Structural studies of Norrin dependent Wnt/β-catenin signaling

Tao-Hsin Chang

A thesis submitted in partial fulfilment of the requirements for the degree of Doctor of Philosophy at the University of Oxford



Somerville College

Nuffield Department of Clinical Medicine

Division of Structural Biology

University of Oxford

Trinity Term 2014

Abstract

Norrin is a secreted cystine-knot growth factor that plays critical roles in vascular development in the brain, retina, and cochlea, as well as the uterus. Although Norrin is unrelated to the lipid-modified morphogens Wnts, Norrin activates the canonical Wnt/β-catenin pathway by binding to receptor Frizzled4 cysteine-rich domain (Fz4-CRD) and co-receptors of low density lipoprotein receptor related protein 5/6 ectodomain (Lrp5/6-ECD) in conjunction with Tetraspanin-12 (Tspan-12). Like Wnts, Norrin has limited extracellular diffusion properties as a result of associating with heparan sulfate proteoglycans (HSPGs). Mutations lead to inherited disordered retinal vascularization diseases such as Norrie disease, familial exudative vitreoretinopathy and coats' disease. However, the molecular mechanism of how Norrin initiates signalling by engagement with Fz4, Lrp5/6, and HSPGs has remained unresolved.

Here, novel strategies for protein production of recombinant human Norrin and Fz4-CRD as well as the complex are developed. The crystal structures of Norrin and its complex with Fz4-CRD, plus complex bound with the heparin mimic sucrose octasulphate, and unliganded structures of Fz4-CRD are presented. These structural data together with biophysical and cellular assays not only reveal the Fz4 and Lrp5/6 binding sites on distinct patches of the Norrin surface, but also indicate the HSPGs binding site on Norrin and Fz4-CRD as well as providing a framework to explain numerous disease-related mutations. Structural comparison with *Xenopus* Wnt8 in complex with mouse Fz8-CRD provides molecular insights for our understanding of ligand-receptor binding specificity and promiscuity, which has important implications for developing therapeutic strategies against Norrin dependent retinal disorders, and cancers caused by abnormal Wnt signaling.

Acknowledgements

I would like to express very much appreciation to my supervisor Professor Yvonne Jones for her patient guidance, support and trust. Advice given by Dr. Radu Aricescu and Dr. Christian Siebold has been a great help in useful critiques of this research work. I am particularly grateful for the assistance given by Dr. Karl Harlos. His willingness to give his time so generously for advice on crystallization and X-ray diffraction data collection has been greatly appreciated.

I would also like to extend my huge thanks to the researchers in STRUBI for their help in sharing with me their knowledge and resources for this project; Dr. Matthias Zebisch for X-ray diffraction data collection and suggestions; Dr. Jonathan Elegheert for help with the MALS and SAXS data analysis; Ms. Weixian Lu and Dr. Yuguang Zhao for help with tissue culture training and assistance; Dr. Tom Walter for the tips on crystallization trials; Ms. Jun Dong for IT support. In particular, I wish to acknowledge the help provided by Ms. Fu-Lien Hsieh for her hard work handling tissue culture, without which the progress of this project would not have been smooth. Thanks are reserved for Ms. Margaret Jones for all her help keeping everything necessary functioning in the wet lab.

I would like to express my thanks to everyone in STRUBI for making this place so enjoyable and I am grateful to have this opportunity to work here for four years. I am also very grateful to the funding sources provided by a Nuffield Department of Clinical Medicine Prize Studentship in conjunction with Clarendon Scholarship and Somerville College Graduate Scholarships.

Finally, I would like to offer my special thanks to my family and friends, especially my wife Fu-Lien, for their love, support and encouragement.

Table of Contents

Abstract I

Acknowledgements II

Table of contents A

Chapter 1 Introduction 1

1.1 Wnt signalling 2

1.2 Norrin mediated Wnt/β-catenin signalling 5

1.2.1 Gene features of Norrie disease protein 6

1.2.2 Norrie disease protein and cystine knot-like growth factor 6

1.2.3 Clinical features of retinal disorders 8

1.2.4 Functional characteristics of the Norrin mediated pathway 9

1.2.5 Molecular mechanism of Wnt and Norrin signalling 11

1.3 Aims 13

Chapter 2 Materials and Methods 15

2.1 Molecular Biology 16

2.1.1 Complementary DNA and expression vectors 16

2.1.2 Construct design, cloning, and mutagenesis 17

2.2 Protein expression in mammalian cells 18

2.2.1 Small-scale protein expression and western blot 18

2.2.2 Pull-down assay 20

2.2.3 Large-scale protein expression 20

2.2.4 Large-scale expression of selenomethionine labelled protein 22

2.3 Protein expression in *Escherichia coli* 22

2.4 Protein production and purification 23

2.4.1 Protein production and purification of Norrin 23

2.4.2 Protein production and purification of Fz4-CRD 24

2.4.3 Protein production and purification of Norrin/Fz4-CRD complex 25

2.4.4 Protein production and purification of Norrin/Fz4-CRD/Lrp6-PE1PE2 complex 25
2.4.5 Reductive lysine methylation 26
2.4.6 Protein purification from *E.coli* 26
2.5 Protein crystallisation and Crystal optimisation 27
2.6. X-ray data collection and processing 30
2.7. Structure determination, refinement, and validation 32
2.8. Structure Analysis 34
2.9. Surface plasmon resonance equilibrium binding studies 34
2.10. Small-Angle X-Ray Scattering Experiment 36
2.11. Size-exclusion chromatography coupled to multi-angle light scattering analysis 37
2.12. Luciferase reporter assay 37
2.13. Heparin Affinity Chromatography 38

Chapter 3 Efficient mammalian expression strategies for production of Norrin pathway components 39

3.1 Summary 40
3.2 Introduction 41
3.3 Aims 42
3.4 Mammalian cell expression system 44
3.5 Pull-down assay to confirm Norrin forms complex with Fz4-CRD 44
3.6 Improvement of Norrin secretion levels 48
3.6.1 The optimization of codon usage and domain boundary 50
3.6.2 A specific signal peptide improves the secretion of Norrin 50
3.6.3 The histone deacetylase inhibitor increases the secretion of Norrin 50
3.6.4 Enhanced Norrin secretion using C-terminal fusion 51
3.6.5 Enhanced Norrin secretion using N-terminal fusion 52
3.7 Protein production of biologically active Norrin 54
3.8 Improvement of Fz4-CRD secretion levels 58
3.8.1 The optimization of the domain boundary 58

3.8.2 Enhanced Fz4-CRD secretion using C-terminal fusion and valproic acid treatment 59
3.9 Protein production of Fz4-CRD 60
3.10 Protein production of Fz5-, Fz7-, and Fz8-CRD 63
3.11 Protein production of Norrin/Fz4-CRD complex 64
3.12 Protein production of Norrin/Fz4-CRD/Lrp6-P1E1P2E2 complex 66
3. 13 Future perspectives 69

Chapter 4 Structural and functional basis of Norrin interaction with Fz4, Lrp5/6, and HSPGs 70
4.1 Summary 71
4.2 Introduction 72
4.3 Aims 74
4.4 The crystal structure of uncomplxed human Norrin 77
4.5 The crystal structure of unliganded human Fz4-CRD 90
4.6 The monomeric state of Fz-CRDs in solution 98
4.7 The crystal structure of human Norrin in complex with Fz4-CRD 103
4.8 Norrin has distinct binding sites for Fz4, Lrp5/6, and HSPGs 115
4.8.1 Verification of Fz4 binding site 124
4.8.2 Verification of HSPGs binding site 133
4.8.3 Analyses of Lrp5/6 binding site on Norrin 136
4.9 Structural comparison of Norrin/Fz4-CRD with Wnt8/Fz8-CRD 139
4.10 Model of Norrin-induced receptor clustering and signallosome formation 146
4.11 Future perspectives 148

Chapter 5 Further discussion 151
5.1 Therapeutic potential of Norrin for retinal disorders 152
5.2 Future structural studies on Norrin and related signalling 153
5.3 Application of engineered Norrin mutants 156
5.3.1 Implication in understanding the signalling mechanism 156
5.3.2 Application in anti-cancer drug development 157

5.3.3 Application to drug delivery in the brain 158

Appendices 159

Appendix 1. Polylinkers of pLEXm based vector variants 160

Appendix 2. List of Formulae 169

Appendix 3. Abbreviations 170

References 173

Chapter 1

Introduction

1.1 Wnt signalling

The Wnt genes encode 19 conserved cysteine-rich secreted palmitoylated glycoproteins that play key roles in the regulation of developmental processes including cell-fate determination, tissue homeostasis and tumorigenesis as well as embryonic development (Angers and Moon, 2009; Logan and Nusse, 2004). Aberrant Wnt signaling leads to severe diseases like cancer, osteoporosis and degenerative illnesses (Logan and Nusse, 2004). Specifically, Wnt proteins are 350 to 400 residues long and feature a conserved pattern of 22-24 cysteine residues (Willert and Nusse, 2012). Lipid modification of a conserved serine reside (Ser209 of Wnt3a typically) is indispensable for intracellular processing, secretion and activity of Wnt proteins (Takada et al., 2006).

Wnt proteins can initiate at least three different pathways including canonical Wnt/β-catenin signalling, non-canonical Wnt/planar cell polarity (PCP) and Wnt/Ca^{2+} signalling (MacDonald et al., 2009; Seifert and Mlodzik, 2007). These thesis focuses on the canonical Wnt/β-catenin signalling pathway.

The current model of the Wnt/β-catenin pathway is summarized in **Figure 1.1**. In the absence of Wnt, β-catenin in the cytoplasm is captured by the destruction complex for phosphorylation and ubiquitination and subsequently degraded by the proteasome (Logan and Nusse, 2004). The destruction complex (Clevers and Nusse, 2012; MacDonald and He, 2012) is a multiprotein complex composed of the scaffolding protein Axin (Zeng et al., 1997), adenomatous polyposis coli (APC) (Munemitsu et al., 1995), glycogen synthase kinase 3 (GSK3) (Liu et al., 2002),

casein kinase 1 (CK1) (Ikeda et al., 1998), Dishevelled (Wong et al., 2003), and β-transducin repeat containing protein (β-TrCP) (Aberle et al., 1997). Basically, β-catenin is phosphorylated by CK1 and then GSK3. The β-TrCP recognizes the phosphorylated β-catenin for further ubiquitination, which would result in it being degraded by the proteasome (Clevers and Nusse, 2012). This regulation mechanism prevents β-catenin accumulation in the cytoplasm and translocation to the nucleus, thus suppressing the expression of Wnt target genes by the T cell factor and lymphoid enhancer factor (TCF/LEF) (Riese et al., 1997).

The canonical Wnt/β-catenin pathway is initiated by the binding of Wnt protein to Frizzled (Fz) receptor (Bhanot et al., 1996) and low-density lipoprotein (LDLR)-related protein 5 and 6 (Lrp5/6) co-receptor (Tamai et al., 2000) on the cellular surface to form a ternary complex. The cytoplasmic protein Dishevelled binds to the C-terminal tail of Fz (Wong et al., 2003) and further recruits the complex composed of Axin, APC, GSK3, and CK1 to interact with the cytoplasmic domain of Lrp5/6 for phosphorylation by GSK3 and CK1 (Davidson et al., 2005). The triggering of complex formation, from the extracellular to intracellular region, leads to the stabilization and subsequent translocation of cytoplasmic β-catenin to associate with members of the TCF/LEF family of transcription co-factors in the nucleus to turn on downstream transcriptional cascades (MacDonald et al., 2009).

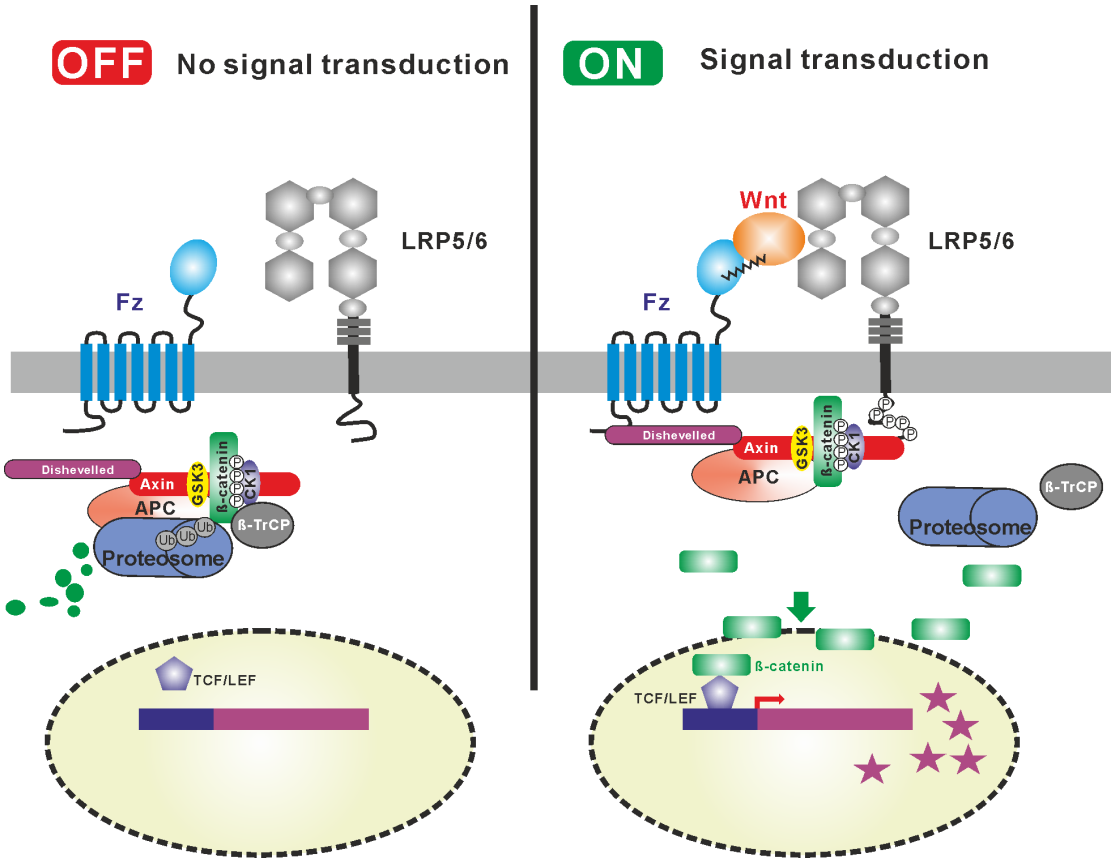


Figure 1.1. Overview of canonical Wnt/β-catenin signalling.
In the absence of Wnt, cytoplasmic β-catenin forms a destruction complex with Axin, Dishevelled, APC, GSK3, CK1, and β-TrCP and is phosphorylated by CK1 and GSK3. The phosphorylated β-catenin is further ubiquitinated by β-TrCP. The phosphorylated and ubiquitinated β-catenin is degraded by the proteasome to recycle the destruction complex. In the presence of Wnt, Wnt engages with the Fz and Lrp5/6 receptors. Dishevelled binds to the C-terminal tail of Fz, resulting in Axin recruitment to Lrp5/6 and phosphorylation via GSK3 and CK1. The destruction complex still interacts with phosphorylated β-catenin, but the ubiquitination by β-TrCP is blocked. Newly synthesized β-catenin is accumulated and translocated into the nucleus where it acts as a co-activator for TCF/LEF to activate the expression of Wnt target genes. APC, adenomatous polyposis coli; GSK3, glycogen synthase kinase 3; CK1, casein kinase 1; β-TrCP, β-transducin repeat containing protein; TCF/LEF, T cell factor and lymphoid enhancer factor.

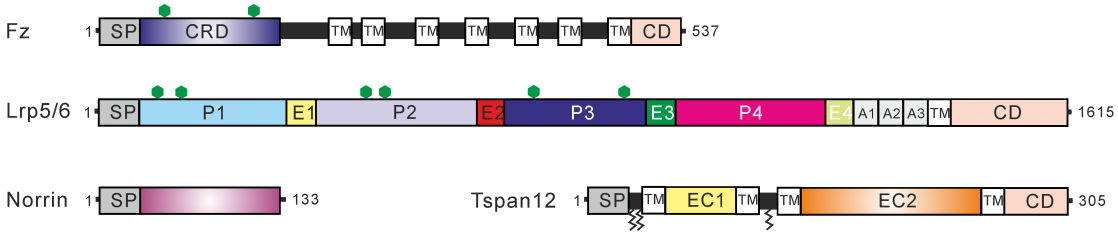


Figure 1.2. Schematic diagrams of Fz4, Lrp5/6, Norrin, and Tspan-12 drawn to linear scale.
SP, signal peptide; CRD, cysteine-rich domain; TM, transmembrane domain; CD, cytoplasmic domain; EC, extracellular domain; P: β-propeller domain; E: epidermal growth factor-like module; A, LDL-receptor class A domain. NetNGlyc (http://www.cbs.dtu.dk/services/NetNGlyc/) predicted N-linked N-acetylglucosamine (GlcNAc) glycoslyation sites are highlighted with green hexagons and S-palmitoylation sites are highlighted by serrations.

1.2 Norrin mediated Wnt/β-catenin signalling

Interestingly, Norrie disease protein (NDP; Norrin), a non-Wnt protein, has been identified to activate canonical Wnt/β-catenin signaling via engagement of the receptor Fz4, co-receptors Lrp5/6, and auxiliary four-pass transmembrane protein Tetraspanin-12 (Tspan-12) (**Figure 1.2**) (Junge et al., 2009; Xu et al., 2004; Ye et al., 2009). The Fz4 receptor is one of ten members of a sub-set of the G protein-coupled receptor (GPCR) family, consisting of an N-terminal extracellular cysteine-rich domain (CRD) which directly bind to Wnts, a seven-pass transmembrane segment, and an intracellular C-terminal domain (Bhanot et al., 1996; Hsieh et al., 1999). The co-receptor Lrp5/6 is a single-pass transmembrane receptor (He et al., 2004), whose ectodomain (Lrp5/6-ECD) contains four tandem β-propeller/epidermal growth factor-like domain (PE) pairs followed by three LDLR type A repeats (Ahn et al., 2011; Bourhis et al., 2011; Chen et al., 2011; Cheng et al., 2011) and interacts with Wnts and Wnt antagonists via a variety of PE pair combinations (Bourhis et al., 2010; Cruciat and Niehrs, 2013).

1.2.1 Gene features of Norrie disease protein

The *NDP* gene (**Figure 1.3**) is located on chromosome Xp11.4 in the human genome. It is composed of three exons and two introns from which a 2.1 kb mRNA is transcribed (Berger et al., 1992a; Chen et al., 1992). The first exon is an untranslated region, which is used to regulate *NDP* gene expression (Kenyon and Craig, 1999). Alternative splicing has not been found. Mutations in the gene of *NDP* cause Norrie disease (Berger et al., 1992b).

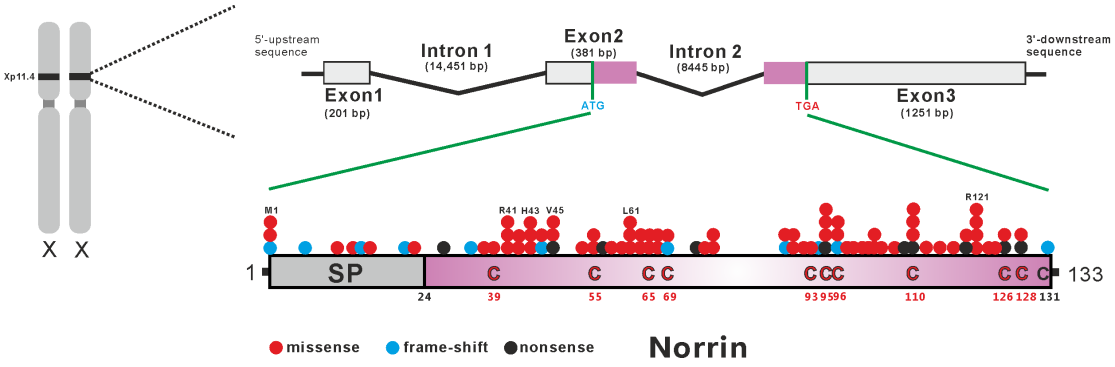


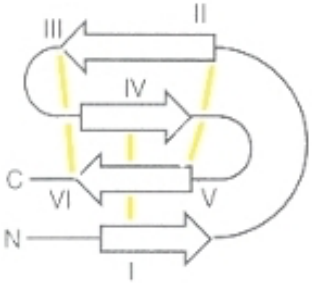
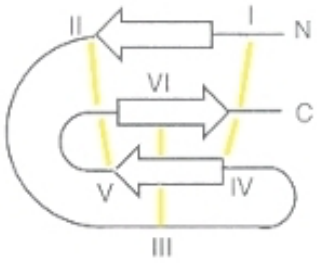
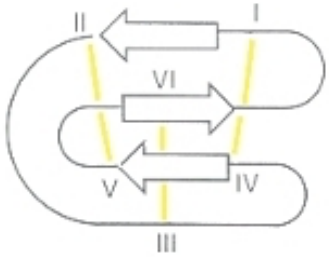
Figure 1.3. Genomic structure of the *NDP* gene.
The gene is located on chromosome Xp11.4 in the human genome. Before mRNA splicing, the pre-mRNA contains three exons and two introns. Norrin is a small-secreted cysteine-rich protein, containing 109 amino acids in the mature form. Over 100 disease-associated mutations in the *NDP* gene have been identified.

1.2.2 Norrie disease protein and cystine knot growth factor

Norrin (**Figure 1.2**) encoded by the *NDP* gene a small cysteine-rich secreted protein (of only 109 amino acid residues in the mature form; unrelated to Wnts in sequence), revealing weak homology (below 15% sequence identity) to the C-terminal cystine knot growth factors including transforming growth factor (TGF)-β, bone morphogenetic protein (BMP), and platelet-derived growth factor (PDGF) (Berger et al., 1992a; Chen et al., 1992; Meindl et al., 1992; Meitinger et

al., 1993). The cystine knot is a kind of protein structural motif (Daly and Craik, 2011; McDonald and Hendrickson, 1993). It consists of three disulfide bridges that are arranged in a unique topology in which two disulfide bridges along with their connecting backbone segments form an embedded ring through which a third disulfide bridge penetrates, forming a knot. As shown in **Table 1.1**, the cystine knot is further classified into three types (Daly and Craik, 2011; McDonald and Hendrickson, 1993; Sun and Davies, 1995), including cystine knot growth factor, inhibitor cysine knot (alternate name Knottin), and cyclic cystine knot (alternate name cyclotide).

Table 1.1 Features of cystine knot protein family. The cartoon models show the differences between cystine knot protein families (arrows, the β-strands; I-VI, the number of cysteine residues; N, the N-terminus of polypeptide, C, the C-terminus of polypeptide, yellow lines, the disulphide bridges. Figures are adapted from http://www.cyclotide.com/knots.html.

cystine knot growth factor	**inhibitor cysine knot**	**cyclic cystine knot**
		
1. Three disulfide bridges 2. Penetrating disulfide bond (cysteine I-IV)	1. Three disulfide bridges 2. Penetrating disulfide bond (cysteine III-VI)	1. Three disulfide bridges 2. Penetrating disulfide bond (cysteine III-VI) 3. Cyclization of the polypeptide backbone

Because of the technical difficulty in obtaining sufficient Norrin protein for functional characterization, there is limited knowledge regarding Norrin.

Previously reported studies indicate that Norrin binds to the extracellular matrix and heparin (Bao et al., 2012; Hsieh et al., 1999; Kikuchi et al., 2007; Logan and Nusse, 2004). Norrin, similar to the morphogen Wnt, has the property of interaction with heparan sulphate proteoglycans (HSPGs) and limited spatial diffusion (Ohlmann et al., 2010; Perez-Vilar and Hill, 1997; Smallwood et al., 2007; Xu et al., 2004). HSPGs have been proposed to regulate the local distribution of ligand and receptor at the cell surface potentially acting as an introductory agency for ligand and receptor (Malinauskas et al., 2011; Malinauskas and Jones, 2014).

HSPGs consist of a core protein that is heavily modified with glycosaminoglycans (GAGs). GAGs are single chain polysaccharides that are composed of repeating disaccharides with a uronic acid and an amino sugar (Baeg et al., 2001). The disaccharides of glucuronic acid and N-acetylglucosamine form heparan sulfate. Membrane HSPGs can be divided into two families, called glypicans and syndecans (Yan and Lin, 2009). Mammals carry six glypican genes and four syndecan. Glypicans are anchored to the cell membrane via glycosylphosphatidylinositol (GPI) and have 2-3 GAG attachment sites to membrane-proximal regions of the protein. Syndecans are type I transmembrane proteins with up to five GAG attachment sites mainly containing heparin sulfate chains.

1.2.3 Clinical features of retinal disorders

Mutations in the *NDP* gene cause an X-linked recessive genetic disease that accompanies auditory impairment, mental retardation, and retinal dysplasia

(Berger et al., 1992a; Chen et al., 1992). The phenotypes of dysfunction in retinal vascularization (**Figure 1.4**) are also characterized in humans having Familial Exudative Vitreoretinopathy (FEVR), Retinopathy Of Prematurity (ROP) and Coats' disease, as defects in the *Fz4*, *Lrp5*, or *Tspan-12* genes (Gong et al., 2001; Hiraoka et al., 2010; Nikopoulos et al., 2010a; Poulter et al., 2010; Robitaille et al., 2002; Shastry, 2010; Toomes et al., 2004; Yang et al., 2011; Zhang et al., 2011). Moreover, missense mutations in the *NDP* gene have been identified to be highly relevant to FEVR and ROP as well (Shastry et al., 1997a; Shastry et al., 1997b). Patients who suffer from Norrie disease often present with blindness at birth, whereas the majority of FEVR patients display a mild phenotype.

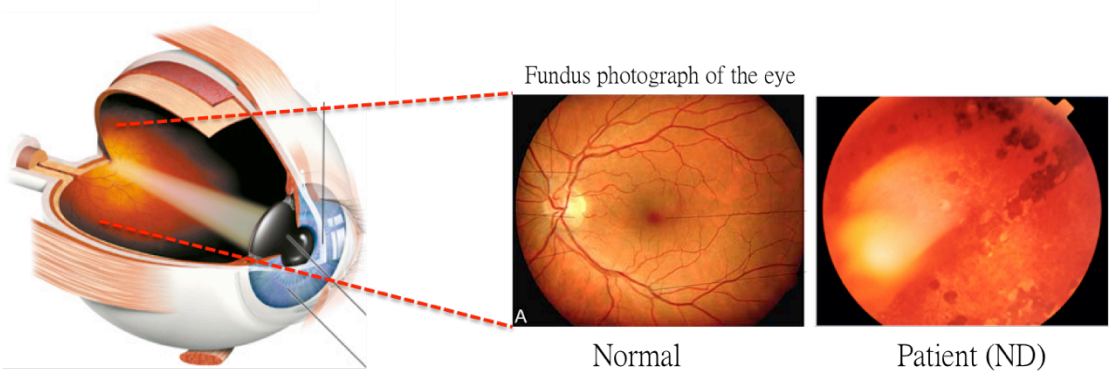


Figure 1.4. Retinal defects characteristic of Norrie disease.
The left panel shows the retinal region imaged for a fundus photograph. The fundus photographs reveal normal blood vessel distribution on a healthy retina (middle panel) and impaired vascularization on the Norrie disease patient's retina (right panel).
Figures are adapted from http://www.fevr.net and Csak *et al*., 2006 (Csak et al., 2006).

1.2.4 Functional characteristics of the Norrin mediated pathway

The *NDP* gene knock-out mice reveal an overall impaired retinal vascularization and ocular abnormalities, which is similar to those observed in Norrie disease

patients (Richter et al., 1998). Highly similar phenotypes are found in other gene knock-out mice including *FZ4* (Xu et al., 2004), *LRP5* (Kato et al., 2002), and *TSPAN-12* (Junge et al., 2009). These findings support the hypothesis that dysfunctional Norrin mediated signalling results in impaired retinal vascularization, in agreement with cell-based assays showing that most of the mutations result in defects in the activation of signalling (Xu et al., 2004). In adults, Norrin has not only angiogenic properties in the retina, cochlea, and uterus (Luhmann et al., 2005; Rehm et al., 2002), but also neuroprotective effects on retinal neurons (Ohlmann et al., 2010; Seitz et al., 2010), as well as an essential role for maintaining the blood-retina barrier (Paes et al., 2011; Ye et al., 2009) and blood-brain barrier (Wang et al., 2012).

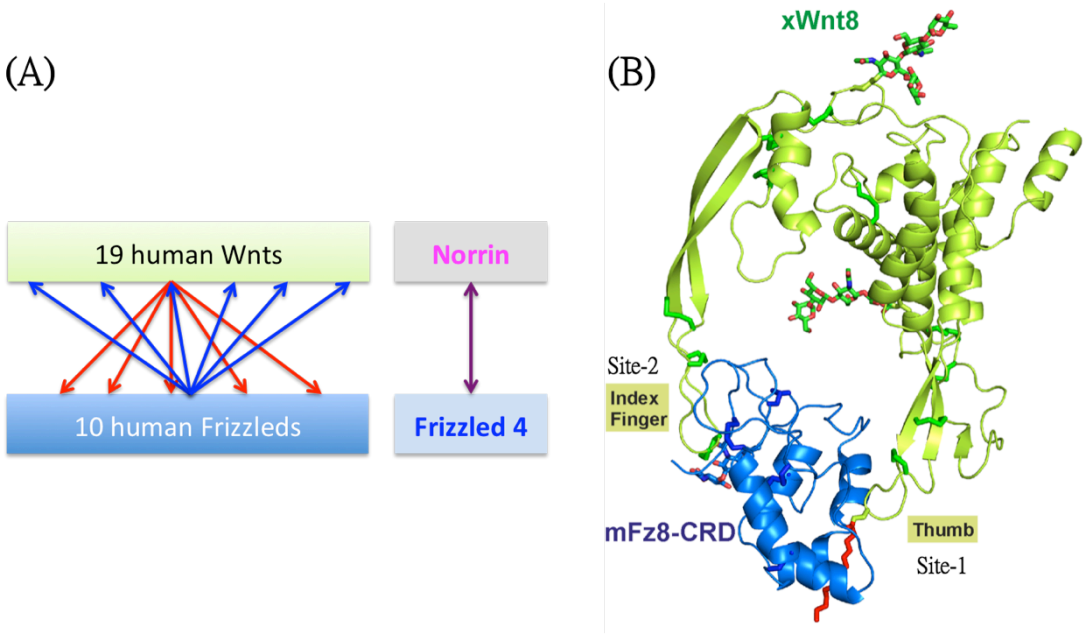


Figure 1.5. Comparison of Wnt and Norrin interaction networks and crystal structure of *Xenopus* Wnt8/Fz8-CRD complex.
(A) Interaction networks of Wnt and Fz pairs as well as Norrin and Fz pairs. **(B)** *Xenopus* Wnt8 (green) in complex with mouse Fz8-CRD (blue). The disulphide bonds (green, xWnt8; blue, mFz8-CRD) and palmitoleic acid (red) covalently attached to the thumb region of Wnt8 are shown as sticks. N-linked glycans are shown in blue for Fz8-CRD and green for Wnt8.

1.2.5 Molecular mechanism of Wnt and Norrin signalling

A confounding complexity (**Figure 1.5A**) in Wnt signalling results from the combination of 19 Wnt proteins, 10 Fz receptors and at least two Lrp5/6 co-receptors. It has been demonstrated that each Wnt binds to multiple Fz receptors, each Fz receptor responds to multiple Wnts, and different Wnt proteins interact with different regions of the ectodomain of Lrp5/6 (Bao et al., 2012; Hsieh et al., 1999; Kikuchi et al., 2007; Logan and Nusse, 2004). Therefore, whether and how different combinations of Wnt/Fz/Lrp might trigger the response in certain biological processes is obscure so far.

In contrast to Wnt proteins, Norrin (**Figure 1.5A**) shows highly selective binding to Fz4-CRD, but not to the other CRDs of the nine Fzs and five secreted Frizzled-related proteins (sFRPs) (Junge et al., 2009; Smallwood et al., 2007; Xu et al., 2004). A previous study has indicated that the binding regions on Fz4-CRD for Norrin and *Xenopus* Wnt8 are largely overlapped (Smallwood et al., 2007). But, *Xenopus* Wnt8 also binds to Fz2, 5, 7 and 8 (Dann et al., 2001; Hsieh et al., 1999; Janda et al., 2012). Intriguingly, unlike the specificity of Norrin paired with Fz4-CRD, Fz4-CRD has been demonstrated to bind to several canonical Wnt proteins (Wnt2b, Wnt3a and Wnt8a) and a non-canonical Wnt5a (Hsieh et al., 1999; Mikels and Nusse, 2006; Smallwood et al., 2007) as well as the non-Wnt proteins including Tsukushi (a secreted leucine-rich repeat-containing protein) (Ohta et al., 2011) and complement C1q (Naito et al., 2012).

The recently published crystal structure of *Xenopus* Wnt8 in complex with mouse Fz8-CRD (**Figure 1.5B**) shows that Wnt8 comprises two structural subdomains:

a larger N-terminal domain comprising a six α-helix core, and two protruding β-hairpins, one of which is covalently linked with palmitoleic acid, and a C-terminal domain that is a cytokine-like hairpin loop (Janda et al., 2012). The hand-like Wnt structure uses its extended thumb with lipid attachment to insert into a hydrophobic groove in the Fz8-CRD, and index finger protruding from the C-terminal domain to contact a second hydrophobic depression (pocket) in Fz8-CRD (**Figure 1.5B**).

Taken together, Norrin appears to function like a Wnt with properties such as binding to Fz and Lrp5/6 for the activation of signalling, and interaction with HSPGs for distribution in the extracellular region. This is despite a complete absence of primary sequence homology with the Wnt family. However, Norrin mediated signalling shows highly selective interaction with Fz4 and engages additionally with Tspan-12, which acts as an enhancer to increase signalling response, characteristics that are different from Wnt signalling.

1.3 Aims

As discussed above, Norrin regulates vascularization in retina and brain to maintain the blood-retina barrier and blood-brain barrier, respectively. However, structural and biophysical analyses are very limited, as a result of the technical difficulties in obtaining recombinant Norrin and its binding partners, relative to functional studies of Norrin mediated signalling. The main aim of this thesis is to obtain structural knowledge regarding the molecular architecture of Norrin in complex with the ectodomains of Fz4 and Lrp5/6, to elucidate the mechanism of Norrin mediated signalling, and to understand the action of disease-associated mutations.

Chapter 2

Materials and Methods

2.1 Molecular Biology

2.1.1 Complementary DNA and expression vectors

Synthetic complementary DNA (cDNA) clones (codon-optimized for expression in mammalian cells) of Norrin from human (UniprotKB/Swiss-prot Q00604), *Xenopus* (NCBI accession number NP_001154869), and *Zebrafish* (NCBI accession number XP_001338820) as well as *Xenopus* Frizzled4 cysteine-rich domain (Fz4-CRD, residues 1-166; UniprotKB/Swiss-prot Q9PT62) were obtained from GeneArt (Invitrogen). The cDNA templates of human receptors including Fz4 (UniprotKB/Swiss-prot Q9ULV1; IMAGE ID: 40082087), Fz7 (UniprotKB/Swiss-prot O75084; IMAGE ID: 4549389), and Tspan-12 (UniprotKB/Swiss-prot O95859; IMAGE ID: 5275953) and mouse receptors containing Fz5 (UniprotKB/Swiss-prot Q9EQD0; IMAGE ID: 40088671) and Fz8 (UniprotKB/Swiss-prot Q61091; IMAGE ID: 8861081) were purchased from SourceBioScience. The cDNA clones encoding human Lrp6 (UniprotKB/Swiss-prot O75581) and Lrp5 (UniprotKB/Swiss-prot O75197) were provided by Drs. Shuo Chen and E. Yvonne Jones (University of Oxford, UK). The *E. coli* expression vectors of Human Rhinovirus (HRV)-3C protease either carrying a N-terminal glutatione S-transferase (GST) or 6xHis tag were gifts from the Oxford Protein Production Facility UK.

For expression in mammalian cell lines, several vectors based on the pLEXm backbone were used: pHLsec, pHL-FcHis, and pHL-Avitag3 (Aricescu et al., 2006) plus pHLsec-1D4 (a gift from Drs. N. Mitakidis and A. R. Aricescu, University of Oxford, UK) and pHL-mVenus (a gift from Drs. A. Clayton and A. R. Aricescu,

University of Oxford, UK). These vectors (**Appendix 1**) typically have the same multiple cloning sites; most typically, constructs were inserted using the AgeI and KpnI restriction sites, introducing an optimized Kozak sequence at the 5' end, a N-terminal secretion signal and a C-terminal 6xHis tag or a C-terminal highly specific epitope (nine residues, TETSQVAPA, derived from bovine rhodopsin; named as Rho-1D4) that is recognized by the Rho-1D4 monoclonal antibody for the vector pHLsec-1D4 (Molday and MacKenzie, 1983). The EcoRI restriction site was used in place of AgeI when it was necessary to replace the secretion signal in the plasmid with native secretion signal from the target protein or with other secretion signals from high secretion proteins. In the pHL-Avitag3 vector used for biophysical binding assays, the biotin ligase (BirA) recognition site (fifteen residues, GLNDIFEAQKIEWHE) is located C-terminal to the insert, prior to the 6xHis tag. The vectors pHL-FcHis and pHL-mVenus contain a HRV 3C protease cleavage site (LEVLFQ/GP) C-terminal to the insert followed by the human IgGγ1 Fc region or monoVenus (Genbank DQ092360), respectively, prior to the 6xHis tag.

For improvement of protein secretion and purification, a series of vectors incorporating optimized secretion peptides or fusion tags, including a mammalian expression codon-optimized *Saccharomyces cerevisiae* small ubiquitin-like protein (SUMO**;** UniprotKB/Swiss-prot Q12306; residues 2-96)(Peroutka et al., 2008) and alkaline phosphatase (UniProtKB/Swiss-Prot: P05187) from the APtag-2 vector (Flanagan and Cheng, 2000), at either the N- or C-terminus were designed in this study by using the above vectors as the backbones (**Appendix 1**). Two newly designed expression vectors were used to

solve the protein expression problem for Norrin and Fz4-CRD, respectively, and are described briefly below. The vector of pHLIgκ-STR-8H-SUMO-1D4 contains a murine Igκ-chain secretion signal (Coloma et al., 1992), followed by a Strep-II tag, 8xHis tag, SUMO **(**residues 2-96), a HRV-3C protease cleavage site, insert of target, and finally a Rho-1D4 (Molday and MacKenzie, 1983). The vector of pHL-mVenus-12H contains a C-terminal HRV-3C protease cleavage site followed by a linker, the monoVenus (Nagai et al., 2002), and finally a tandem 6xHis tag.

2.1.2 Construct design, cloning, and mutagenesis

Constructs were designed considering the domain boundaries listed on the UniprotKB/Swiss-prot Internet protein database (http://www.uniprot.org/), information from the protein disorder prediction program RONN (http://www.strubi.ox.ac.uk/RONN/) (Yang et al., 2005) and overall protein features including protein physical and chemical parameters, secondary structure, and surface entropy analyses using Expert Protein Analysis System (ExPASy) ProtParam (http://expasy.org/), XtalPred Server (http://ffas.burnham.org/XtalPred-cgi/xtal.pl) (Slabinski et al., 2007), and Surface Entropy Reduction prediction server (http://services.mbi.ucla.edu/SER/) (Goldschmidt et al., 2007).

The coding sequences were amplified by polymerase chain reaction (PCR) using *Pyrobest*™ (TaKara) according to the manufacturer's protocol and designed oligonucleotides (MWG Biotech) included restriction sites or extended sequences, to allow restriction-based or *In-Fusion*™ (Clontech) cloning methods to be used, respectively. Basically, primers were designed to have a Tm value

between 60-65°C and ideally a GC content of approximately 60%. Mutagenesis was performed using a two-step overlapping PCR procedure. Norrin mutants for biophysical and cellular assays were obtained from GeneArt (Invitrogen).

All PCR reactions were verified by agarose gel electrophoresis and purified using QIAquick Kit (QIAGEN). Purified PCR product and vectors were digested with the corresponding restriction enzymes (New England Biolabs), ligated using the Quick Ligation™ Kit (New England Biolabs), and transformed into the Library Efficiency DH5α™ competent cells (Invitrogene) according to the manufacture's protocols. Transformed cells were spread on Luria-Bertani medium (LB)-agar plates containing 100 μg/ml carbenicillin and incubated overnight at 37 °C. Two colonies for each construct were picked and used to inoculate overnight cultures to purify plasmid DNA using QIAprep Spin Miniprep Kit (QIAGEN) according to the manufacture's protocol. Clones were verified by DNA sequencing (Source Bioscience DNA sequencing facility, Department of Biochemistry, University of Oxford).

2.2 Protein expression in mammalian cells

2.2.1 Small-scale protein expression and western blot

The two human embryonic kidney (HEK) cell lines 293T and N-acetylglucosaminyl transferase I (GnTI)-deficient 293S were the main expression systems (Aricescu et al., 2006; Reeves et al., 2002). Both cell lines were maintained in Dulbecco's Modified Eagle Medium (DMEM, Sigma) supplemented with 5 μg/ml L-Glutamine (L-Glu, Sigma), 5 μg/ml non-essential amino acids

(NEAA, Invitrogen) and 10% [v/v] Fetal Bovine Serum (FBS, Invitrogen) in a humidified 37 ^{o}C incubator with 5% CO_2.

Protein expression and secretion of all constructs was initially tested in small-scale trials in HEK293T cells. Cells were seeded in 12-well plates (Corning) with $0.2x10^6$ cells per well and incubated with 5% CO_2 at 37 ^{o}C until a final density of 80-90% was achieved. Media was exchanged to DMEM supplemented with 2% [v/v] FBS, 5 µg/ml NEAA and L-Glu and cells per well were transfected with 2 µg of DNA with 4 µl lipofectamine 2000 (Invitrogen) according the manufacture's protocol. The cell media were collected two days post-transfection and prepared for analyses by western blot to check the secretion expression level. Cell media were centrifuged to remove cell debris. The stringent quality control mechanisms specific to the mammalian cell secretory pathway ensure that secreted proteins are correctly folded (Trombetta and Parodi, 2003).

These samples were analysed by sodium dodecyl sulfate polyacrylamide gel electrophoresis (SDS-PAGE) gels transferred onto a nitrocellulose membrane (GE Healthcare Life Sciences) at 100 mA for an hour using 10 % [v/v] methanol in NuPAGE transfer buffer and XCell SuperLockTM Mini-Cell (Invitrogen). The western blot analysis was performed using the standard method (Alegria-Schaffer et al., 2009) with anti-PentaHis (Anti-His, 1:1000 dilution, Qiagen) or Rho-1D4 monoclonal antibodies (Anti-1D4, 1 µg per ml, Flintbox, University of British Columbia) as primary antibody and goat anti-mouse IgG-horseradish peroxidise conjugate (1:5000 dilution, Sigma). The signal was visualized by

Enhanced Chemiluminescence western blotting detection kit (ECL, GE Healthcare Life Sciences).

2.2.2 Pull-down assay

For the Immobilised Metal Affinity Chromatography (IMAC) pull-down assay, we cloned human Norrin (residue 25-133) and Fz4-CRD (residues 40-160) into pHLsec vector (Aricescu et al., 2006) in frame with a C-terminal Rho-1D4 and 6xHis tag, termed as Norrin-1D4 and Fz4-CRD-His, respectively. HEK293T cells were transfected with the DNA mix (pLEXm, Fz4-CRD-His and pLEXm, Norrin-1D4 and pLEXm, Fz4-CRD-His and Norrin-1D4, separately) using Lipofectamine 2000 (Invitrogen) according to the manufacture's protocol. The conditioned media (2 ml per each reaction) were collected 2 days post transfection and add 10 ml phosphate buffered saline (PBS), pH 7.4 before incubation with the Co^{2+}-charged beads (25 µl; TALON®Clontech) at 4 ^{o}C overnight. The beads were washed with buffer containing PBS, pH 7.4, 10 mM Imidazole and eluted in 25 mM Tris, pH 7.5, 0.5 M NaCl, 0.5 M Imidazole. The eluted samples were subjected to SDS-PAGE, followed by immunoblotting with the appropriate antibodies.

2.2.3 Large-scale protein expression

Typically, scale-up of protein production was performed by transfection of HEK293S (Reeves et al., 2002), HEK293T for Norrin due to no predicted N-linked glycosylation sites, or HEK293T cells in the presence of the class I α-mannosidase inhibitor, kifunensine (Toronto Research Chemicals Inc.) (Chang et al., 2007) in expanded surface roller bottles (2125 cm^2, Greiner Bio-One) with a

cocktail of 2 mg of purified DNA (Endotoxin-Free Plasmid Giga Kit, Qiagen) and 4 mg polyethylenimine (PEI, Aldrich) per liter of cell media, reduced FBS levels from 10[[v/v] to 2% [v/v]. The roller bottles were incubated with 5% CO_2 at 37 ^{o}C following transfection. Seven to eight days post transfection, media were clarified by centrifugation at 4000*g* for 20 min and sterilized by filtration using Steritop™ Filter units (Millipore), then stored at 4 °C.

The N-linked glycosylation pathway produces a high diversity in the N-linked glycans present on glycoproteins, which may interfere with protein crystallisation. Two strategies were used to prevent the progress of N-linked glycosylation pathway beyond an infant high mannose glycan to hybrid and complex glycans in order to produce the glycoproteins with a homogeneous population of *N*-linked glycans. For the first strategy, after transfection, HEK293T cell growth media had added 5 μM kifunensine (Toronto Research Chemicals), a specific inhibitor of α-mannosidase I (Chang et al., 2007). The treatment halts the N-linked glycosylation pathway in the *cis*-Golgi at the $Man_9GlcNAc_2$ stage. For the second strategy HEK-293S cells were used, these cells are deficient in the N-acetylglucosaminyltransferase I enzyme (GnTI). Therefore, the N- linked glycosylation pathway is stalled at the simplified $Man_5GlcNAc_2$ glycan unit in the medial Golgi (Reeves et al., 2002). For both strategies, endoglycosidase-F_1 (Endo-F_1) is able to hydrolyze the oligomannose-type N-linked glycans to a single N-acetylglucosamine residue, whereas hybrid and complex *N*-linked glycans are resistant to this enzyme.

2.2.4 Large-scale expression of selenomethionine labelled protein

For the preparation of selenomethionine (SeMet) labelled proteins, the cell media was discarded 24 hr post-transfection and the cells were washed with PBS (2× 35mL per roller bottle). At this stage, Dulbecco's Modified Eagle's Medium lacking both L-methionine and L-glutamine (MP Biomedicals) and supplemented with 2 mM L-glutamine (Sigma), 40μg/ml SeMet (Eburon Organics) and 2 % [v/v] dialyzed FBS (lacking methionine) was added to the cells. After 4 days expression, the medium was harvested and cleared by centrifugation and filtration.

2.3 Protein expression in *Escherichia coli*

The *E. coli* expression system was used for expression of HRV 3C protease and *Flavobacterium meningosepticum* Endo-F_1. The constructs for expression of Endo-F_1 (with either N-terminal GST-tag or 12xHis and GST tandem tag) were transformed to *E. coli* Rosetta 2 (DE3) pLysS (Novagen) and induced with 0.2 mM isopropyl β-thiogalactopyranoside (IPTG) in Luria-Bertani (LB) medium containing 100 μg/ml carbenicillin at 15 °C overnight. The constructs for expression of 3C protease (with either N-terminal GST-tag or 6xHis-tag) were transformed to *E. coli* Rosetta 2 (DE3) pLysS (Novagen) and induced with 0.2 mM IPTG in LB medium in the presence of 0.5% [v/v] glucose and 100 μg/ml carbenicillin (for GST-tagged protein expression) or 50 μg/ml kanamycin (for His-tagged protein expression) at 15 °C overnight. Cell pellets were harvested and resuspended in extraction buffer (50 mM Tris, pH 8.0, 20 mM imidazole, 0.3

M NaCl, 1 mM tris(2-carboxyethyl) phosphine hydrochloride (TCEP), and 2 ng/ml of benzonase (Novage), and Protease Inhibitor Cocktail (Roche)).

2.4 Protein production and purification

2.4.1 Protein production and purification of Norrin

Norrin was expressed in HEK293T cells in the presence of 4 mM valproic acid, a histone deacetylase inhibitor (Backliwal et al., 2008), used to increase the expression level of secreted protein. Because recombinant Norrin carried two affinity tags (N-terminal 8xHis and C-terminal Rho-1D4 tag), two alternative protein purification strategies could be applied.

In the first purification flowchart, Norrin conditioned media were passed through the 1D4-affinity beads prepared by covalently coupling purified Rho-1D4 antibody to CNBr-activated Sepharose 4 Fast Flow (GE Healthcare Life Sciences) according to the manufacturer's protocol. The beads were washed thoroughly with buffer containing 25 mM Tris, pH 7.5, 0.5 M NaCl, 10% [w/v] Glycerol, 0.5% [w/v] CHAPS and the protein eluted in 25 mM Tris, pH 7.5, 0.5 M NaCl, 10% [w/v] Glycerol, 0.5% [w/v] CHAPS, 250 μM TETSQVAPA peptide (GenScript). The eluted sample was incubated with the homemade GST-tagged HRV-3C protease to remove the SUMO-tagged fusion protein. The untagged Norrin was purified by 1D4-affinity beads followed by size-exclusion chromatography (SEC, Superdex 200 10/300 GL High Performance, GE Healthcare Life Sciences) in 10 mM HEPES, pH 7.5, 0.7 M NaCl, 0.5% [w/v] CHAPS.

In the second purification flowchart, Norrin conditioned media were dialyzed against PBS buffer plus 0.4 M NaCl. Recombinant protein was further purified from the dialyzed media by IMAC (TALON®Clontech) and eluted in 25 mM Tris, pH7.5, 0.15 M NaCl, 0.5 M Imidazole. The purified sample was dialyzed against 25 mM Tris, pH 7.5, 1M NaCl, 10% [w/v] Glycerol and treated with His-tagged HRV-3C protease to remove the SUMO-tagged fusion protein. The untagged sample was further isolated by IMAC and further purified by SEC (SEC, Superdex 200 10/300 GL High Performance, GE Healthcare Life Sciences) in 10 mM HEPES, pH 7.5, 0.7 M NaCl, 0.5% [w/v] CHAPS or 10 mM acetate buffer, pH 4.0, 0.5 M NaCl, 0.5% [w/v] CHAPS.

2.4.2 Protein production and purification of Fz4-CRD

For purification of Fz4-CRD, protein was produced in HEK293T cells in the presence of 5 µM kifunensine (Toronto Research Chemicals Inc.) (Chang et al., 2007). The conditioned media were dialyzed and recombinant protein was purified by IMAC (TALON®Clontech). The purified sample was dialyzed against 25 mM Tris, pH 7.5, 0.5 M NaCl, 10% [w/v] Glycerol and treated with His-tagged HRV 3C protease and Endo-F_1 (Chang et al., 2007; Grueninger-Leitch et al., 1996). The deglycosylated and untagged sample was purified by IMAC (TALON®Clontech) and further polished by SEC (Superdex 75 16/600 column, GE Healthcare Life Sciences) in 10 mM HEPES, pH 7.5, 0.15 M NaCl. Purification of Fz4-, Fz5-, Fz7-, and Fz8-CRD for functional assays followed the same

procedure to that described above, except protein was expressed in HEK293T cells and the treatment by Endo-F_1 was omitted.

2.4.3 Protein production and purification of Norrin/Fz4-CRD complex

Norrin and Fz4-CRD were co-expressed in HEK293T cells in the presence of 5 μM kifunensine and 4 mM valproic acid. Complex was isolated from dialyzed conditioned media by IMAC (TALON®Clontech). The eluted sample was dialyzed against 25 mM Tris, pH 7.5, 0.5 M NaCl, 10% [w/v] and treated with GST-tagged HRV-3C protease and Endo-F_1. The deglycosylated and untagged complex was further purified by IMAC (TALON®Clontech) and GST-affinity beads (GE Healthcare Life Sciences) and subsequently isolated by SEC (Superdex 200 16/600 column, GE Healthcare Life Sciences) in 10 mM HEPES, pH 7.5, 0.7 M NaCl.

2.4.4 Protein production and purification of Norrin/Fz4-CRD/Lrp6-PE1PE2 complex

For preparation of ternary complex of Norrin/Fz4-CRD/Lrp6-PE1PE2, the three components were co-expressed in HEK293T cells in the presence of 5 μM kifunensine and 4 mM valproic acid. The conditioned media were dialyzed against PBS buffer plus 0.4 M NaCl and complex was purified by IMAC (TALON®Clontech). The eluted sample was dialyzed against 25 mM Tris, pH 7.5, 0.5 M NaCl, 10% [w/v] and treated with His-tagged HRV-3C protease and Endo-F_1. The deglycosylated and untagged complex was further purified by IMAC

(TALON®Clontech) and further isolated by SEC (Superdex 200 16/600 column, GE Healthcare Life Sciences) in 10 mM HEPES, pH 7.5, 0.5 M NaCl.

2.4.5 Reductive lysine methylation

For preparation of methylated protein, surface lysine methylation (Walter et al., 2006) was performed on proteins during the last steps of purification (typically after SEC or IMAC) in the HEPES based buffer condition. A reducing agent, 20 mM dimethylamine borane complex (ABC, Fluka) and a methyl source, 40 mM formaldehyde, were added to approximately 0.5-1 mg/ml protein solution and incubated at 4 °C for 0.5 hr. The concentrations of both reagents were then doubled and the reaction left to continue at 4 °C for 0.5 hr. A further 10 mM ABC was added to the reaction, which was incubated at 4 °C for 1 hr. Then 0.2 M Tris, pH 7.5 was added to quench with the excess of ABC and formaldehyde. The reaction mixture was centrifuged to remove any precipitated protein and concentrated before further purification by SEC.

2.4.6 Protein purification from *E.coli*

Cell lysate was prepared by a French Press method (Cell Disruption Solutions, Constant Systems), centrifuged at 20,000 rpm for 60 min at 4 °C to remove cell debris, and filtered with a 45 μm syringe filter (Appleton Woods). For purification of His-tagged protein, the supernatant was loaded onto a Ni-charged chelating sepharose column (GE Healthcare Life Science) pre-equilibrated in 50 mM Tris, pH 8.0, 20 mM imidazole, 0.3 M NaCl, 1 mM TCEP. The beads were washed with extraction buffer and eluted with buffer containing 25 mM Tris, pH

7.5, 0.15 M NaCl, 0.5 M Imidazole, 1 mM TCEP. For purification of GST-tagged protein, the supernatant was incubated with GST-affinity beads (GE Healthcare Life Sciences) at 4 °C for 1 hr. The beads were collected on a gravity flow column, washed with extraction buffer, and the protein was eluted in 50 mM Tris, pH 8.0, 0.3 mM NaCl, 1 mM TCEP, 10 mM reduced Glutathione (Sigma). Finally, HRV 3C protease was dialysed against 20 mM Tris, pH 7.5, 0.15 M NaCl, 1 mM TCEP, 1 mM EDTA, 20% [w/v] Glycerol, whereas Endo F_1 was dialysed against 20 mM Tris, pH 7.5, 0.15 M NaCl, 20% [w/v] Glycerol.

2.5 Protein crystallisation and Crystal optimisation

Typically, protein fractions from SEC that were found to be >95% pure by SDS-PAGE were pooled and concentrated by Amicon-Ultra centrifugal filter unit (Millipore) immediately prior to crystallisation trials.

A pre-crystallization trial (PCT, Hampton) was then performed to ensure that protein was at a suitable concentration for full screen trials. Initial screening of crystallization conditions was performed as sitting drop vapor diffusion crystallisation trials in 96-well Greiner plates consisting of 100 nl protein solution and 100 nl reservoir equilibrated against 95 ul reservoir solution using a Cartesian Technologies dispensing instrument (Walter et al., 2005). Typically, up to 960 different conditions were tested from the commercially available crystallisation screening kits from three companies: Hampton Research, Emerald Biosystems, and Molecular Dimensions. Because crystals obtained from initial crystallisation screening were usually not suitable for data collection,

optimizations of crystallisation conditions were performed by varying the pH, reservoir dilution, additive screening, and ratio of protein to reservoir (Walter et al., 2005). Crystallisation plates were placed in a The Automation Partnership storage vault maintained at 294 K and imaged via a Veeco visualization system (Mayo et al., 2005). Crystallisation conditions for all protein structures described in this thesis are provided in **Table 2.1**.

Table 2.1 Crystallization and cryoprotection conditions for crystal structures presented in this thesis.

Protein	**Protein concentration**	**Space group**	**Crystallisation condition**	**Cryoprotection**[a]
Norrin Crystal form I	5 mg/ml	$P2_12_12_1$	0.1 M sodium acetate, pH 5.0, 5% [w/v] PGA-LM, 30% [w/v] PEG550MME	None[b]
Norrin Se-Met Crystal form I	5 mg/ml	$P2_12_12_1$	0.1 M sodium acetate, pH 5.0, 5% [w/v] PGA-LM, 30% [w/v] PEG550MME	None[b]
Norrin Crystal form II	5 mg/ml	$P2_12_12_1$	0.1 sodium acetate, pH 5.0, 5% [w/v] PGA-LM, 4% [w/v] PEG2000MME, 24% [w/v] PEG550MME	30% [v/v] PEG550MME
Norrin Crystal form III	5 mg/ml	$C121$	0.1M citrate, pH 5.0, 30% [w/v] PEG6000	30% [v/v] glycerol
Fz4-CRD Crystal form I	60 mg/ml	$P2_12_12_1$	1.6 M tri-sodium citrate, pH 6.5	1.8 M tri-sodium citrate
Fz4-CRD Crystal form II	60 mg/ml	$P6_1$	0.1 M HEPES, pH 7.5, 0.1 M NaCl, 1.6 M ammonium sulfate	23% [v/v] sucrose
Norrin/Fz4-$CRD_{methylated}$	10 mg/ml	$P4_322$	0.1 M Bicine, pH 9.0, 10% [w/v] PEG6000	30% [v/v] glycerol
Norrin/Fz4-CRD/SOS[c]	10 mg/ml	$P6_122$	0.1 M Tris, pH 8.0, 0.15 M NaCl, 8% [w/v] PEG8000	20% [v/v] PEG200 plus 10 mM SOS

[a] Crystals were soaked in mother liquor supplemented with cryoprotection reagents.

[b] The crystals of Norrin crystal form I were frozen directly and showed strong ice rings.

[c] protein complex of Norrin/Fz4-CRD was mixed with 10 mM SOS (Toronto Research Chemicals Inc.) prior to crystallization.

2.6. X-ray data collection and processing

Cryoprotection and subsequent X-ray diffraction data collection at low temperature (100K) are essential as they allow a complete data set to be obtained by reducing the problem of radiation damage. Cryoprotectants such as glycerol, ethylene, and low molecular weight polyethylene glycol were used to protect crystals from the damaging effects of ice formation. Alternatively, if there was a cryoprotectant present in the crystallisation condition the crystals could be mounted directly. For crystals grown in high salt conditions, sodium malonate, sodium citrate, and sucrose could be used as cryoprotectants (Bujacz et al., 2010; Holyoak et al., 2003)

After the introduction of a suitable cryoprotectant (**Table 2.1**), the crystals were flash frozen at 100 K in liquid nitrogen. X-ray diffraction data were collected at 100K at Diamond Light Source (Oxfordshire, UK) at the beamlines I03, I04, I04-1, and I24. At the synchrotron, the online data collection strategy program determined the optimum orientation of the crystal at which to start data collection, exposure time for the elimination of radiation damage, and degree of oscillation and crystal rotation for the complete data set collection according to the space group and mosaicity (the measurement of the spread of crystal plane orientations).

For SeMet-labelled protein crystals, a fluorescence scan was carried out to establish the exact wavelength at the absorption edge. Redundant data were collected at the peak wavelength (0.9795 Å) using the data collection strategy as

described above, except that the intensities for Friedel pairs ($I_{h,k,l}$ and $I_{-h,-k,-l}$) were not merged, to enable phasing attempts using single-wavelength anomalous dispersion (SAD) strategies.

X-ray diffraction data processing included several steps: (1) assignment of Miller indices (*hkl*) to each reflection, (2) determination of the point group and unit cell dimensions of the crystal lattice, (3) integration of reflection intensities, (4) merging and scaling of the reflection intensities. Data quality was assessed and high resolution limits were determined according to the following criteria: Completeness (the percentage of unique reflections that are measured in the dataset)**,** Redundancy (the ratio of total measured reflections to unique measured reflections in the dataset), Mean I/σ(I) (the ratio of signal intensity to the error in measurement of the signal intensity ; the criteria used in the thesis is ≥ 1.5), and R_{pim} (the measurement of the consistency of the dataset and represents the deviation between equivalent measurements).

All diffraction data were indexed and integrated using XIA2 (Winter, 2010) coupled with XDS (Kabsch, 2010) or IMOSFLM (Battye et al., 2011), and scaled and merged using Aimless (Evans and Murshudov, 2013). The Program TRUNCATE (French S. and Wilson K., 1978) of the CCP4 software suite (Collaborative Computation Project, Number 4, 1994) was used to calculate structure factor amplitudes from the reflection intensities (Formula 1, **Appendix 2**). A subset of 5% of randomly selected diffraction data were used for calculating R_{free} (Brunger, 1993).

2.7. Structure determination, refinement, and validation

The structure of Norrin crystal form I was solved using highly redundant SAD data collected at the Se absorption edge (0.9795 Å). In order to increase anomalous signal, four data sets, from two crystals were merged using XIA2 (Winter, 2010). Four (16 Se-Met sites) or six (24 Se-Met sites) Norrin molecules per asymmetric unit would give approximately 70% and 56% solvent contents, respectively. HKL2MAP (Sheldrick, 2010) was used to identify the heavy atom (Se) sites by using the resolution range (999-3.7 Å) for calculation and outputted 22 Se sites with anomalous signal. Six Se sites were further removed because of the low occupancies (<0.35). Sixteen Se sites were then fed into PHENIX AUTOSOL (Adams et al., 2002), resulting in an initial phases (figure of merit of 0.29) and an interpretable density modified electron map generated by RESOLVE (Terwilliger, 2003). An initial model generated by BUCCANEER (Cowtan, 2006) was used to solve the high-resolution native structures.

The structure of Fz4-CRD was determined by molecular replacement (MR) in the program PHASER (McCoy, 2007) using mouse Fz8-CRD (PDB ID: 1IJY) as the search model, which was modified by CHAINSAW (Schwarzenbacher et al., 2004) to remove unaligned residues and truncate the side-chains of nonconserved residues to the gamma position based on sequence alignment.

For the determination of Norrin/Fz4-CRD$_{methylated}$, Norrin was used as search model for MR in PHASER (McCoy, 2007) to obtain the initial phases. The additional electron density corresponding to Fz4-CRD was clearly discernible

after density modification with PARROT (Cowtan, 2010). Subsequently, the complex structure was solved by searching for Fz4-CRD with MR in PHASER (McCoy, 2007) after the first solution of Norrin was located.

All other structures were solved by molecular replacement in PHASER (McCoy, 2007) using refined Norrin and Fz4-CRD as search models. All models were completed by manual rebuilding in COOT (Emsley and Cowtan, 2004) and refinement in REFMAC5 (Murshudov et al., 1997) and PHENIX (Adams et al., 2010) with translation libration screw refinement. During the iterative rounds of model building and refinement, a number of variable parameters were monitored to ensure consistency between observed diffraction data and atomic coordinates, including R_{work} (a linear R-value which represents the deviation of the model structure factors from the data structure factors calculated from 95 % of the reflections; formulae 2, **Appendix 2**), R_{free} (calculation similar to R_{work} but from a randomly assigned 5 % of reflections which are excluded from the refinement process; formulae 3, **Appendix 2**), geometrical constraints including bond length and angle, atomic position, non-crystallographic symmetry, and B-factor distribution. In addition, the gap between R_{work} and R_{free} is a quantitative measure of the bias introducted and differences lower than 5% should be targeted during the course of the refinement. All final models were validated with MOLPROBITY (Chen et al., 2010) for structural analysis and assessment of stereochemical quality. The omit electron density map was used to validate specific features in atomic models, for example, presence of the bound ligand of SOS (**Figure 4.2G**). Final refinement and validation statistics for all crystal structures are presented in **Chapter 4**.

2.8. Structure Analysis

Amino acid sequence alignments were constructed using ClustalW (Thompson et al., 1994). Structure superposition was performed within CCP4 using the SSM algorithm (Krissinel and Henrick, 2004). Electrostatic potential calculations were generated using APBS tools (Baker et al., 2001), surface sequence conservation was calculated using CONSURF (Ashkenazy et al., 2010) and interface areas of proteins were analyzed with the PISA web server (Krissinel and Henrick, 2007). High-quality images of the molecular structures were created with PyMOL Molecular Graphics System (Delano Scientific). Schematic figures and other illustrations were prepared using Corel Draw (Corel Corporation).

2.9. Surface plasmon resonance equilibrium binding studies

SPR experiments were performed using a Biacore T200 machine (GE Healthcare Life Sciences) at 25°C in 10mM HEPES, pH 7.5, 0.15 M NaCl, 0.005% [w/v] Tween20. For *in vivo* biotinylation (Penalva and Keene, 2004), Norrin wild-type or mutants in pHL-Avitag3 vector (Aricescu et al., 2006) were co-expressed with BirA-ER in HEK293T. Mutant proteins were secreted at similar levels to the wild-type protein. The mammalian cell secretory pathway uses its stringent quality control mechanism to ensure that secreted proteins are correctly folded (Trombetta and Parodi, 2003).

The biotinylated Norrin variants were immobilized onto the surface of a CM5 sensor chip (GE Healthcare Life Sciences) on which approximately 8500 resonance units (RUs) of streptavidin were coupled via primary amines using the following protocol (O'Callaghan C et al., 1999).

1. Activate the CM5 sensor chip surface with a freshly prepared mixture of 0.4 M EDC (N-(3-dimethylaminopropyl)-N′-ethylcarbodiimide hydrochloride from GE Healthcare Life Sciences) and 0.1 M NHS (N-hydroxysuccinimide from GE Healthcare Life Sciences).
2. Immobilise streptavidin (0.5 mg/ml in 10 mM sodium acetate pH 4.0; Sigma) on the surface of sensor chip to give 8000–9000 RUs.
3. Deactivate sensor chip surface with ethanolamine pH 8.5.
4. Wash with SPR running buffer until baseline is reached.

Fz4-CRD proteins used as analytes were expressed in HEK293T cells to ensure full glycosylation and prepared as described above. Protein concentrations were determined from the absorbance at 280 nm using calculated molar extinction coefficients. The signal from SPR flow cells was corrected by subtraction of a blank and reference signal from a mock coupled flow cell. In all experiments analysed, the experimental trace returned to baseline line after a regeneration step with 0.1 M phosphate pH 3.7, 2M NaCl, 1% [v/v] Tween20. The data were fitted to a 1:1 Langmuir adsorption model ($B = B_{\max}C/(K_d + C)$, where B is the amount of bound analyte and C is the concentration of analyte in the sample) for the calculation of dissociation constant (K_d) values using Biacore Evaluation software (GE Healthcare Life Sciences). Data points correspond to an average from two independent dilution series.

2.10. Small-Angle X-Ray Scattering Experiment

SAXS measurements were performed at the BM29 beamline at the European Synchrotron Radiation Facility (ESRF, Grenoble, France). Scattering data were collected at 20°C, a wavelength of 0.0995 nm and a sample-to-detector distance of 1 m. The 1D scattering profiles were generated and initial data processing was performed at BM29 using the automatic pipeline of AUTOSUB (Pernot et al., 2013). Fz4-CRD was prepared in 10 mM HEPES, pH 7.5, 0.15 M NaCl and measured at concentrations in serial dilutions between 0.16 and 6.08 mg/ml for the deglycosylated state and at concentrations of 0.97 and 1.45 mg/ml for the glycosylated state. Other samples were measured at concentrations of 0.75, 1.26, and 2.43 mg/ml in 10 mM HEPES, pH 7.5, 0.7 M NaCl, 0.5% CHAPS [w/v] for Norrin and at concentrations of 0.53, 0.78, 1.02, and 2.14 mg/ml in 10 mM HEPES, 0.5 M NaCl for Norrin/Fz4-CRD complex. Ten consecutive frames of 10 sec each were measured for each sample, with buffer samples measured in between. The radiation damage of each frame was monitored and any affected frames were excluded from further processing. The data processing including buffer subtraction, image averaging, and curve merging was performed by using PRIMUS (Petoukhov et al., 2012). Merged curves were generated using the low angle part of the lowest concentration curve and the high angle part of the highest concentration curve. The radius of gyration (R_g) was determined from the Guinier plot using AutoRg (Petoukhov et al., 2012). The maximum particle dimension (D_{max}), distance distribution function ($P(r)$) and Porod volume of the hydrated particle were evaluated using GNOM (Svergun, 1992). The molecular

weight of samples was calculated by comparison with the reference bovine serum albumin (BSA) and obtained by dividing the Porod Volume by 1.66 (Rambo and Tainer, 2011). Theoretical X-ray scattering patterns from structural models were calculated and fitted into experimental X-ray scattering curves using FoXS (Schneidman-Duhovny et al., 2010). All-atom modeling of flexible glycans and missing loops in combination with energy minimization were performed using AllosMod-FoXS (Guttman et al., 2013; Weinkam et al., 2012)

2.11. Size-exclusion chromatography coupled to multi-angle light scattering analysis

SEC-MALS experiments were performed by using SEC on an analytical Superdex S200 10/300 GL column (GE Healthcare Life Sciences) connected to online static light-scattering (DAWN HELEOS II, Wyatt Technology), differential refractive index (Optilab rEX, Wyatt Technology) and Agilent 1200 UV (Agilent Technologies) detectors. Purified sample (50 μM Fz-CRD proteins or 25 μM Norrin/Fz4-CRD complex) was injected into a column equilibrated in 10 mM HEPES, pH 7.5 and 0.15 M NaCl. Data were analyzed using the ASTRA software package (Wyatt Technology).

2.12. Luciferase reporter assay

The stable HEK293STF cell lines (Xu et al., 2004)a gift from Jeremy Nathans) carrying the Super Top Flash firefly luciferase reporter system with tandems LEF/TCF binding sites for β-catenin before luciferase reporter gene were split into 96-well plates and transfected 24 hr later with 200 ng DNA per well using

Lipofectamine 2000 (Invitrogen) according to the manufacturer's protocol. For assessment of interface mutants used in SPR experiments, the DNA mix contained 80 ng Norrin plasmid, 40 ng each of Fz4 and Lrp6 plasmids, 20 ng each of Tspan-12 and constitutive *Renilla* luciferase plasmid (pRL-TK from Promega). The firefly and *Renilla* luciferase activities were measured 48 hr later with Dual-Glo luciferase reporter assay system (Promega) using an Ascent Lunimoskan luminometer (Labsystems). For evaluation of recombinant Norrin protein and SOS inhibition, the DNA mix (80 ng pLEXm plasmid, 40 ng each of Fz4 and Lrp6 plasmids, 20 ng each of Tspan-12 plasmid, and constitutive *Renilla* luciferase plasmid) was used for transfection. Cells were stimulated 6 hr post transfection with 9 μg/ml Norrin, 9 μg/ml Norrin preincubated with 2 mM SOS for 15 min, or control 9 μg/ml Fetal Calf Serum (FCS). The Dual-Glo luciferase reporter assays were performed 48 hr later. The firefly luciferase activity was normalized to *Renilla* luciferase activity (relative light unit, RLU). Luciferase reporter assays were performed three times in triplicate.

2.13. Heparin Affinity Chromatography

Protein sample was freshly purified by SEC and then adjusted in 100 mM HEPES, pH 7.5, 0.25 M NaCl. Purified protein (0.5 mg/ml, 0.5 ml) was loaded onto a 1 ml HiTrap heparin HP column (GE Healthcare Life Sciences) equilibrated in 20 mM Tris, pH 7.5, 0.15 M NaCl and eluted with a linear NaCl gradient to 20 mM Tris, pH 7.5, 2M NaCl, 5% [w/v] glycerol over fifteen column volumes. Elution was monitored by absorption at 280 nm.

Chapter 3

Efficient mammalian expression strategies for production of Norrin pathway components

3.1 Summary

Our preliminary expression trials in mammalian cells reveal only marginal amounts of Norrin and Frizzled4 cysteine-rich domain (Fz4-CRD) could be detected in conditioned media, in agreement with previous protein expression experiments in mammalian and insect cells (Ke et al., 2013; Ohlmann et al., 2010; Perez-Vilar and Hill, 1997; Shastry and Trese, 2003). Thus, there are technical difficulties in obtaining sufficient quantities of recombinant proteins for advanced biochemical and structural studies. Here, I developed several methodologies (**Figure 3.1**) including signal peptide screening, N- and C-terminal fusion as well as the supplement of histone deacetylase inhibitor (iHDAC) to solve the expression problem in human embryonic kidney (HEK) 293 cells. N-terminally small ubiquitin-like modifier (SUMO) tagged Norrin in combination with the optimum signal peptide and addition of iHDAC gave a significant boost in protein secretion levels. For Fz4-CRD having optimized boundaries along with C-terminal yellow/green fluorescence protein fusion and treatment with iHDAC yielded sufficient protein sample. The successful expression strategy used for Fz4-CRD was also applied to other Fz-CRDs to produce sufficient recombinant proteins for functional studies described in **Chapter 4**. Finally, I used these efficient protein expression strategies to produce recombinant proteins including Norrin, Fz4-CRD, and binary complex of Norrin/Fz4-CRD as well as ternary complex of Norrin/Fz4-CRD/Lrp6 for structural and functional studies presented in **Chapter 4**.

3.2 Introduction

Wnt signalling regulates multiple biological and pathological processes including angiogenesis, inflammation, and tumorigenesis (Anastas and Moon, 2013; Clevers and Nusse, 2012; Logan and Nusse, 2004). Norrin (Norrie disease protein, NDP) is a cystine-knot like growth factor, distinct from the morphogen Wnt, however, Norrin interacts with Wnt receptor Frizzled 4 (Fz4) and co-receptor low density lipoprotein receptor related protein 5/6 (Lrp5/6) plus the auxiliary four-pass transmembrane protein Tetraspanin-12 (Tspan-12) to active the canonical Wnt/β-catenin pathway (Junge et al., 2009; Perez-Vilar and Hill, 1997; Xu et al., 2004; Ye et al., 2009). In function, the Norrin mediated pathway regulates vascularization in retina, brain, and cochlea; unsurprisingly, mutations lead to inherited retinal diseases, which are usually accompanied by mental retardation and hearing loss in patients (Nikopoulos et al., 2010b; Ohlmann and Tamm, 2012; Ye et al., 2010). In molecular mechanism, unlike Wnts which have promiscuous interactions with Fz receptors, Norrin specifically binds to Fz4-CRD but not the 14 other CRDs of Fz and secreted Frizzled-related protein (sFRP) family members (Angers and Moon, 2009; Smallwood et al., 2007). Structural analyses of Norrin mediated signalling are very limited due to a lack of available methods to obtain recombinant proteins.

Norrin-deficient mice have a severely impaired intraretinal vascular architecture (Rehm et al., 2002), however, this pathologic phenotype could be rescued by using a transgenic approach to express ectopic Norrin (Ohlmann et al., 2005). Overexpression of Norrin in wild-type mice could also enhance vascular

regrowth into vaso-obliterated retinal areas to build intraretinal capillaries during oxygen-induced retinopathy (Ohlmann et al., 2010). Norrin mediated signalling is also required to maintain blood-retina barrier (BRB) integrity (Paes et al., 2011; Wang et al., 2012). Deficient BRB and retinal vascularization are highly related to a variety of ophthalmic disorders, including age-related macular degeneration and diabetic retinopathy (Ye et al., 2010; Zhou et al., 2014). In combination, these observations suggest that recombinant Norrin has therapeutic potential for treatment of genetic retinal disorders and vitreoretinal diseases. Therefore, there is an eager demand for development of a reliable and efficient expression system of production for biologically active Norrin and its associated proteins.

We note that during the preparation of this thesis Ke *et al*., independently reported a refolding method to produce active recombinant Norrin fused with a N-terminal Maltose Binding Protein (MBP-Norrin) from *E coli* inclusion bodies and published the crystal structure of MBP-Norrin (Ke et al., 2013), however, MBP-Norrin only retains half of the signalling activity of untagged Norrin.

3.3 Aims

The aim of the studies presented in **Chapter 3** is to develop new strategies for protein production of Norrin and Fz4-CRD and to set up a protein expression and purification system for the isolation of protein complexes.

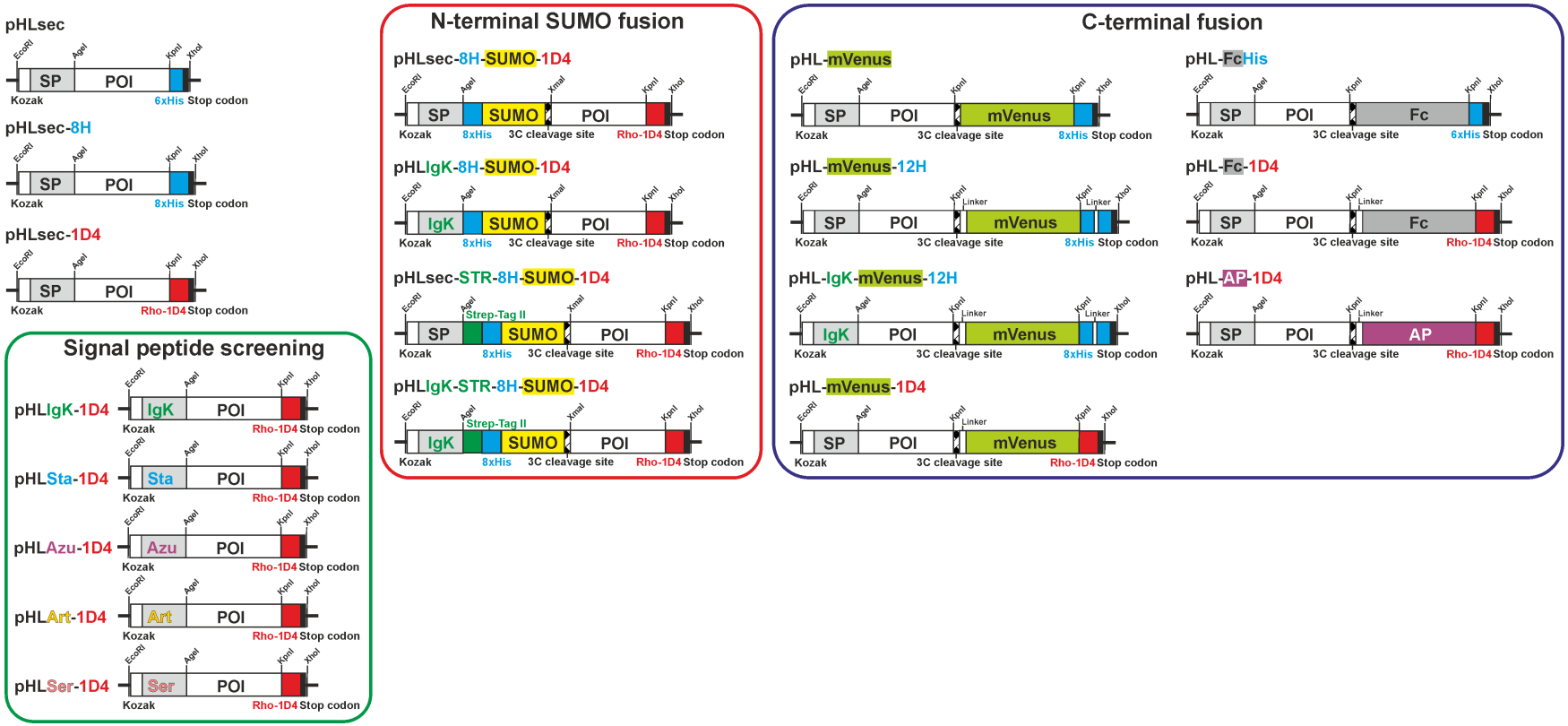


Figure 3.1. Overview of expression vectors presented in this thesis.
All expression constructs reported here are derived from the pHLsec vector backbone. In order to improve the secreted protein expression level, three classes of vectors were generated. Class I vectors were used for screening the optimum signal peptide for secretion (including IgK, murine Igκ-chain; Sta, human stanniocalcin-1; Azu, human azurocidin; Art, artefact engineered signal peptide; Ser, rat serum albumin). Class II vectors were N-terminal SUMO fusion derivatives. Class III vectors were a series of derivatives containing different C-terminal fusions (including mVenus, yellow/green fluorescence protein; Fc, human IgGγ1 FC region; AP, human alkaline phosphatase). Detailed information is presented in **Appendix 1**

3.4 Mammalian cell expression system

Mammalian cell expression is particularly suitable for the production of extracellular or secreted proteins of mammalian origin, due to the requirement for posttranslational modifications and chaperones in protein synthesis (Chang et al., 2007). pHLsec (**Figure 3.1**; **Appendix 1**) is a high-copy number plasmid containing the ampicillin resistance gene, an optimized Kozak sequence, and secretion signal sequences, making it an ideal vector for protein expression in mammalian cells (Aricescu et al., 2006). I hence used pHLsec as a backbone and developed derivatives for enhancement of protein production in mammalian cells (**Figure 3.1**; **Appendix 1**).

3.5 Pull-down assay to confirm Norrin forms complex with Fz4-CRD

The constructs of Norrin and Fz4-CRD were designed based on the prediction of domain boundaries and disordered regions along with analysis of homologous structures (**Figure 3.2** and **Figure 3.3**) as described in **Chapter 2 Materials and Methods** (2.1.2 Construct design, cloning, and mutagenesis). Human Fz4-CRD (residues 40-160, including ten conserved cysteine residues) was cloned into the pHLsec vector (Aricescu et al., 2006) in frame with a C-terminal hexahistidine tag, which is referred to here after as hFz4-CRD-His. These conserved cysteine residues have been demonstrated to stabilize the protein fold of CRD (Dann et al., 2001; Stiegler et al., 2009; Zhang et al., 2011).

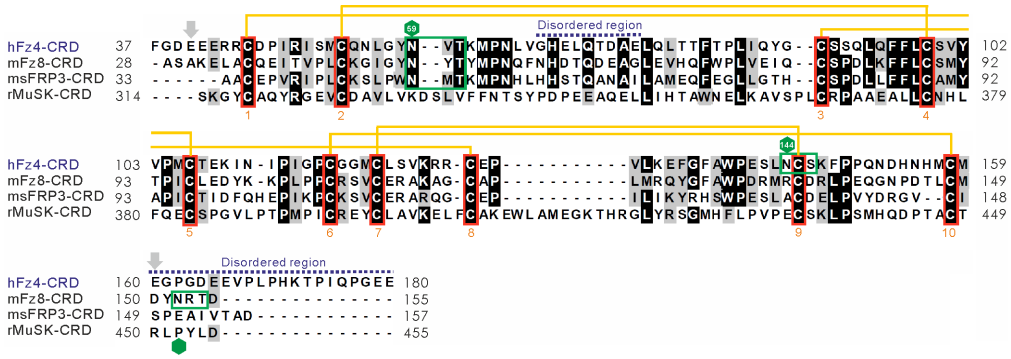


Figure 3.2. Multiple sequence alignment of the cysteine-rich domain (CRD), including human Fz4-CRD, mouse Fz8-CRD (PBD code: 1IJY), mouse sFRP3-CRD (PBD code: 1IJX), and rat Muscle skeletal tyrosine protein kinase receptor (MuSK) (PBD code: 3HKL). Identical and similar sequences are shaded in black and grey, respectively. Dashes indicate the sequence gaps introduced to optimize the sequence alignment. Ten conserved cysteine residues forming five disulphide bridges, marked in yellow lines, are highlighted by red boxes and labelled as numerals below the alignment. The boundaries of Fz4-CRD for the initial pull-down assay (**Figure 3.5**) are marked by grey arrows. The N-glycosylation sites are marked by green hexagons and boxes. The disordered regions of hFz4-CRD predicted by RONN (http://www.strubi.ox.ac.uk/RONN/) are indicated by blue dashed lines.

Human Norrin has limited homology to the cystine-knot growth factors, including the transforming growth factor (TGF-β) superfamily, based on the conserved spacing of cysteine residues in the sequence and is presumed to share a similar protein fold to cystine-knot growth factors, although sharing less than 15% sequence identity (**Figure 3.3**). In addition, four cysteine residues, which are absent in the TGF-β superfamily, are highly conserved across vertebrate Norrins (**Figure 3.4**) and these have been reported to be highly relevant in Norrie Disease (Meindl et al., 1992; Smallwood et al., 2007; Ye et al., 2010). Human Norrin (residues 25-133; mature form after cleavage of signal peptide) was hence engineered into the pHLsec-1D4 vector (**Figure 3.1**) with a Rho-1D4 tag in the C-terminus, referred to here after as hNorrin-1D4.

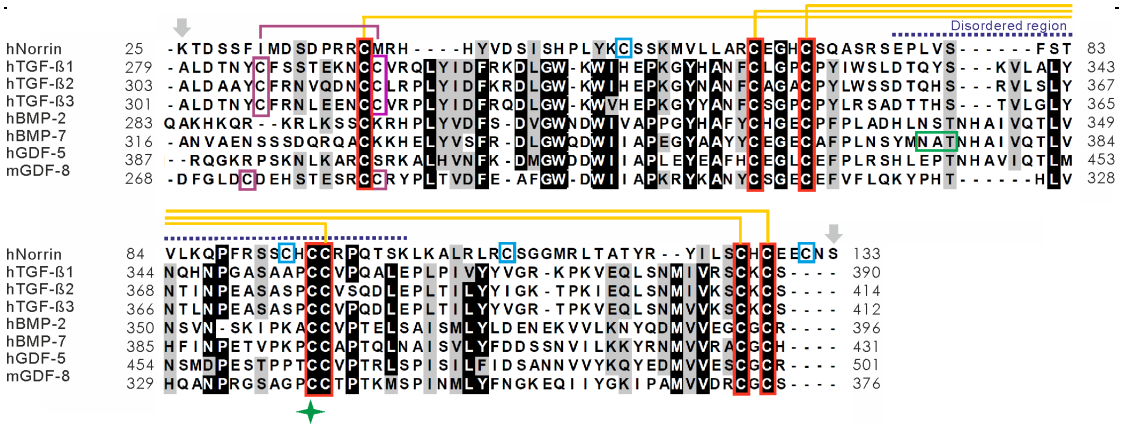


Figure 3.3. Sequence alignment of human Norrin with TGF-β superfamily proteins. Conserved cysteine residues across TGF-β superfamily members are marked in red boxes. The intramolecular disulphide bonds are drawn in yellow lines and the cysteine residues used for the interchain disulphide bridge are marked by a green cross. Two additional conserved cysteine residues found in some TGF-β proteins are boxed and lined in purple. Cysteine residues found in Norrin but absent from the TGF-β superfamily are coloured cyan boxes. The boundaries of Norrin for the initial pull-down assay (**Figure 3.5**) are marked by grey arrows. The N-linked glycosylation sites are marked by green boxes and the disordered regions predicted by RONN (http://www.strubi.ox.ac.uk/RONN/) are denoted by blue dashed lines. Identical and similar sequences are shaded in black and gray, respectively. Dashes indicate the sequence gaps introduced to optimize the sequence alignment.

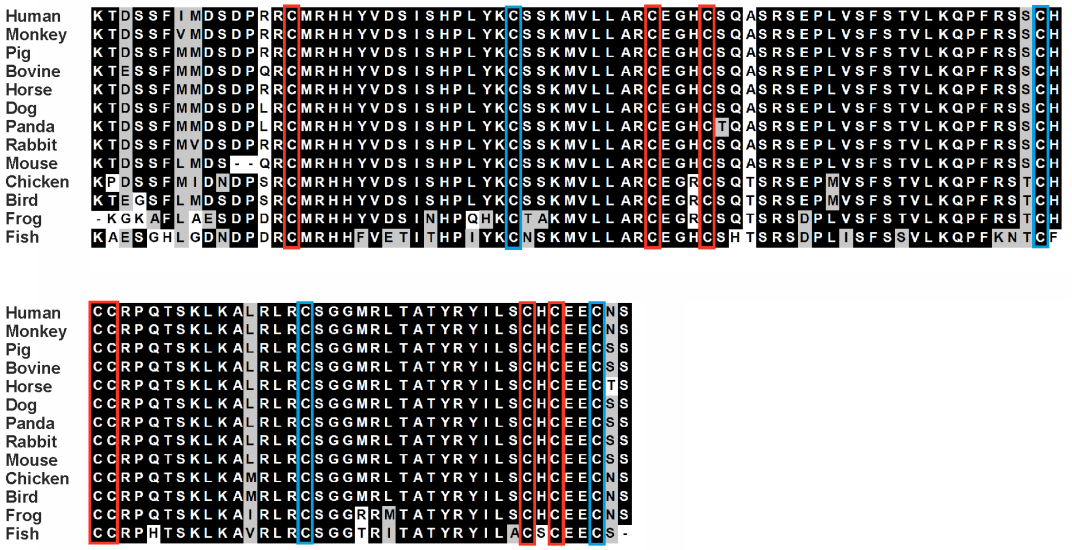


Figure 3.4. Multiple sequence alignment of Norrin proteins in vertebrates. Conserved cysteine residues in TGF-β superfamily are boxed in red. Norrin dependent conserved cysteine residues are marked in cyan boxes. All sequences presented here have the N-terminal signal peptides omitted. Identical and similar sequences are shaded in black and grey, respectively. Dashes indicate the sequence gaps introduced to optimize the sequence alignment.

Small-scale expression trials in HEK293T cells revealed that Norrin and Fz4-CRD are produced in secreted soluble form (**Figure 3.5**; bottom panel). Protein levels of Norrin and Fz4-CRD appear to be improved by co-expression in a 1:1 mix of the two constructs of hNorrin-1D4 and hFz4-CRD-His (**Figure 3.5**; bottom panel). Notably, the expression levels of Norrin and Fz4-CRD are extremely low by comparison with other proteins studied in the Jones' group.

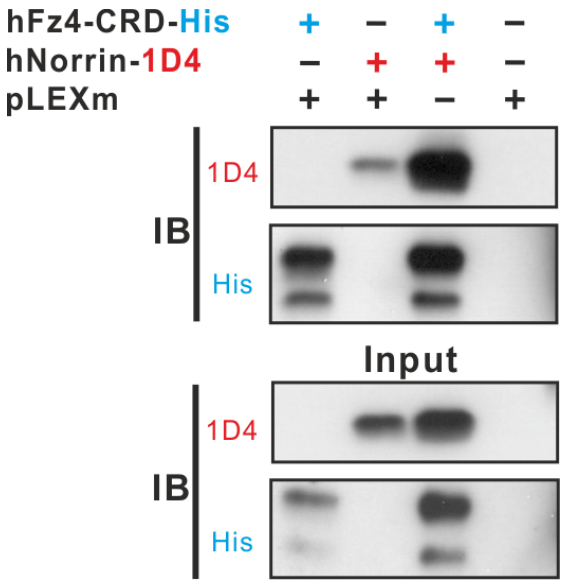


Figure 3.5. Norrin forms complex with Fz4-CRD in solution.
Pull-down assay presents the binding of Norrin to Fz4-CRD. HEK293T cells were co-transfected with human Fz4-CRD (residues 40-160) with C-terminal His tag (hFz4-CRD-His) and pLEXm (empty vector), human Norrin (residues 25-133) with C-terminal Rho-1D4 tag (hNorrin-1D4) and pLEXm, hFz4-CRD-His and hNorrin-1D4, or pLEXm. The proteins from the conditioned medium were pulled down by IMAC using Co^{2+} beads. After thorough washes, the precipitates and input samples were immunoblotted (IB) separately with the anti-1D4 and anti-His antibodies. (More details about experiment protocol can be found in **Chapter 2.2.2** Pull-down assay)

To address whether Norrin forms a stable complex with Fz4-CRD *in vitro*, a pull-down assay was performed (**Figure 3.5**). HEK-293T cells were co-transfected with empty vector and hNorrin-1D4, hFz4-CRD-His, or hNorrin-1D4 and hFz4-CRD-His. Immobilized metal affinity chromatography (IMAC) was used to pull-down His-taggged Fz4-CRD from the conditioned media. Western blot analysis using antibody against the Rho-1D4 tag confirmed that Rho-1D4 tagged Norrin was successfully complexed with the His-tagged Fz4-CRD (**Figure 3.5**). As a negative control, media from cells overexpressing only Rho-1D4 tagged Norrin were used to verify the binding.

3.6 Improvement of Norrin secretion levels

As a result of the technical difficulties in obtaining sufficient quantities of the proteins, the structural properties of uncomplexed Norrin and Fz4-CRD as well as the complex of Norrin/Fz4-CRD remain poorly defined, although Norrin mediated signalling and disease-associated mutations are increasingly understood at the cellular and clinical level (Ohlmann and Tamm, 2012; Xu et al., 2012; Yang et al., 2012). Furthermore, Norrin may be a potent factor to induce angiogenesis in microvascular endothelia cells and suppress the defects that result from oxygen-induced retinal damage during Retinopathy Of Prematurity (ROP) (Ohlmann et al., 2010). Hence the development of a system to produce sufficient quantity and quality of protein is urgently needed. I therefore investigated traditional and novel methodologies.

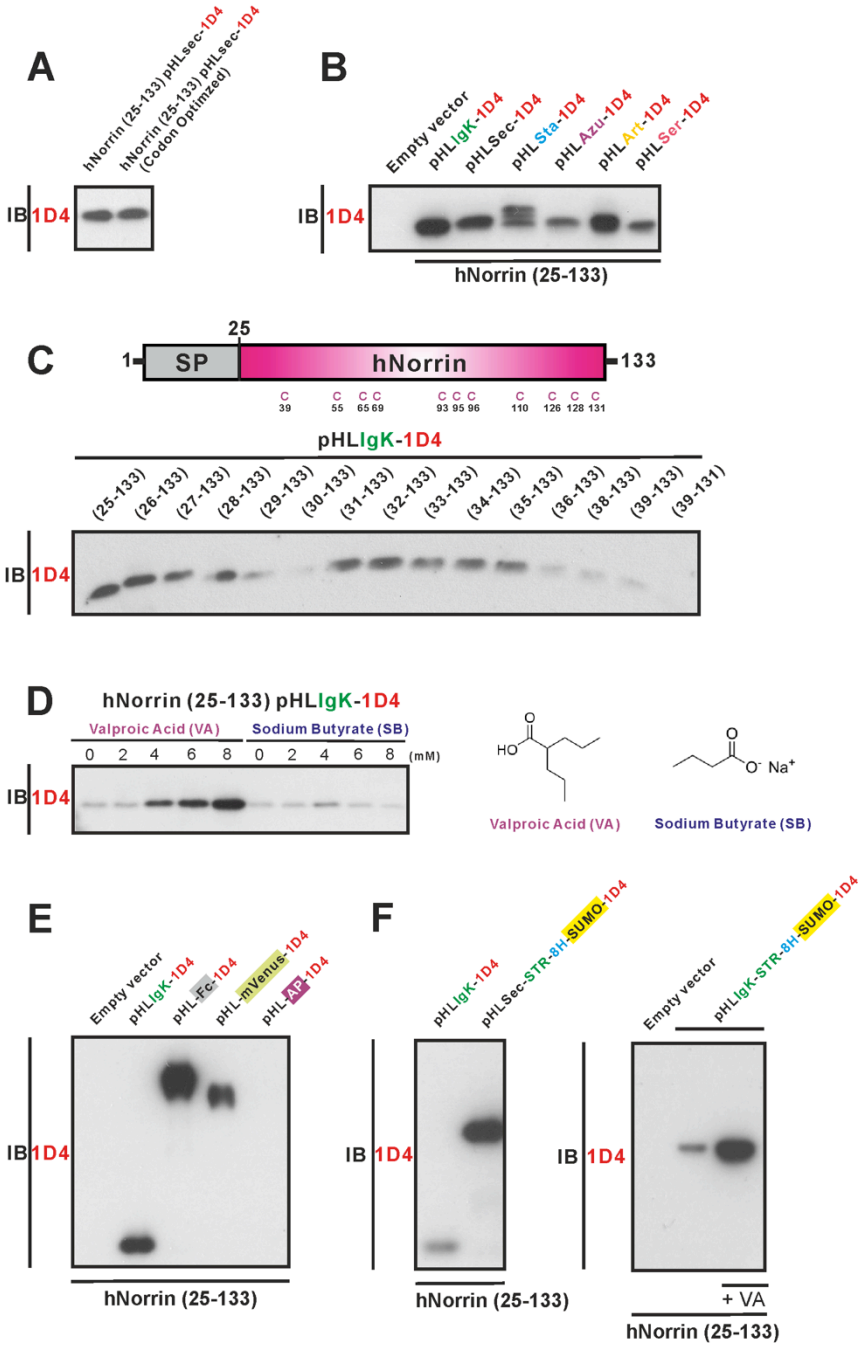


Figure 3.6. Expression trials for human Norrin constructs. Conditioned media from transfected HEK293T cells, except for data in (**D**) using HEK293S cells, were immunoblotted (IB) following SDS-PAGE under reduced conditions. **(A)** Comparison of secretion levels between initial and codon optimized constructs. **(B)** The optimization of signal peptide for enhancement of Norrin secretion. **(C)** Modification of the N- and C-terminal boundaries of Norrin. The conserved cysteine residues forming disulphide bridges are labelled. **(D)** Histone deacetylase inhibitors including valproic acid and sodium butyrate were used to increase the secretion of Norrin. **(E)** C-terminally Fc tagged Norrin has remarkably enhanced secreted expression. **(F)** N-terminal SUMO fusion significantly improves Norrin secreted expression. The expression level of SUMO tagged Norrin was further boosted for HEK293T cells treated with valproic acid post transfection.

3.6.1 The optimization of codon usage and domain boundary

A codon optimized construct of human Norrin did not show improvement in protein secretion (**Figure 3.6A**). Norrin from *Xenopus* and *Zebrafish* were selected for expression trials but did not give better results than the human form (data not shown). Extensive modifications in protein boundaries also failed to improve the secretion of Norrin (**Figure 3.6C**), although this strategy is successfully applied in many cases in the Jones' group. Notably, the 11 conserved cysteine residues were retained in all constructs.

3.6.2 A specific signal peptide improves the secretion of Norrin

A variety of pHLsec-1D4 vector variants were generated to replace the original signal peptide (SP) of chicken receptor protein tyrosine phosphatase sigma with the SP of murine Igκ-chain (Coloma et al., 1992), human stanniocalcin-1 (Liu et al., 2009), human azurocidin (Olczak and Olczak, 2006), artifact engineered (Barash et al., 2002), or rat serum albumin (Shi et al., 2011; Zou and Sun, 2004). Information on these vectors is summarized in **Appendix 1**. Western blots showed that the SP of the murine Igκ-chain gives the greatest improvement in Norrin secretion (**Figure 3.6B**).

3.6.3 The histone deacetylase inhibitor increases the secretion of Norrin

Histone deacetylase inhibitors (iHDACs) have been demonstrated to increase transient gene expression in mammalian cells by suppressing the negative epigenetic effects that for the transfected DNA were associated with deacetylated

histones and silenced the gene expression (Backliwal et al., 2008; Monneret, 2005; Riu et al., 2007). Two iHDACs, valproic acid and sodium butyrate, were used (**Figure 3.6D**). Surprisingly, the addition of valproic acid at the optimum concentration of 8 mM in HEK293S cells could remarkably boost the secretion levels of Norrin, in contrast to sodium butyrate (**Figure 3.6D**). This protocol may provide a generally useful approach for those difficult to express proteins in mammalian cells for which large quantities are required for X-ray crystallography experiments. One recent successful case in STRUBI (University of Oxford) is human type-A γ-aminobutyric acid receptor (Miller and Aricescu, 2014).

3.6.4 Enhanced Norrin secretion using C-terminal fusion

I was inspired by the work of Qiang Xu (Johns Hopkins University School of Medicine), they reported that alkaline phosphatase (AP) fused to the C-terminus of mouse Norrin resulted in an enhancement in protein secretion, compared to wild-type (Xu et al., 2004). C-terminally Rho-1D4 tagged proteins including human IgGγ1 FC region (Fc), monomeric yellow/green fluorescence protein (mVenus) and AP were created to test this strategy (**Figure 3.1**; **Appendix 1)**. As shown in **Figure 3.6E**, only the Fc tag can provide a significant enhancement in the production of Norrin in our mammalian expression system, while mVenus and AP fusions appeared to decrease the secretion of Norrin into the conditioned media.

3.6.5 Enhanced Norrin secretion using N-terminal fusion

Peroutka *et al*, report that an engineered small ubiquitin-like modifier (SUMO) fusion with double mutations of R64T and R71E was successfully used to improve recombinant protein expression in mammalian cells (Peroutka et al., 2008). The mutations resulted in the engineered SUMO fusion being resistant to cleavage by endogenous deSUMOylases within the cell. The following two vectors both containing signal peptide from pHLsec and a C-terminal 1D4 tag were created (**Figure 3.1**; **Appendix 1)**: pHLsec-8H-SUMO-1D4, having a N-terminal octahistidine tag followed by an engineered SUMO and 3C protease cleavage site and pHLsec-STR-8H-SUMO-1D4, having an additional Strep-Tag II prior to an octahistidine tag of pHLsec-8H-SUMO-1D4. As shown in **Figure 3.6F**, SUMO tagged Norrins revealed remarkable boosts in the secretion of Norrin, better than Fc tagged Norrin, as judged by comparing the western blot intensities of Rho-1D4 tagged Norrin (**Figure 3.6E**). In addition, the SUMO fusion expression strategy was successfully applied in several cases in the Jones' group. Hence, the SUMO fusion strategy may be a valuable tool for structural studies involving eukaryotic proteins that are difficult to express. SUMO fusion in combination with addition of iHDAC significantly boosts the secreted expression level of Norrin (**Figure 3.6F**). In addition, the SUMO tagged Norrin can be used to co-express with Fz4-CRD for protein complex studies without concern that SUMO impairs the binding to FZD4-CRD, because previous studies have used AP fusion proteins plus one or three Myc epitopes at the N-terminus or C-terminus of Norrin to assess Norrin binding to Fz4-CRD and SUMO (94 amino acids in length) is a small protein (Smallwood et al., 2007; Xu et al., 2004).

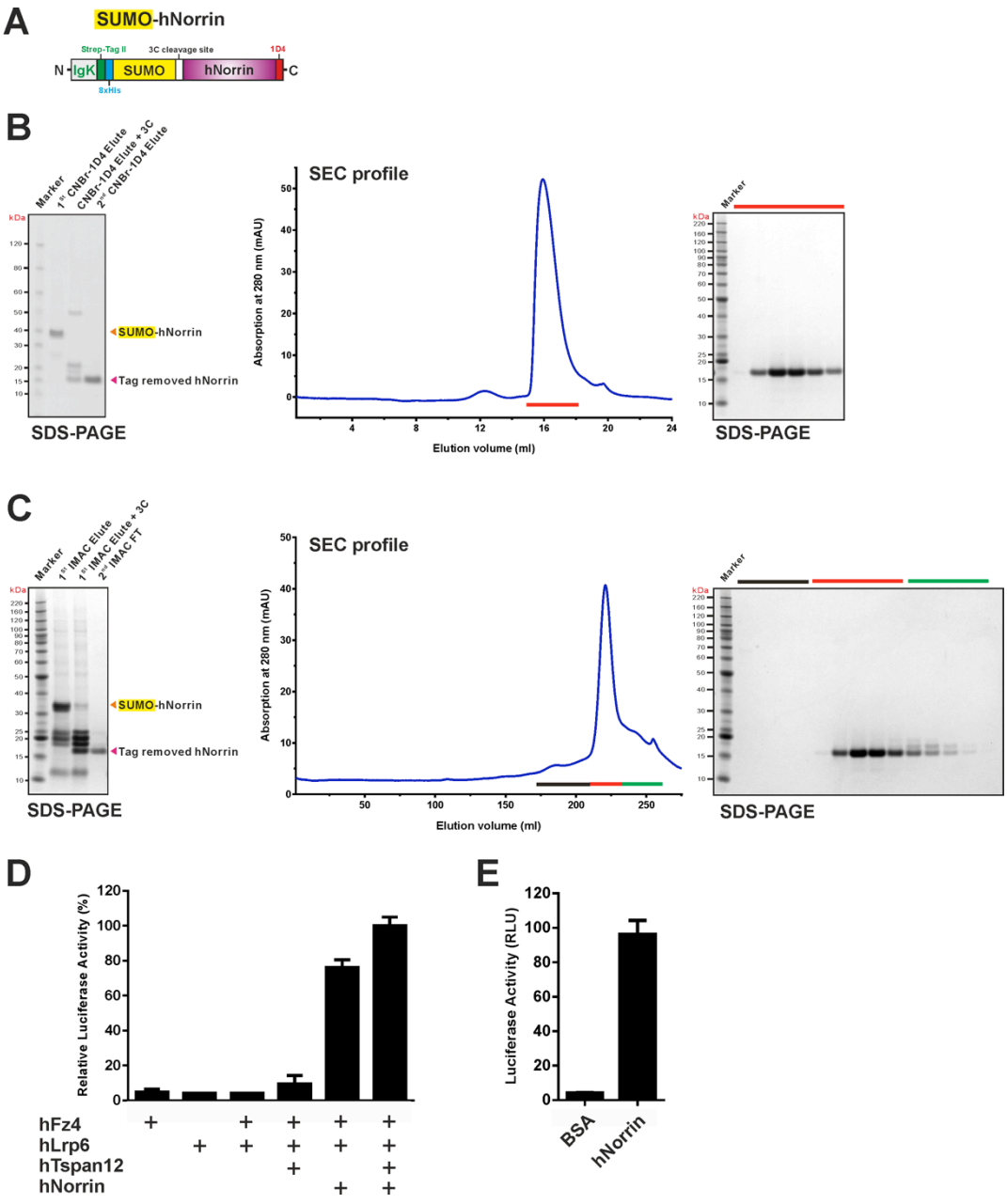


Figure 3.7. Protein purification of biological active recombinant human Norrin. (A) Schematic diagrams of the expression construct of Norrin. **(B)** SDS-PAGE analysis of protein purification procedure by CNBr-1D4 beads. SEC elution profile (left panel) and SDS-PAGE under reducing condition (right panel) with fraction analysis. **(C)** SDS-PAGE analysis of protein purification procedure of SUMO-tagged Norrin by two steps of IMAC. SEC elution profile (left panel) and SDS-PAGE under reducing condition (right panel) with fraction analysis. **(D)** Luciferase reporter assays with HEK293STF cells transfected with the indicated plasmids to set up a reliable system for measurement of signalling activity. **(E)** Purified recombinant Norrin (9 µg/ml) activates the canonical Wnt/β-catenin pathway. HEK293STF cells transfected with human receptors (Fz4, Lrp6, and Tspan-12) plus control *Renilla* luciferase plasmid and stimulated with recombinant Norrin. RLU: relative light unit. Error bars indicate standard deviations (n = 3).

3.7 Protein production of biologically active Norrin

The construct of human Norrin in pHLIgk-STR-8H-SUMO-1D4 vector was transiently transfected in HEK293T cells for large-scale protein expression, because there is no predicted N-linked glycosylation site within the sequence and HEK293T cells typically provide higher protein expression levels than HEK293S cells (Zhao et al., 2011). Because SUMO-tagged Norrin fusion protein carried N-terminal His-tag and C-terminal Rho-1D4 tag (**Figure 3.7A**), either IMAC or CNBr-activated beads conjugated with Rho-1D4 antibody (CNBr-1D4) could be used for purification.

As shown in **Figure 3.7B**, SUMO-tagged Norrin was isolated from conditioned media produced in HEK293T cells with treatment of valproic acid (the optimum concentration is 4 mM in HEK293T cells) by CNBr-1D4. The eluted SUMO-tagged Norrin was digested with home made GST-tagged HRV 3C protease (**Figure 3.8A**) to remove SUMO fusion. The untagged Norrin was isolated by CNBr-1D4 and subjected to size-exclusion chromatography (SEC) using Superdex200 in 10 mM HEPES, pH 7.5, 0.7 M NaCl, 0.5 %[w/v] CHAPS. The final protein yield of Norrin was 0.2 mg from one liter of conditioned media. Norrin was purified in the monodisperse state (**Figure 3.7B**). Notably, after removing SUMO fusion, Norrin was stabilized in the presence of detergent CHAPS, similar to the protein preparation of Wnts (Willert et al., 2003).

Alternatively, high purity recombinant Norrin (**Figure 3.7C**) could be isolated by using two steps of IMAC in combination with treatment by home made His-

tagged HRV 3C protease (**Figure 3.8B**), although a huge amount of contaminant was found in the first IMAC eluted sample. About 0.5 mg Norrin could be purified from one liter of conditioned media. In addition, homogenous Norrin could also be purified by SEC (Superdex200) in 10 mM acetate buffer, pH 4.0, 0.5 M NaCl, 0.5 %[w/v] CHAPS. The recombinant untagged Norrin actually is more stable in acidic buffer than in neutral conditions.

Both purification flowcharts were successfully applied in the purification of recombinant Norrin. However, two steps of IMAC was adopted as a standard purification procedure for two reasons: IMAC gives a 2.5 fold increase in protein yield compared to CNBr-1D4 and IMAC is a more cost-efficient method compared to CNBr-1D4 because of the price of antibody and the limited regeneration cycles of CNBr-1D4 beads.

To assess the biological activity of recombinant Norrin, the stable HEK293STF cells (Xu et al., 2004) carrying the Super Top Flash firefly luciferase reporter and transiently transfected with *Renilla* luciferase plasmid was used for the cell-based luciferase reporter assay. As shown in **Figure 3.7D**, a reliable and sensitive assay system was set up to achieve the best signal to noise ratio. On the basis of previous cellular assays, the maximum activity of Norrin mediated canonical Wnt/β-catenin signalling requires all receptors including Fz4, Lrp5/6, and Tspan-12 on cell surface for response to Norrin binding (Junge et al., 2009). As shown in **Figure 3.7E**, a high level of luciferase activity was detected for

HEK293STF cells transfected with human receptors of Fz4, Lrp6, and Tspan-12 and stimulated with the purified recombinant Norrin.

In total, a novel system was created for expression and purification of biologically active recombinant Norrin. The recombinant protein would not only be used for structural and functional studies described in **Chapter 4** but also has therapeutic potential for treatment of genetic retinal disorders and vitreoretinal diseases discussed in **Chapter 5**.

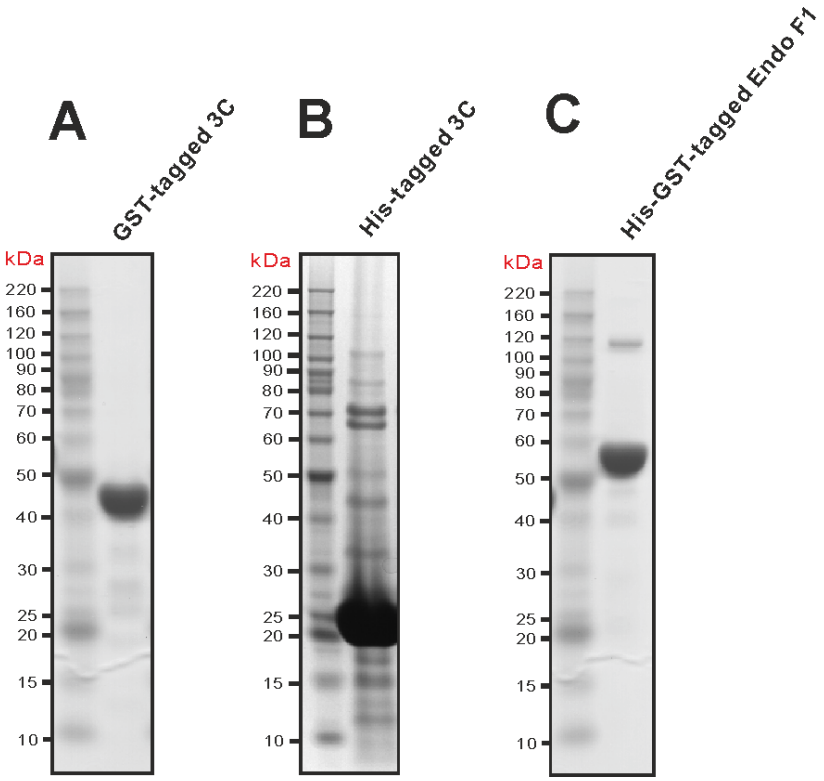


Figure 3.8. Home made HRV 3C protease and Endo-F_1. (A) The N-terminally GST-tagged HRV 3C protease. **(B)** The N-terminally His-tagged HRV 3C protease. **(C)** The N-terminally His- tandem GST-tagged Endo-F_1.

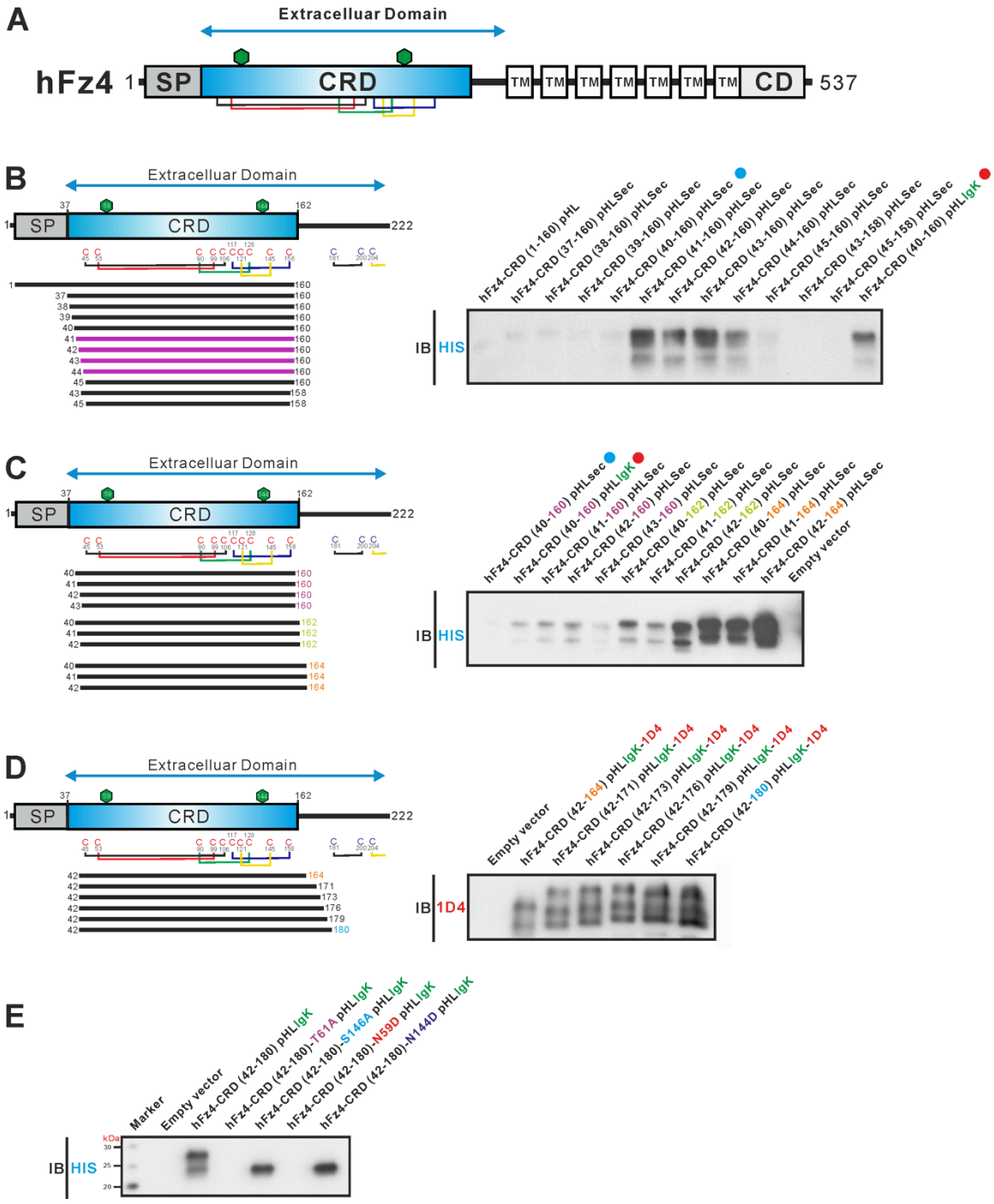


Figure 3.9. Expression trials for human Fz4-CRD constructs.
(A) Schematic diagram of human Fz4. SP, signal peptide; CRD, cysteine-rich domain; TM, transmembrane domain; CD, cytoplasmic domain. **(B)-(D)** Schematic diagrams of the ectodomain of hFz4 (left panel) and western blots (right panel) are shown to illustrate the secreted expression levels of a series of constructs. Ten conserved cysteine residues forming disulphide bridges are drawn in coloured lines and two N-glycosylation sites are highlighted by green hexagons. **(B)** Modifications of the N-terminal boundaries of hFz4-CRD. **(C)** and **(D)** Optimization of the C-terminal boundaries of hFz4-CRD. **(E)** The mutagenesis studies and expression trials demonstrated that the first N-glycosylation site of hFz4 is critical for its secretion.

3.8 Improvement of Fz4-CRD secretion levels

As shown in **Figure 3.5**, the expression level of human Fz4-CRD was very low in contrast to mouse Fz8-CRD (data not shown). My preliminary purification trials revealed that less than 0.04 mg of Fz4-CRD was purified from one liter of conditioned media. Obtaining sufficient quantities of the Fz4-CRD for structural and functional studies was hence proving to be challenging. Here, I optimized the domain boundary and used the fusion strategy for improvement of the secretion level of human Fz4-CRD in mammalian cells.

3.8.1 The optimization of the domain boundary

Exhaustive attempts at construct engineering by modification of the N- and C-terminal boundaries of the extracellular domain (**Figure 3.9A**) were targeted for cloning and expression trials to improve the secretion of Fz4-CRD. Notably, the 10 conserved cysteine residues were retained. As shown in **Figure 3.9B**, variation of the starting residue (from 41 to 44), separately, provided much better secretion expression levels than the initial construct (residues 40-160). Western blots indicated that the signal peptide of the murine Igκ-chain further improved the secretion of Fz4-CRD (**Figure 3.9B**) using these same boundaries. The screening of various C-terminal boundaries revealed remarkable boosts in the secretion levels of Fz4-CRD (**Figure 3.9C**) and finally a construct (residues 42-180; further extension at the C-terminus is not possible, because extending beyond residue 180 will include a extra cysteine residue) is the best domain boundary for expression (**Figure 3.9D**). Because mouse Fz8-CRD and sFRP3-CRD were previously crystallized as forms with mutations in N-linked

glycosylation sites (Dann et al., 2001), I then tested this strategy for human Fz4-CRD. The western blot demonstrated the first N-linked site is critical for the secretion of hFz4-CRD (**Figure 3.9E**). The mutants with S146A and N144D may be suitable for structural studies if wild-type Fz4-CRD in isolation or in complex with Norrin fails to crystallize.

3.8.2 Enhanced Fz4-CRD secretion using C-terminal fusion and valproic acid treatment

As shown in **Figure 3.10A**, the C-terminal mVenus fusion further boosts the secreted expression of Fz4-CRD and reveals a similar expression level to C-terminal Fc fusion (**Figure 3.10B**). Furthermore, the addition of 4 mM valproic acid could further improve the secretion levels of Fz4-CRD (**Figure 3.10C**).

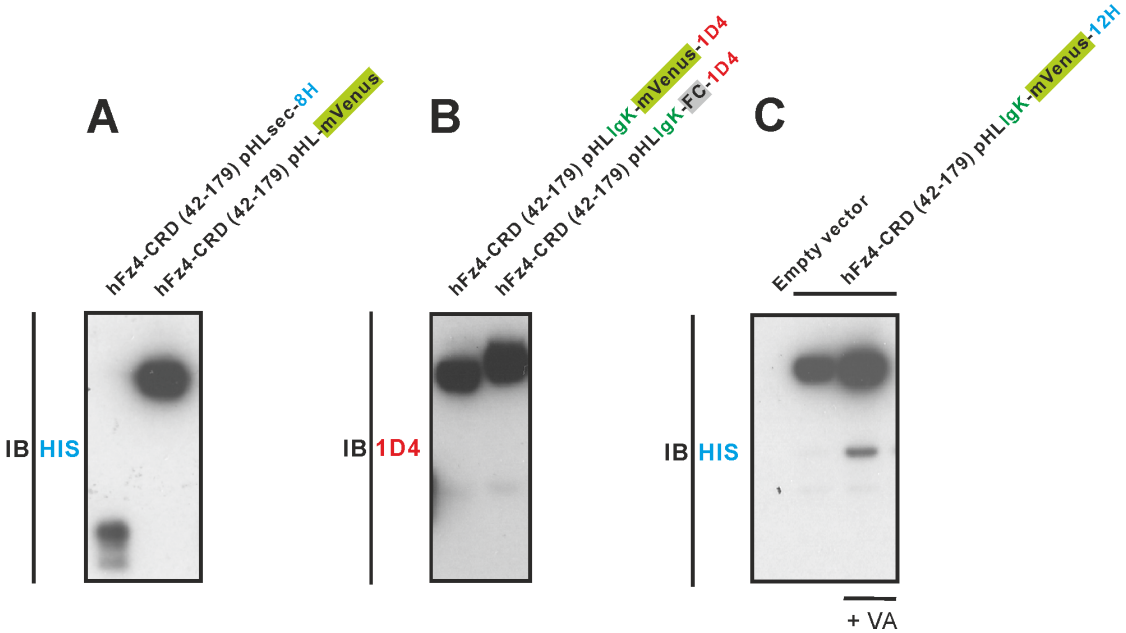


Figure 3.10. The C-terminal fusion and treatment by valproic acid improve the secreted expression of Fz4-CRD. Conditioned media from HEK293T cells transfected with the indicated constructs were immunoblotted (IB) following SDS-PAGE under reduced conditions **(A)** The C-terminally mVenus tagged Fz4-CRD has better secretion. **(B)** There is no difference between the C-terminal Fc and mVenus fusion. **(C)** The addition of valproic acid into HEK293T cells post transfection boosts the level of secreted expression.

3.9 Protein production of Fz4-CRD

The Fz4-CRD construct (**Figure 3.11A**) with the optimum domain boundary (residues 42-179) and murine Igκ signal peptide as well as C-terminal mVenus fusion was expressed in HEK293T cells in the presence of valproic acid and kifunensine (Chang et al., 2007) to limit glycosylation. As shown in **Figure 3.11A**, mVenus-tagged Fz4-CRD was purified from dialyzed conditioned media by IMAC. The eluted sample was treated with home made HRV 3C protease either GST-tagged or His-tagged to remove the mVenus fusion and deglycosylated by His tandem GST-tagged endoglycosidase-F_1 (Endo-F_1; **Figure 3.8C**) cleavage, to leave a single N-acetylglucosamine at each site. The untagged Fz4-CRD was isolated by a reverse IMAC and further purified by SEC (**Figure 3.11A**) using Superdex200 in 10 mM HEPES, pH 7.5, 0.15 M NaCl. The final protein yield of Fz4-CRD is 3 mg from one liter of conditioned media, a significant improvement from the 0.04 mg protein yield in the preliminary protein expression and purification test using the first construct without any modification.

Interestingly, the SEC profile (**Figure 3.11B**) shows that deglycosylated Fz4-CRD protein samples form a range of large aggregations and only have a small portion of monodispersed Fz4-CRD when the C-terminal mVenus fusion is replaced with a Rho-1D4 tag. SDS-PAGE results show untagged Fz4-CRD (**Figure 3.11A**) has higher heterogeneity of glycosylated states than Fz4-CRD carrying a C-terminal Rho-1D4 tag (**Figure 3.11B**) even though both of them were treated with Endo-F_1 for deglycosylation. The protein composition of the aggregation peak appears to be fully deglycosylated Fz4-CRD (**Figure 3.11B**). In total, recombinant Fz4-

CRD is successfully produced in HEK293T cells by a C-terminal mVenus fusion in combination with the optimum domain boundary and signal peptide as well as the treatment of valproic acid. Surprisingly, different fusion tags at the C-terminus appear to affect protein behavior in solution, particularly in deglycosylated states, although the reason is not clear so far.

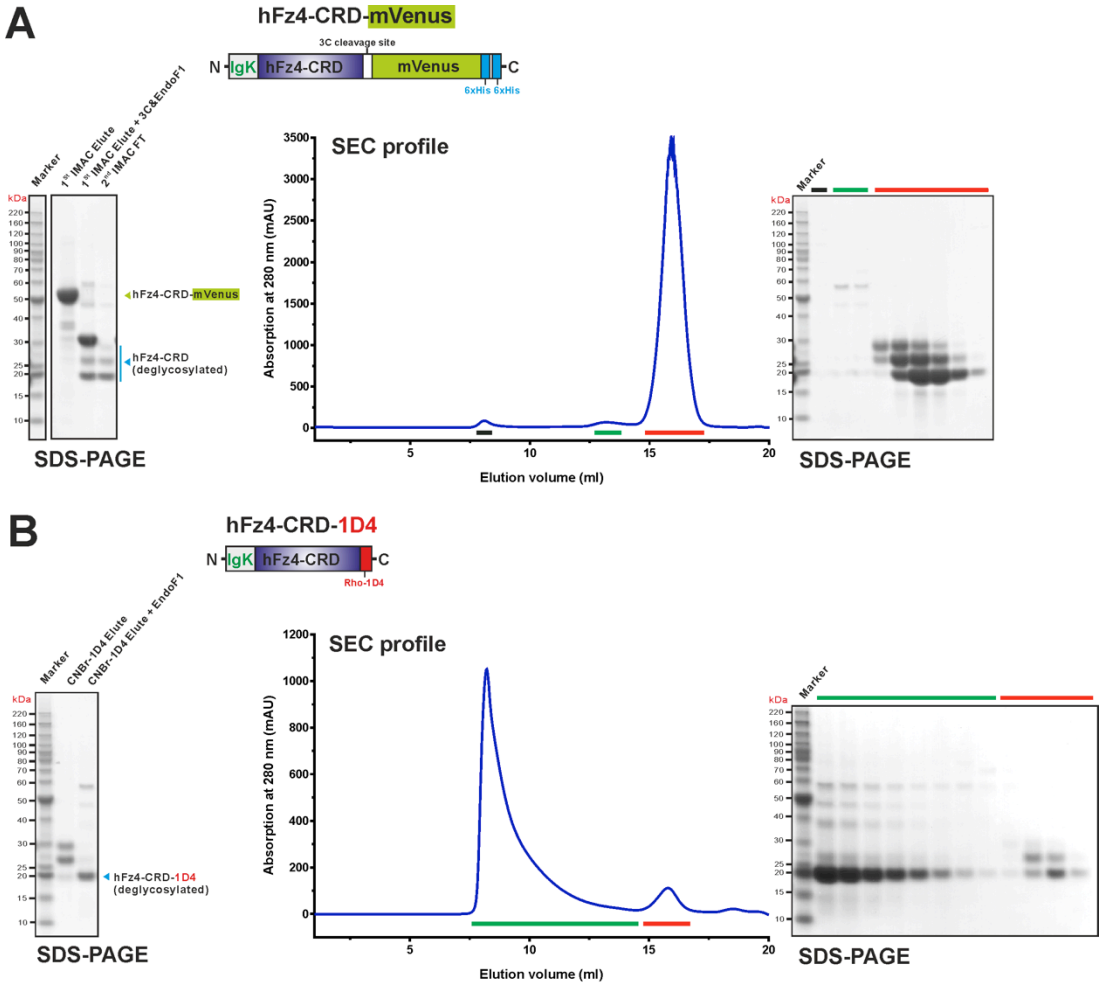


Figure 3.11. Protein purification of recombinant human Fz4-CRD. Schematic diagram of expression construct (top panel), SEC elution profile (left panel; using superdex200 for SEC in 10 mM HEPES, pH7.5 and 0.15 M NaCl), and SDS-PAGE under reducing conditions (right panel) with fraction analysis. **(A)** The purification of C-terminally mVenus tagged Fz4-CRD. **(B)** The purification of C-terminally Rho-1D4 tagged Fz4-CRD.

3.10 Protein production of Fz5-, Fz7-, and Fz8-CRD

The combination of strategies used for Fz4-CRD were also successfully applied for the protein expression and purification of mouse Fz5-CRD (residues 31-176; **Figure 3.12A**), human Fz7-CRD (residues 33-173; **Figure 3.12B**), and two versions of mouse Fz8-CRD_S (residues 30-151; **Figure 3.12C**) and Fz8-CRD_L (residues 30-170; **Figure 3.12D**). The optimisation of the domain boundaries of these Fz-CRDs were performed by Ms. Fu-Lien Hsieh (STRUBI, University of Oxford) on the basis of the boundary of human Fz4-CRD and the crystal structure of mouse Fz8-CRD (Dann et al., 2001). I then used these proteins produced from HEK293T cells to assess the interaction with Norrin by surface plasmon resonance experiments, described in detail in **Chapter 4**.

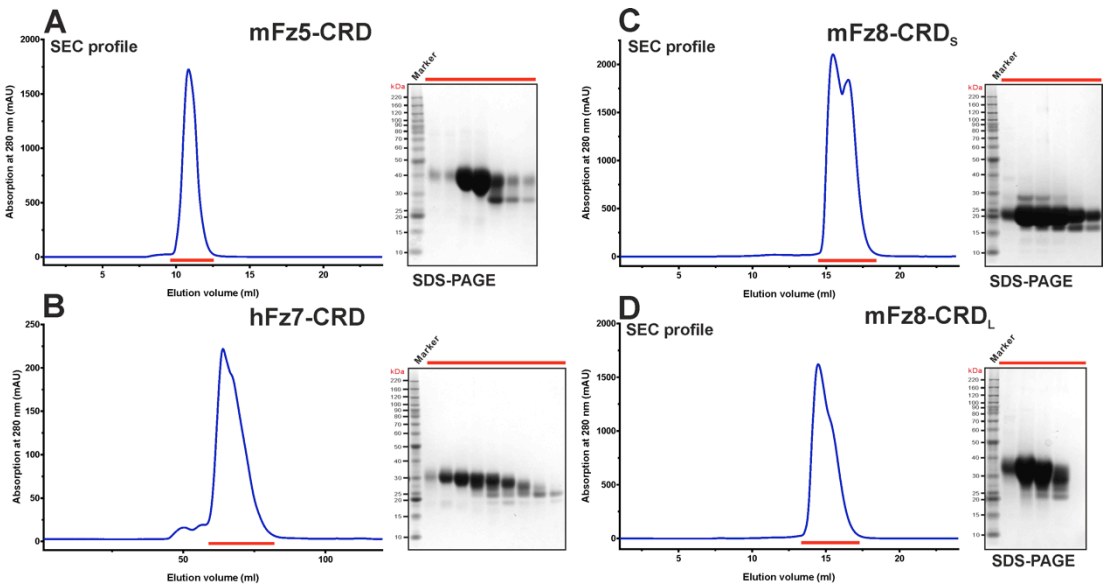


Figure 3.12. Protein purification of recombinant Fz-CRD proteins.
The purification procedure of Fz4-CRD was successfully applied in **(A)** mouse Fz5-CRD (using superdex75 for SEC), **(B)** human Fz7-CRD (using superdex75 for SEC), **(C)** mouse Fz8-CRD_S (using superdex200 for SEC), **(D)** mouse Fz8-CRD_L (using superdex200 for SEC). SEC elution profile (left panel; using 10 mM HEPES, pH7.5 and 0.15 M NaCl as running buffer) and SDS-PAGE under reducing conditions (right panel) with fraction analysis.

3.11 Protein production of Norrin/Fz4-CRD complex

Isolation of the complex of Norrin/Fz4-CRD for structural studies is challenging but critical for understanding the basic mechanism of how Norrin initiates signalling by binding to Fz4-CRD. In addition, structural information would be also important for the studies of Wnt and Fz pairs. In the beginning, I assessed the optimum DNA ratio for co-transfection into HEK293T cells and investigated the effect of valproic acid when Norrin and Fz4-CRD were co-expressed. As shown in **Figure 3.13A**, the optimum DNA ration is 1:1 of Norrin and Fz4-CRD. The treatment of valproic acid boosts both the secreted expression level of Norrin and Fz-CRD (**Figure 3.13B**).

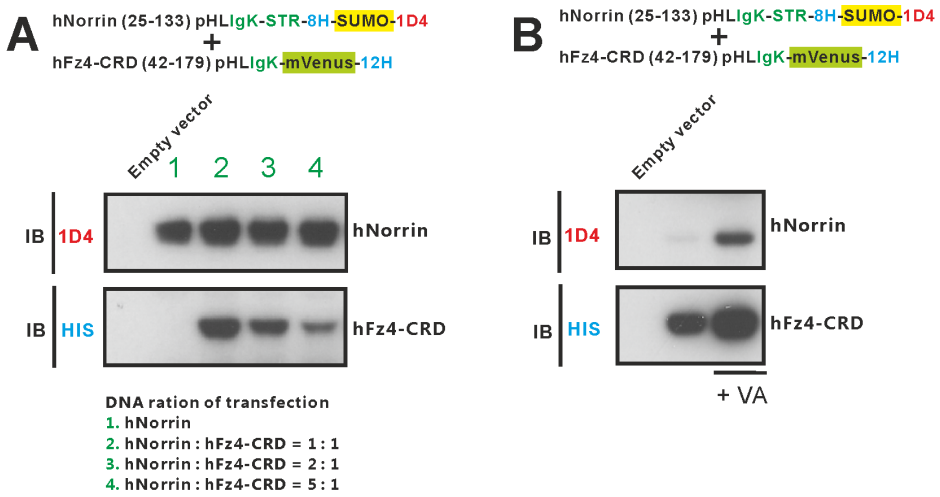


Figure 3.13. Expression trials for the optimization of co-expression.
Conditioned media from transfected HEK293T cells were immunoblotted (IB) following SDS-PAGE under reduced conditions. **(A)** Different DNA ratios of Norrin and Fz4-CRD constructs were transfected into HEK293T cells to assess the optimum transfection condition for complex expression. **(B)** The treatment by valproic acid could increase the level of secreted expression of Norrin and Fz4-CRD.

In combination, the optimum constructs (**Figure 3.14A**) of Norrin and Fz4-CRD were co-transfected at the DNA ratio 1:1 (**Figure 3.13A**) into HEK293T cells in

the presence of 4 mM valproic acid and 5 μM kifunensine (Chang et al., 2007) to express the complex of Norrin/Fz4-CRD for purification. As shown in **Figure 3.14B**, two-steps of IMAC purification in combination with treatment by HRV 3C and Endo F_1 were used to purify the untagged and deglycosylated complex. The monodispersed complex (**Figure 3.14B**) was further isolated by SEC using Superdex200 in 10 mM HEPES, pH 7.5, 0.7 M NaCl (the high concentration of salt is a critical step to maintain complex stability and solubility in solution while the sample is concentrated for SEC). The final complex protein yield is 2 mg from one liter of conditioned media. The crystallization and structure determination of Norrin in complex with Fz4-CRD is described in **Chapter 4**.

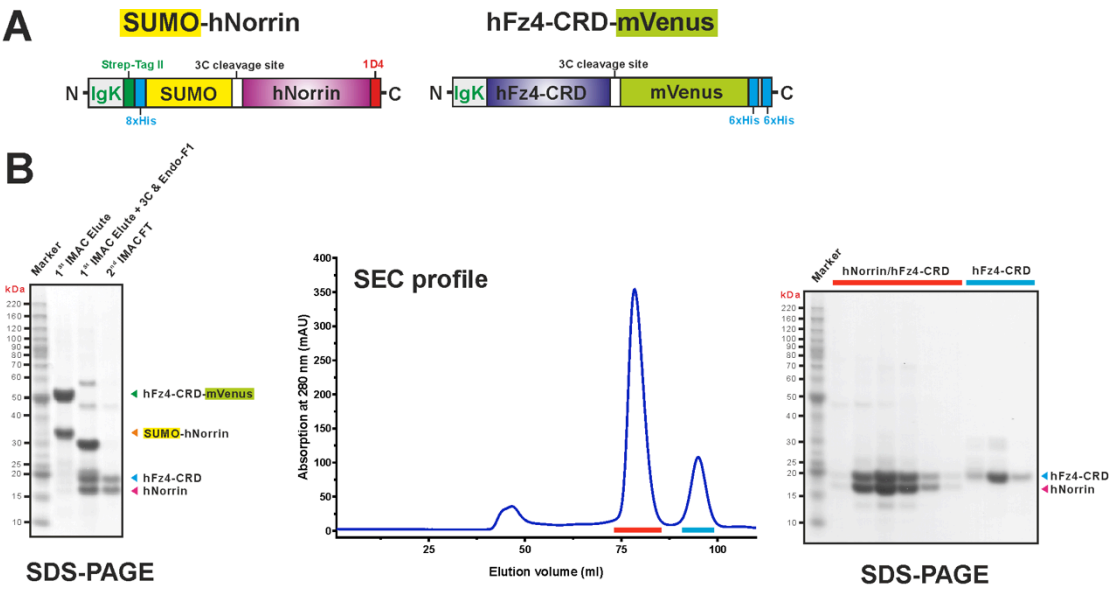


Figure 3.14. Protein purification of Norrin/Fz4-CRD complex.
(A) Schematic diagrams of Norrin and Fz4-CRD expression constructs. **(B)** SDS-PAGE analysis of protein complex purification procedure. Norrin forms a stable complex with Fz4-CRD in solution. SEC elution profiles (left panel) and SDS-PAGE under reducing conditions (right panel) are presented. SEC fractions analysed by SDS-PAGE are marked as red lines for Norrin/Fz4-CRD complex and cyan lines for uncomplexed Fz4-CRD.

3.12 Protein production of Norrin/Fz4-CRD/Lrp6-P1E1P2E2 complex

Like Wnt, Norrin activation of the canonical Wnt/β-catenin pathway also requires engagement with Lrp5/6 (Xu et al., 2004). The Lrp5/6 ectodomain contains four tandem β-propeller/epidermal growth factor-like domain (PE) pairs followed by three LDLR type A repeats (Ahn et al., 2011; Bourhis et al., 2011; Chen et al., 2011; Cheng et al., 2011). Although Lrp5 and Lrp6 are highly homologous receptors involving in canonical Wnt signalling (Joiner et al., 2013), the genetic data revealed that Norrin function is highly dependent on Lrp5 rather than Lrp6 (Nikopoulos et al., 2010b; Xu et al., 2004; Ye et al., 2009).

In the beginning, I therefore tried to understand how Norrin interacts with the ectodomain of Lrp5 from a structural perspective. Extensive expression trials including engineered domain boundary and fusion strategies were performed (**Figure 3.15**). However, all attempts failed to give reasonable secreted expression. The expression level of secreted Lrp5 ectodomain either P1E1P2E2 or P3E3P4E4 is much lower than Lrp6-P3E3P4E4 (Chen et al., 2011) previously studied in the Jones' group. Interestingly, Ke *et al.*, very recently reported that Norrin directly binds to Lrp6-P1E1P2E2 (Ke et al., 2013). Therefore, Lrp6-P1E1P2E2 having the comparable expression level as Lrp6-P3E3P4E4 was then chose and used for the isolation of ternary complex.

Lrp6-P1E1P2E2 (residues 20-629) was cloned into a newly created pHLsec derivative vector (**Figure 3.16A**) in-frame with a C-terminal HRV 3C cleavage

site and 10xHis tag. Transient expression in HEK293T cells in the presence of 4 mM valproic acid and 5 µM kifunensine (Chang et al., 2007) was performed as a co-expression with Norrin carrying a N-terminal SUMO fusion and Fz4-CRD with a C-terminal mVenus fusion (**Figure 3.16A**). Secreted recombinant protein was purified from dialyzed conditioned media by IMAC and subjected to treatment with HRV 3C protease and Endo-F_1 (**Figure 3.16B**). The untagged and deglycosylated sample was purified by reverse IMAC and ternary complex of Norrin/Fz4-CRD/Lrp6-P1E1P2E2 was further isolated by SEC (Superdex200) in 10 mM HEPES, pH 7.5 and 0.5 M NaCl (**Figure 3.16B**). The final protein yield of ternary complex is 0.4 mg from one liter of conditioned media.

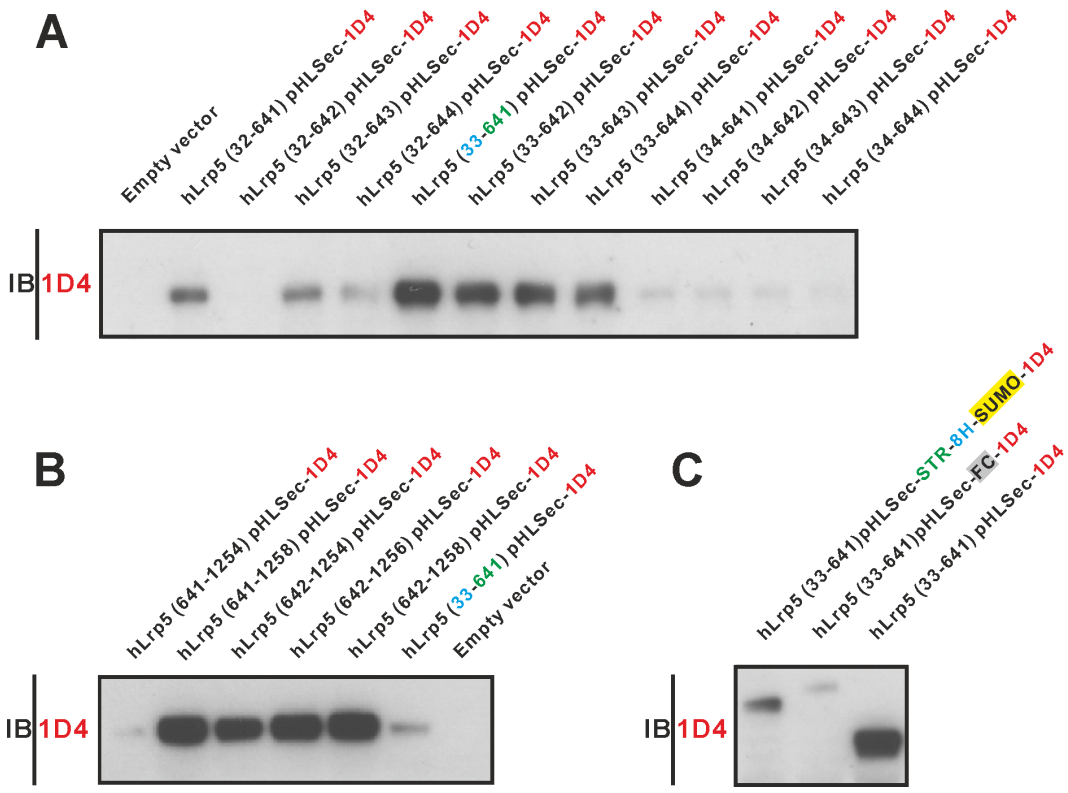


Figure 3.15. Expression trials for human Lrp5 ectodomain constructs. Conditioned media from transfected HEK293T cells were immunoblotted (IB) following SDS-PAGE under reduced conditions. **(A)** Expression trials for a series of Lrp5-P1E1P2E2 constructs. **(B)** Expression trials for a series of Lrp5-P3E3P4E4 constructs. **(C)** The fusion strategy failed in Lrp5.

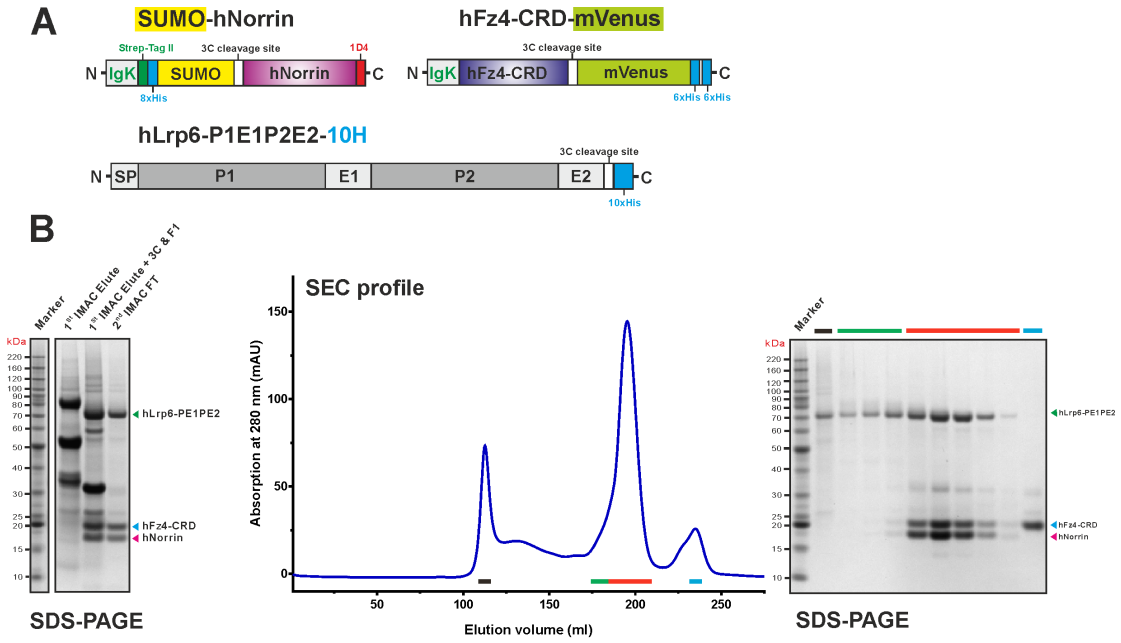


Figure 3.16. Protein purification of Norrin/Fz4-CRD/Lrp6-P1E1P2E2 complex.
(A) Schematic diagrams of expression constructs of Norrin, Fz4-CRD, and Lrp6-P1E1P2E2. **(B)** SDS-PAGE analysis of protein complex purification procedure. SEC elution profiles (left panel) and SDS-PAGE under reducing conditions (right panel) are presented. SEC fractions analysed by SDS-PAGE are marked as red lines for ternary complex and cyan lines for uncomplexed Fz4-CRD.

3. 13 Future perspectives

As described in **Chapter 3**, novel strategies were developed to produce Norrin and its binding partner Fz4-CRD in milligram quantities and a reliable system for complex protein production was set up. **Chapter 4** will present the crystal structure of Norrin and its complex with Fz4-CRD as well as unliganded Fz4-CRD. The functional significance of the Norrin and Fz4-CRD interaction will be addressed in **Chapter 4**, using a series of biophysical and cellular assays. The roles of heparan sulfate proteoglycans and Lrp5/6 in Norrin mediated signalling were investigated in **Chapter 4**, by structural analyses of a complex structure of Norrin/Fz4-CRD/heparan sulfate analogue in combination with cellular and surface plasmon resonance binding assays. The potential application of recombinant Norrin of genetic retinal disorders and vitreoretinal diseases is discussed in **Chapter 5**.

Chapter 4

Structural and functional basis of Norrin interaction with Fz4, Lrp5/6, and HSPGs

4.1 Summary

As described in **Chapter 3**, novel strategies were developed for protein production of recombinant human Norrin and Fz4-CRD as well as complex in milligram quantities. Here, the crystal structures of Norrin in complex with Fz4-CRD and complex bound with sucrose octasulfate (SOS; a synthetic analogue of heparan sulfate) as well as the unliganded states of Norrin and Fz4-CRD are determined and presented (**Table 4.1**). These structures are further validated by solution studies using size-exclusion chromatography coupled to multiangle light scattering (SEC-MALS) and small-angle X-ray scattering (SAXS). The structural and functional analyses in combination with previously reported disease-associated mutations map three distinct sites on the Norrin surface. The sites respond independently to Fz4, Lrp5/6, and heparan sulphate proteoglycans (HSPGs), and all of them are necessary for the activation of Norrin mediated Wnt/β-catenin signalling. Furthermore, structural comparison of Norrin/Fz4-CRD with xWnt8 bound to mouse Fz8-CRD complexes provides insights into Fz binding specificity and promiscuity. Finally, the structural information and engineered Norrin mutants presented in **Chapter 4** open up new avenues for rational and target specific design to enhance or suppress the interactions of Wnt with (co)-receptors for diseases caused by aberrant Wnt signalling.

4.2 Introduction

Norrie Disease Protein (*NDP)* gene encodes Norrin (**Figure 4.1A**), a secreted cystine-knot like growth factor that is unrelated to Wnts in sequence (Berger et al., 1992a; Chen et al., 1992), but like Wnts functionally activates canonical Wnt/β-catenin signalling via interaction with Fz4-CRD and Lrp5/6-ECD (Ke et al., 2013; Xu et al., 2004). Interestingly, mutational mapping studies reveal that Norrin- and *Xenopus* Wnt8 (xWnt8)-binding patches on the Fz4-CRD are largely overlapping (Dann et al., 2001; Smallwood et al., 2007). Moreover, Norrin mediated signalling requires an additional co-receptor, an auxiliary four-pass transmembrane protein Tspan-12, to enhance signalling activity (Junge et al., 2009).

In humans, a huge number of mutations in the *NDP* gene and the receptor genes of *FZ4*, *LRP5*, and TSPAN-12 have been identified for Norrie Disease, an X-linked genetic disease with severe retinal hypovascularization, and a variety of vitreoretinal diseases, including Familial Exudative Vitreoretinopathy (FEVR), Retinopathy Of Prematurity and Coats' Disease (Nikopoulos et al., 2010b; Poulter et al., 2010; Xia et al., 2008). In mice, knock-out mutations in the genes for *NDP* (Richter et al., 1998), *FZ4* (Xu et al., 2004), *LRP5* (Kato et al., 2002), and TSPAN-12 (Junge et al., 2009) further support the notion that dysfunctional Norrin mediated signalling results in impaired retinal vascularization, in agreement with cell-based assays showing that most of the mutations result in defects in the activation of signalling (Xu et al., 2004). In adults, Norrin has not only angiogenic properties in the retina, cochlea, and uterus (Luhmann et al., 2005; Rehm et al.,

2002) but also neuroprotective effects on retinal neurons (Ohlmann et al., 2010; Seitz et al., 2010) , as well as an essential role in maintaining the blood-retina barrier (Paes et al., 2011; Ye et al., 2009) and blood-brain barrier (Wang et al., 2012).

It is noteworthy that Norrin shows highly selective binding to Fz4 but not to the other 9 Fz receptors, which is different from the promiscuous Wnt and Fz pairs: each Wnt binds to multiple Fz receptors and each Fz receptor interacts with multiple Wnts (Bao et al., 2012; Hsieh et al., 1999; Kikuchi et al., 2007; Logan and Nusse, 2004). In addition, Norrin, similar to Wnt morphogens, has the property of interacting with HSPGs and limited spatial diffusion (Ohlmann et al., 2010; Perez-Vilar and Hill, 1997; Smallwood et al., 2007; Xu et al., 2004).

Relative to functional studies of Norrin mediated signalling, structural analyses are very limited due to technical difficulties in obtaining recombinant Norrin and its binding partners. I developed novel strategies (**Chapter 3**) to overcome the bottleneck.

4.3 Aims

The main aim of this chapter will be to obtain structural information for Norrin in complex with Fz4-CRD plus unliganded Norrin and Fz4-CRD. Structural analyses in combination with biophysical and cellular assays will aim to understand Norrin mediated signalling at the molecular level to answer the following major questions.

1. How does Norrin initiate signalling by binding to Fz4-CRD, Lrp5/6, and HSPGs?
2. How do disease-associated mutations affect Norrin mediated signalling?
3. The similarity and difference between Norrin and Wnt

Table 41. Data collection and refinement statistics.

	Norrin/Fz4-CRD/SOS	Norrin/Fz4-$CRD_{methylated}$	Norrin	Norrin Se-Met	$Norrin_{methylated}$	Norrin	Fz4-CRD	Fz4-CRD
Crystal form			I	I	II	III	I	II
Data Collection								
Source	DLS I04-I	DLS I04	DLS I24	DLS I03	DLS I04	DLS I04	DLS I24	DLS I24
Wavelength (Å)	0.9200	0.9795	0.9686	0.9795	0.9795	0.9795	0.9686	0.9686
Space group	$P6_122$	$P4_322$	$P2_12_12_1$	$P2_12_12_1$	$P2_12_12_1$	$C121$	$P2_12_12_1$	$P6_1$
Unit cell dimensions (Å/°)								
a / α	119.14 / 90	98.92 / 90	46.37 / 90	45.82 / 90	102.67 / 90	86.76 / 90	72.61 / 90	76.07 / 90
b / β	119.14 / 90	98.92 / 90	79.10 / 90	78.78 / 90	53.06 / 90	38.10 / 93.97	102.14 / 90	76.07 / 90
c / γ	119.15 / 120	120.42 / 120	234.30 / 90	232.78 / 90	96.13 / 90	177.20 / 90	116.51 / 90	204.50 / 90
Wilson B-factor ($Å^2$)	111.1	48.28	46.95	82.75	36.9	51.9	35.9	58.85
Resolution (Å)[a]	47.34 - 3.00 (3.18 - 3.00)	49.46 - 2.30 (2.38 - 2.30)	65.56 - 2.40 (2.49 - 2.40)	116.39 - 3.18 (3.26 - 3.18)	33.65 - 2.00 (2.05 - 2.00)	44.19 - 2.30 (2.38 - 2.30)	41.77 – 2.20 (2.27 – 2.20)	47.37 – 2.40 (2.49 – 2.40)
No. of unique reflections[a]	10503 (1648)	26816 (2514)	34722 (3384)	14982 (1113)	36272 (2635)	26073 (2538)	44268 (3802)	25975 (2724)
Multiplicity[a]	19.6 (20.6)	6.0 (5.6)	5.6 (5.7)	33.3 (9.9)	5.6 (5.8)	5.8 (6.0)	4.3 (4.4)	4.0 (4.1)
Completeness (%)[a]	100 (100)	98.9 (97.2)	99.9 (100)	99.9 (99.9)	100 (100)	99.2 (97.7)	99.2 (99.7)	99.5 (99.4)
Mean I/σ(I)[a]	14.6 (1.6)	10.7 (1.4)	7.8 (1.9)	20.2 (3.0)	9.1 (1.7)	16.7 (2.0)	12.8 (2.0)	14.5 (2.2)
R_{pim} (all) (%)[a]	3.1 (54.8)	4.5 (56.1)	6.1 (42.3)	2.8 (23.4)	4.1 (58.3)	2.8 (36)	4.1 (49.5)	2.6 (33.9)
Refinement								
Molecules Per ASU	2	3	6	6	4	4	4	4
Solvent content (%)	69.6	66.3	53.5		49.1	54.3	62.0	51.9

R_{work} / R_{free} (%)[b,c]	21.5 / 26.7	19.7 / 22.1	21.6 / 26.2	23.3 / 24.8	22.1 / 25.0	17.7 / 22.3	20.3 / 24.3
r.m.s deviations[d]							
bond lengths (Å)	0.005	0.004	0.009	0.005	0.006	0.01	0.005
bond angles (°)	1.18	0.93	1.08	1.07	1.03	1.35	0.94
B-factor (Å^2) / No. atoms							
Protein	113.1 / 1759	63.2 / 2557	70.3 / 4930	57.1 / 3187	90.7 / 3104	46.5 / 3866	75.6 / 3877
Ligand	133.2 / 83	71.7 / 39	91.5 / 101	73.2 / 10	71.6 / 72	66.7 / 70	72.3 / 99
Water	0 / 0	57.1 / 115	55.2 / 164	50.5 / 122	142.1 / 54	43.3 / 148	67.8 / 69
Ramachandran plot							
Favored regions (%)	95.5	97	96.7	97.2	96.0	99.0	97.0
Allowed regions (%)	4.5	3	3.3	2.8	4.0	1.0	3.0
Number of outliers	0	0	0	0	0	0	0
PDB accession code							

[a]Values in parentheses correspond to the highest resolution data shell.

[b]R_{work} is the R-factor = $(\sum|F_o| - \sum|F_c|) / \sum|F_o|$ where F_o and F_c are observed and calculated structure factors, respectively.

[c]R_{free} is the R-factor calculated using 5% of the data that were excluded from the refinement.

[d]The r.m.s deviation is the root-mean-square deviation from ideal protein geometry.

4.4 The crystal structure of uncomplxed human Norrin

Norrin was crystallized in three crystal forms (**Table 4.1**). The first structure of Norrin (crystal form I) was determined by using selenomethionine-labeled proteins for phasing (**Figure 4.1** and **Figure 4.2A**). The Norrin structures reveal an elongated disulphide-linked dimer stabilized by extensive disulfide bridges (**Figure 4.1C** and **4.2B**). This is consistent with our small-angle x-ray scattering (SAXS) measurement that Norrin exists as dimer in solution (**Figure 4.1E** and **Table 4.2**), whereas an early study reported that Norrin forms oligomers (Perez-Vilar and Hill, 1997). Each monomer comprises three β-hairpins (A, β1-β2 strands; B, β3-β4 strands; C, β5-β6 strands) and a β7 strand at the C-terminus as well as four intermolecular disulphide bonds: one (Cys55-Cys110; termed as II) is a Norrin specific disulphide bridge connecting the β1-β2 loop with the β5-β6 loop and three form the classical cystine-knot motif in which the Cys39-Cys96 (I) disulphide passes through a eight-residue ring bounded by the Cys65-Cys126 (III) and Cys69-Cys128 (IV) disulphides (**Figure 4.1B** and **4.1C**).

The two monomers assemble as a head-to-tail dimer by three novel intermolecular disulphide bonds (Cys93-Cys95, Cys95-Cys93, and Cys131-Cys131) flanked by the cystine knots in each monomer (**Figure 4.1C** and **4.3**). Dimerization buries an extensive surface area of 3600 $Å^2$ corresponding to 22 % of the surface of each monomer (**Figure 4.1C**). The dimer interface is further stabilized by extensive hydrogen bonds and hydrophobic interactions contributed by hairpin B of one monomer contacting with hairpins A and C of the other monomer (**Figure 4.1D** and **Table 4.3**). Disruption of the dimer by either

Cysteine-to-Alanine mutations of intermolecular disulphide bonds or mutations of hydrophobic residues at the dimer interface results in a loss of Norrin-mediated signalling (Ke et al., 2013; Smallwood et al., 2007).

Superposition of all molecules in the asymmetric unit from our three crystal forms with MBP-Norrin (root-mean-square (r.m.s.) deviation of 1.5 Å over 190 equivalent Cα atoms; **Table 4.4**) reveals a high degree of conformational plasticity in the β1-β2 loop, β3-β4 loop, and β5-β6 loop (**Figures 4.4A**). The flexibility inherent in these regions is consistent with the relatively high crystallographic B factor values (**Figures 4.4B**), this flexibility may be relevant to biological function. Searching the homologous structures using the DALI server (Holm and Rosenstrom, 2010) revealed the closest match to the Norrin structure is the recently reported human C-terminal cystine-knot domain of Von Willebrand factor (VWF-CTCK; **Figure 4.4C**) with r.m.s. deviation of 2.5 Å over 82 equivalent Cα atoms per monomer (Zhou and Springer, 2014). Interestingly, VWF-CTCK adopts the same disulphide bond arrangement as Norrin, although the sequence identity between Norrin and VWF-CTCK is low, about 19% (**Figure 4.4D**). Zhou *et al.*, further suggested that the highly crosslinked dimeric architecture of VWF-CTCK possesses the characteristics of resistance to hydrodynamic force and disulphide reduction (Zhou and Springer, 2014). In combination, Norrin therefore uses a specialized dimerization mechanism to maintain its integrity of structure and function.

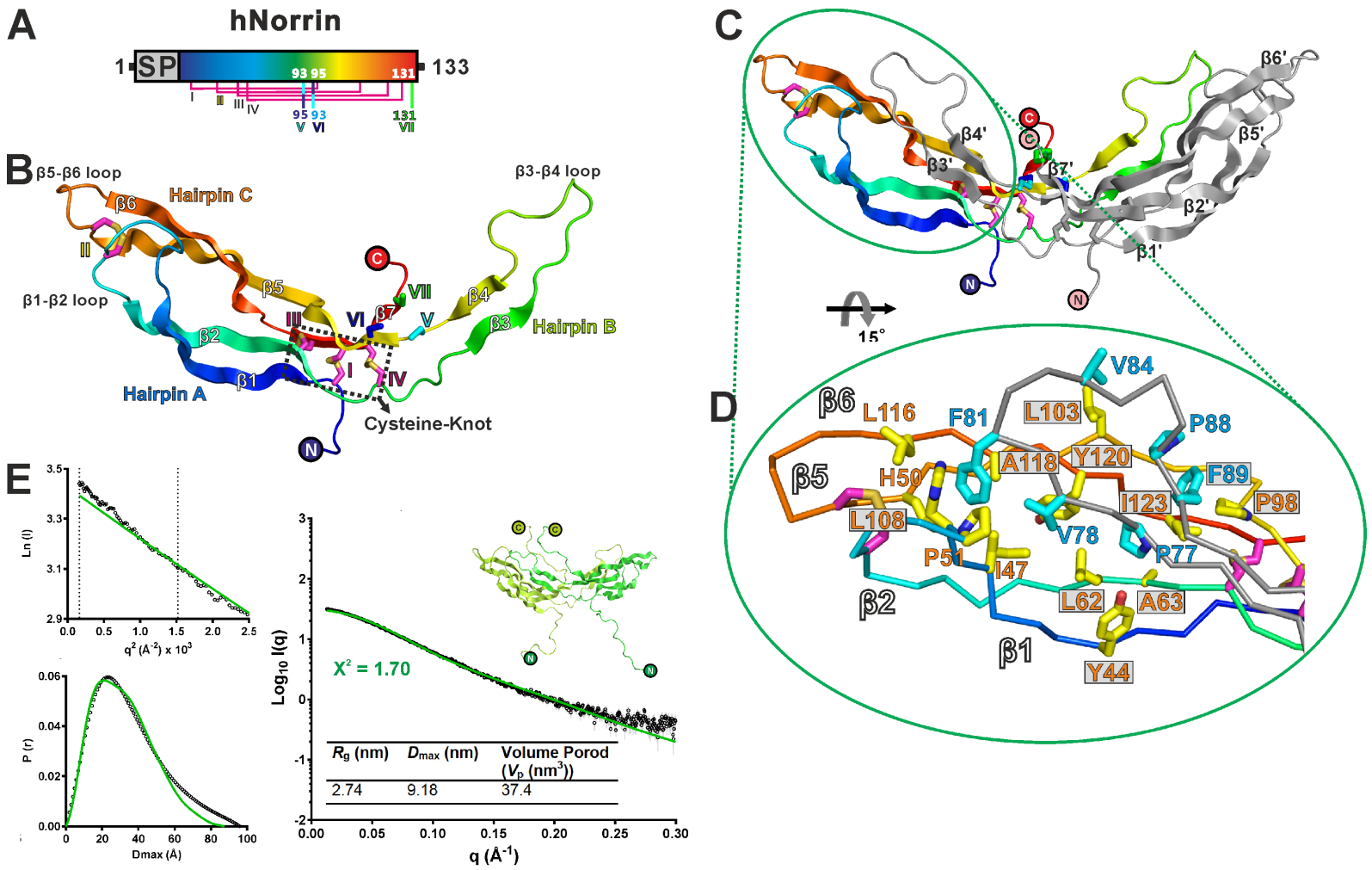


Figure 4.1. Structural characteristics of Norrin.

Figure 4.1 (continued).
(A) Schematic domain organization of human Norrin (SP, signal peptide). The crystallization construct of Norrin (residues 25-133) is coloured in rainbow. The disulphide bonds derived from the crystal structures are numbered and drawn as lines. **(B)** Ribbon diagram of Norrin showing the monomer in rainbow colouring from N-terminus (blue) to C-terminus (red) with elements of β-strands numbered. Four intramolecular disulphide bonds are shown as magenta sticks (see also **Figure 4.3**). The residues of Cys93, Cys95, and Cys131 used for intermolecular disulphide bridges are shown as cyan, blue, and green sticks, respectively. The encircled N and C indicate the N- and C- termini. **(C)** Cartoon representation of dimeric Norrin (crystal form III) with secondary structure elements numbered. The disulphide bonds are shown as sticks. Three intermolecular disulphide bonds (Cys93-Cys95, Cys95-Cys93, and Cys131-Cys131) used for the dimer formation are flanked by two cystine-knot motifs from each monomer, with colour-coding as cyan, blue, and green for residues of Cys93, Cys95, and Cys131, respectively. The filled circles denote the N- and C-termini. **(D)** Structural details of hydrophobic interactions for Norrin dimerization beyond the cystine-knot motif. The selected residues on hairpin A and C (β1, β2, β5, and β6 strands) forming hydrophobic contacts with hairpin B from another monomer are shown as yellow sticks. The hydrophobic residues on hairpin B are shown as cyan sticks. The disease mutations are denoted as grey filled boxes. See also **Table 4.8** for lists of all residues involved in Norrin dimerization. **(E)** SAXS analysis of Norrin. The right inset presents the experimental scattering data (black circles) and calculated scattering pattern (green line) are shown to a maximal momentum transfer of q = 0.30 $Å^{-1}$, and the Norrin solution structure model is shown in cartoon representation. Inset SAXS parameters including R_g, D_{max}, and Volume Porod (V_p). The upper left inset shows the experimental (black circles) and calculated (green line) Guinier region. The dashed lines delimit the range of fitting for Radius of gyration (R_g) analysis ($R_g \cdot S \leq 1.3$). The down left inset shows the experimental (black line) and calculated (green line) pair distance distribution $P(r)$ curve. The measured molecular weights of 33.5 kDa and 22.5 kDa that were obtained from forward scattering of sample ($I(0)$) by comparison with reference BSA and by dividing the Volume Porod by 1.66, respectively, are close to the theoretical molecular weight of Norrin dimer (27.2 kDa).

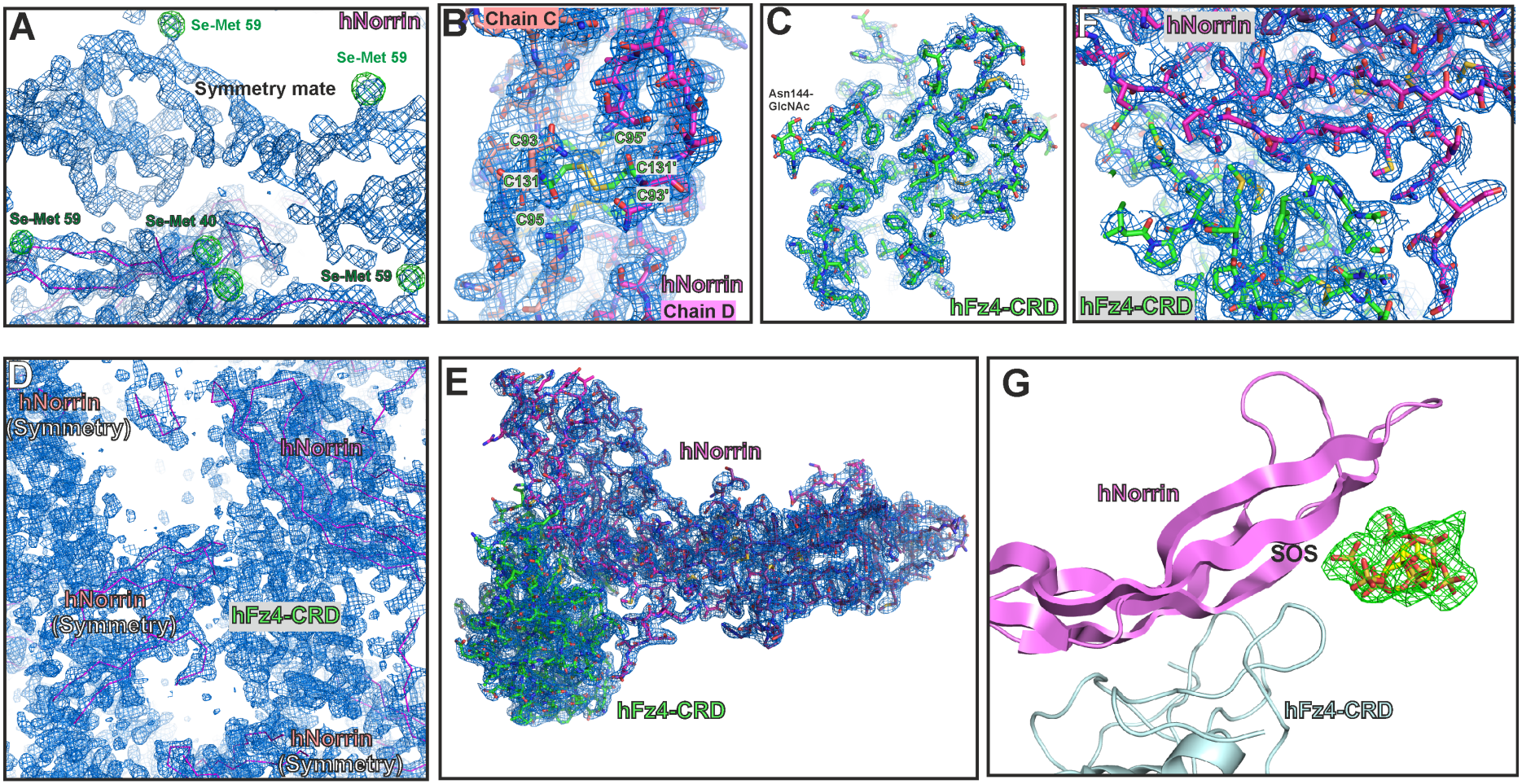


Figure 4.2. Electron density maps.

Figure 4.2 (continued).
(A) The initial density modified map from PHENIX AUTOSOL (Terwilliger, 2000; Terwilliger et al., 2009) calculated with experimental Se-Met SAD phases is contoured at 1.5 σ and shown as blue mesh. The initial model from BUCCANEER (Cowtan, 2006) is shown as magenta ribbon. The anomalous difference map for Se-Met is contoured at 4 σ as green mesh with Se-Met residues labelled. **(B)** The sigmaA-weighted 2|F_O|-|F_C| electron density map of the refined structure of Norrin crystal form II (stick model; chain C and D) at 2 Å is contoured at 1.2 σ as blue mesh. The cysteine residues of Cys93, Cys95, and Cys131 forming intermolecular disulphide bonds are coloured as green sticks. **(C)** Overall sigmaA-weighted 2|F_O|-|F_C| electron density map of the final model of Fz4-CRD crystal form I (shown as green stick model) is contoured at 1.2 σ as blue mesh. **(D)** Initial electron density map of the Norrin/Fz4-$CRD_{methylated}$ complex is contoured at 1.5 σ after molecular replacement in PHASER (McCoy, 2007) using dimeric Norrin crystal form I as search model (magenta ribbon) and further density modification in PARROT (Cowtan, 2010). The additional electron density corresponding to the molecule of Fz4-CRD is clearly visible. **(E)** Overall sigmaA-weighted 2|F_O|-|F_C| electron density map after refinement contoured at the 1.0 σ level as blue mesh for the complex of Norrin/Fz4-$CRD_{methylated}$, shown as stick model. **(F)** Zoom-in view of the electron density map from **(E)** presents the interaction interface between Norrin and Fz4-CRD. **(G)** The sigmaA-weighted |F_O|-|F_C| electron density maps were calculated with omission of the SOS molecules from the refined model, followed by several cycles of refinement and contoured at the 4 σ level as green mesh.

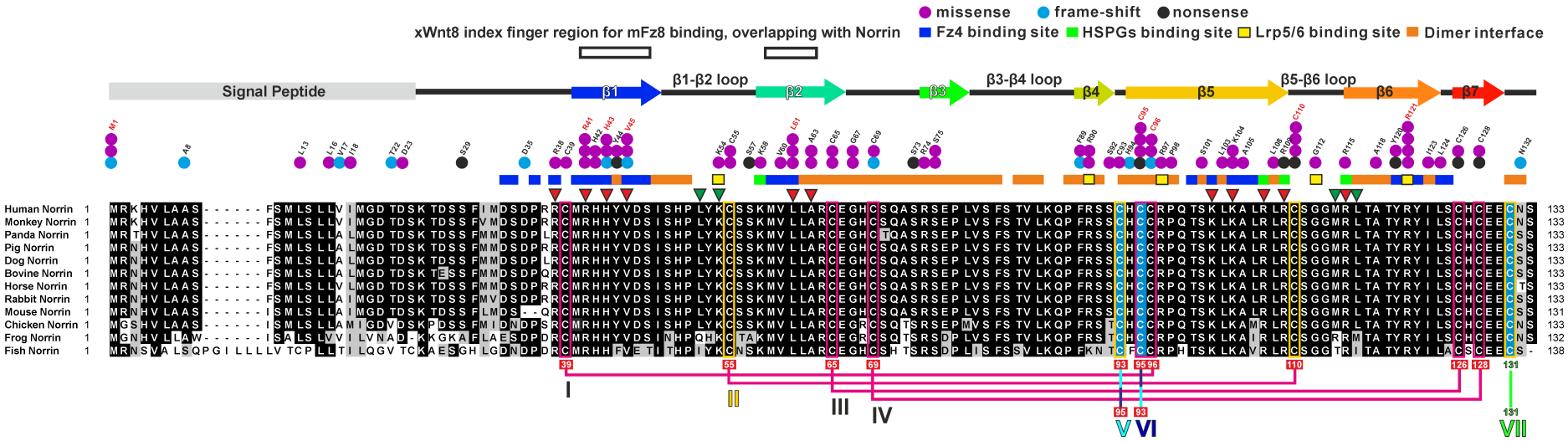


Figure 4.3. Multiple sequence alignment of Norrin proteins in vertebrates.

Figure 4.3 (continued).
The sequence alignment was performed by using the ClustalW program (Larkin et al., 2007). Secondary structure element colouring corresponds to **Figure 4.1B** and is displayed above the alignment. Identical and similar sequences are shaded in black and grey, respectively. Dashes indicate the sequence gaps introduced to optimize the sequence alignment. The magenta boxes represent conserved cysteine residues in the cystine-knot growth factor superfamily, whereas the yellow boxes denote Norrin specific conserved cysteine residues. Disulphide bridges are numbered and are drawn in magenta lines for the intramolecular disulphide bonds. Three cysteine residues (highlighted in cyan) that form intermolecular disulphide bridges are drawn in cyan, blue and green lines. Red and green triangles indicate the mutation sites for SPR binding and luciferase assays. Residues involved in the binding of Fz4, HSPGs, and Lrp5/6 are marked with blue, green, and yellow filled boxes, respectively. Residues involved in dimerization are highlighted with orange filled boxes. Black boxes above the secondary structure assignments denote the region of the xWnt8 index finger involved in mFz8-CRD binding, which overlaps with Norrin β1 and β2 for hFz4-CRD binding (See also **Figure 4.24B**). Disease-associated residues are marked by coloured dots according to the types of mutations (purple, missense; cyan, frame-shift; black, nonsense). Cysteine residues identified as disease-associated residues are marked below the sequence with red filled boxes. The NCBI accession numbers are: Human Norrin, NP_000257; Monkey Norrin, XP_528948; Panda Norrin, XP_002928194; Pig Norrin, NP_001106528; Dog Norrin, XP_855261; Bovine Norrin, AAI12739; Horse Norrin, XP_001490401; Rabbit Norrin, XP_002719919; Mouse Norrin, NP_035013; Chicken Norrin, XP_416765; Frog Norrin, NP_001154869; Fish Norrin, XP_001338820.

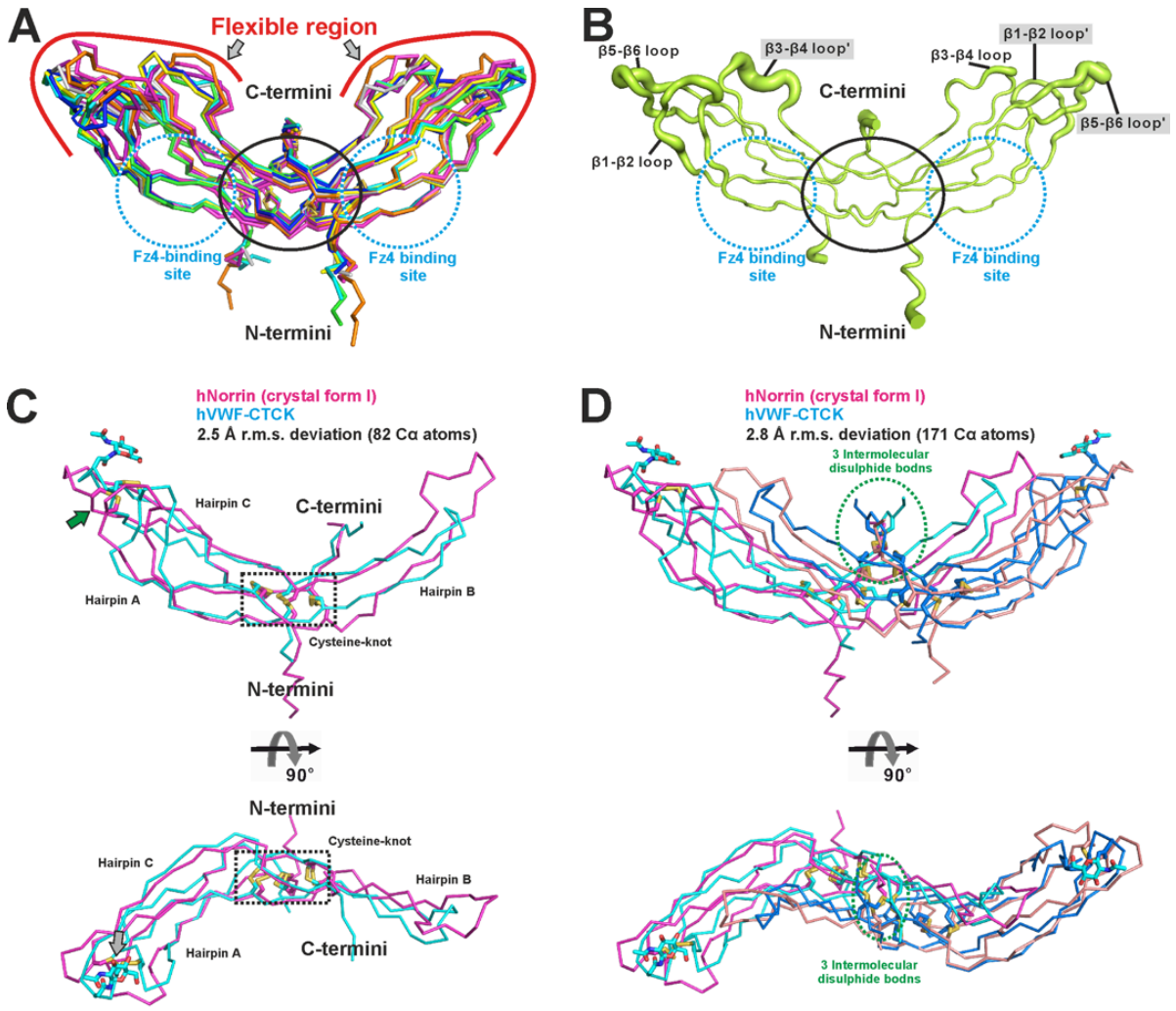


Figure 4.4. Structural rigidity and flexibility of uncomplexed Norrin and superimposition with VWF-CTCK.

Figure 4.4 (continued).
(A) and **(B)** Structural plasticity of loop regions (β1-β2 loop, β3-β4 loop, and β5-β6 loop), the fold is conserved for areas involved in dimerization and the Fz4 binding site. The flexible regions are highlighted as red lines. The well ordered regions include the cystine-knot motifs plus intermolecular disulphide linked areas (black circle) and two Fz4 binding sites (cyan dotted circle). **(A)** Ribbon diagram of superimpositions of Norrin molecules from the asymmetric unit of crystal form I (green, chain A and B; cyan, chain C and D; magenta, chain E and F), crystal form II (yellow, chain A and B; blue, chain C and D), crystal form III (grey, chain A and B; purple, chain C and D), and MBP-Norrin (cyan; PDB ID: 4MY2). See also **Table 4.4** for detailed information on superimposition. **(B)** Representative Norrin dimer displayed with the B factor of the Cα atoms defining the diameter of the Cα tube (small tube means structural rigidity; large tube indicates structural flexibility). **(C)** and **(D)** Structural comparison of Norrin with VWF-CTCK. Ribbon diagram of superimpositions of Norrin crystal form I (magenta/wheat for chain A/B; omitting Rho-1D4 tag from chain A) with VWF-CTCK (cyan; PDB ID: 4NT5) in monomer **(C)** or dimer **(D)**. Overall, both structures adopt a similar fold (β-structure; three hairpins; same disulphide arrangement) except for conformational changes, although the sequence identity is 19%. Similar to Norrin, VWF-CTCK has 11 cysteine residues, comprising 4 intramolecular and 3 intermolecular disulphide bonds. But, each monomer of VWF-CTCK has a N-linked glycan (shown as cyan sticks) on the β5-β6 loop near to Norrin and hWF-CTCK specific disulphide bonds (highlighted as a green arrow) and a shorter hairpin B.

Table 4.2. **Molecular properties of the proteins determined by Small-Angle X-ray Scattering (SAXS).**
Fz4-CRD reveals monomeric states and Norrin forms a dimer, the Norrin/Fz4-CRD complex has a 2:2 stoichiometry in solution. See also **Table 4.7**, SEC-MALS experiments.

Proteins	**N-Glyc state**	R_g **(nm)**[a]	D_{max} **(nm)**[b]	**Volume Porod** (V_p **(nm^3))**	$MW_{Theoretical}$ **(kDa)**[c]	$MW_{Measured}$ **(KDa)**[d]	$MW_{Measured}$ **(KDa)**[e]	**Protein assembly**
Fz4-CRD	deglyc[f]	1.98	6.93	33.0	17.1 (monomer) 34.2 (dimer)	15.9	19.9	monomer
Fz4-CRD	glyc[g]	2.24	7.84	41.1	21.4 (monomer) 42.8 (dimer)	23.7	24.7	monomer
Norrin		2.74	9.18	37.4	13.6 (monomer) 27.2 (dimer)	33.5	22.5	dimer
Norrin/Fz4-CRD	deglyc[f]	3.41	11.92	93.8	61.3 (2:2 complex) 44.2 (2:1 complex)	57.9	56.5	2:2 complex

[a]Rg is Radius of gyration, calculated from Guinier plot using AutoRg (Petoukhov et al., 2012).

[b]*D*max is the maximum dimension of the particle, calculated by GNOM (Svergun, 1992).

[c]The theoretical molecular weight ($\mathbf{MW_{Theoretical}}$) is predicated from amino acid sequence plus 2.35 kDa per N-linked glycosylation site for full glycosylated protein produced from HEK293T cells or 203 Da per site for deglycosylated protein produced from HEK293T cells in the presence of the N-glycosylation processing inhibitors, kifunensine with limited glycosylation and treated with endoglycosidase-F_1. See **Chapter2** for detailed procedure.

[d]The measured molecular weight ($\mathbf{MW_{Measured}}$) is calculated from forward scattering of sample ($I(0)$) by comparison with reference bovine serum albumin (BSA).

[e]The measured molecular weight ($\mathbf{MW_{Measured}}$) is obtained by dividing the Volume Porod (V_p (nm^3)) by 1.66 (Rambo and Tainer, 2011).

[f]The proteins were produced from HEK293T cells in the presence of kifunensine with limited glycosylation and treated with endoglycosidase-F_1.

[g]The proteins were produced from HEK293T cells with full glycosylation.

Table 4.3. List of hydrogen bond and salt-bridge interactions in the Norrin dimer interface, related to Figure 4.1.

Missense and nonsense mutations are highlighted as filled grey and purple backgrounds, respectively.

Monomer A	Distance (Å)	Monomer B
ARG 64 [NH2]	3.68	GLU 76 [OE2]
CYS 65 [N]	3.04	SER 75 [O]
CYS 65 [O]	2.99	SER 75 [N]
GLU 66 [OE1]	3.48	ARG 74 [NH1]
GLU 66 [OE2]	2.73	ARG 74 [NH1]
GLY 67 [N]	3.23	SER 73 [O]
GLY 67 [O]	3.07	SER 73 [N]
GLY 67 [O]	3.37	SER 73 [OG]
HIS 68 [NE2]	2.83	SER 70 [O]
SER 73 [N]	2.92	GLY 67 [O]
SER 73 [O]	2.98	GLY 67 [N]
SER 73 [OG]	3.55	GLY 67 [O]
SER 73 [OG]	2.85	CYS 96 [N]
SER 75 [N]	2.78	CYS 65 [O]
SER 75 [O]	2.76	CYS 65 [N]
SER 80 [N]	3.12	THR 119 [O]
SER 80 [O]	3.68	THR 119 [OG1]
SER 80 [O]	2.92	THR 119 [N]
THR 83 [O]	3.69	THR 119 [OG1]
CYS 96 [N]	2.81	SER 73 [OG]
THR 119 [N]	2.86	SER 80 [O]
THR 119 [O]	3.17	SER 80 [N]
THR 119 [OG1]	3.42	SER 80 [OG]
THR 119 [OG1]	3.50	SER 80 [O]

Table 4.4. Structural comparison of Norrin proteins and MBP-Norrin.
Pairwise superposition of dimeric Norrin molecules in the asymmetric units from the apo and complex structures and MBP-Norrin (PDB accession code: 4MY2) are shown as root mean square (r.m.s) deviation (Å)[a] values and the number of aligned Cα atoms (in brackets).

	Norrin I			**Norrin II**		**Norrin III**		**MBP-Norrin (PDB: 4MY2)**	**Norrin/Fz4-$CRD_{methylated}$**	**Norrin/ Fz4-CRD/SOS**
	Chain AB	Chain CD	Chain EF	Chain AB	Chain CD	Chain AB	Chain CD	Chain AB	Chain AB	Chain AB
Norrin I										
Chain AB	–									
Chain CD	0.77 (202)	–								
Chain EF	1.91 (189)	1.91 (191)	–							
Norrin II										
Chain AB	1.08 (190)	1.03 (193)	1.68 (182)	–						
Chain CD	0.94 (187)	0.94 (189)	1.80 (182)	0.82 (194)	–					
Norrin III										
Chain AB	1.34 (193)	1.22 (195)	1.55 (196)	0.96 (188)	1.20 (185)	–				
Chain CD	1.29 (194)	1.14 (194)	1.52 (190)	1.09 (190)	1.31 (189)	0.88 (194)	–			
MBP-Norrin (PDB: 4MY2)										
Chain AB	1.91 (189)	1.74 (189)	1.19 (196)	1.38 (183)	1.74 (188)	1.12 (192)	1.29 (191)	–		
Norrin/Fz4-$CRD_{methylated}$										
Chain AB	0.99 (196)	1.03 (194)	1.74 (185)	1.05 (192)	1.74 (194)	1.23 (189)	1.03 (188)	1.57 (186)	–	
Norrin/Fz4-CRD/SOS										
Chain AB	1.50 (196)	1.44 (199)	1.46 (196)	1.05 (185)	1.40 (188)	0.88 (196)	0.94 (195)	1.05 (192)	1.11 (199)	–

[a] The r.m.s deviation values were calculated for equivalent Cα atoms using CCP4 program SUPERPOSE using the SSM algorithm (Krissinel and Henrick, 2004).

4.5 The crystal structure of unliganded human Fz4-CRD

The Norrin binding partner, Fz4-CRD (residues 42-179) containing 10 conserved cysteine residues was crystallized in two crystal forms and their structures determined (**Table 4.1** and **Figure 4.5**) by using mouse Fz8-CRD (Dann et al., 2001) as a search model for molecular replacement. The structure of Fz4-CRD adopts a globular fold, consisting of four α helices and connecting loops (**Figure 4.5** and **4.6**), stabilized by five disulphide bridges (Cys45-Cys106, Cys53-Cys99, Cys90-Cys128, Cys117-Cys158, Cys121-Cys145). The N-acetylglucosamines on two N-linked glycosylation sites at Asn59 and Asn144 are visible in the electron density map (**Figure 4.5**), the conserved Asn59-linked glycosylation site is critical for protein folding (**Figure 4.6** and **3.9E**). Superposition of all Fz4-CRD molecules in the asymmetric units from two crystal forms reveals a well-ordered protein fold, except for the C-termini regions (**Figure 4.7A** and **Table 4.6**). The conserved disulphide bonds in Fz-CRD superfamily members are essential for functional activity. FEVR disease mutant C45Y results in protein mis-folding while retained in the endoplasmic reticulum, in agreement with Drosophila Smoothened (Smo) Cysteine-to-Alanine mutations (Rana et al., 2013; Zhang et al., 2011). Structural comparison shows Fz4-CRD resembles the CRDs of mouse Fz8 and secreted Frizzled-related protein 3 (sFRP3) with average r.m.s. deviation of 1.2 Å over 115 equivalent Cα atoms, in contrast to other CRDs of muscle-specific kinase (MuSk) and Smo showing structural conformational rearrangements with average r.m.s. deviation of 2.3 Å over 86 equivalent Cα atoms (**Table 4.6** and **Figure 4.7B-G**).

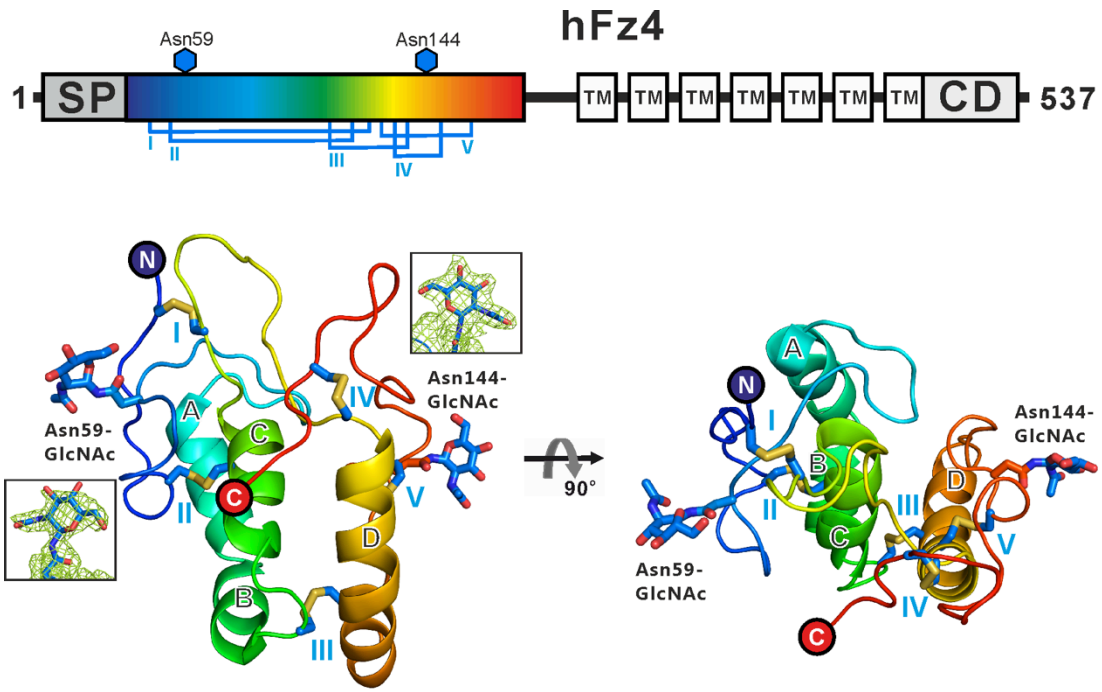


Figure 4.5. Crystal structure of unliganded human Fz4-CRD.
Schematic domain organization of human Fz4 (SP, signal peptide; CRD, cysteine-rich domain; TM. transmembrane domain; CD, cytoplasmic domain). The crystallization construct of Fz4 (residues 42-179) is coloured in rainbow. The disulphide bonds derived from the crystal structures are numbered and drawn as lines. The N-linked glycosylation sites are denoted as hexagons filled with blue. Cartoon representation of Fz4-CRD in rainbow colouring from blue N-terminus to red C-terminus. The α-helices are labelled A-D. Asn-linked N-acetyl-glucosamines (GlcNAc) and disulphide bonds are shown as blue sticks. The encircled N and C indicate the N- and C- termini.

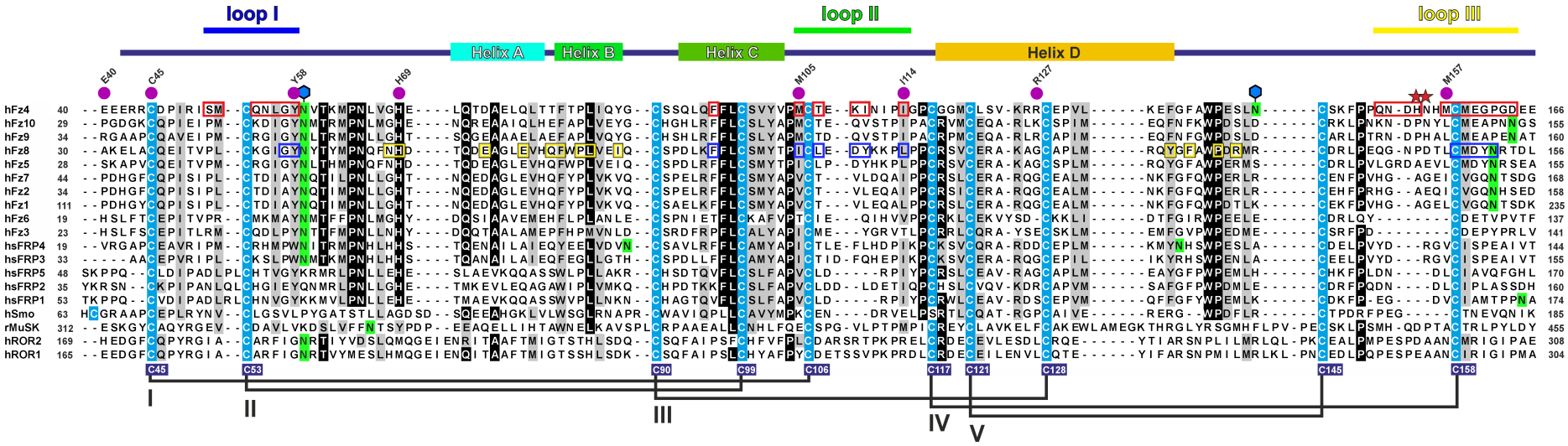


Figure 4.6. Multiple sequence alignment of cysteine-rich like domains.

Figure 4.6 (continued).
The sequences were aligned by using the ClustalW program (Larkin et al., 2007). Secondary structure assignment colouring corresponds to **Figure 4.5** and is displayed above the alignment. Identical and similar sequences are shaded in black and grey, respectively. Dashes indicate the sequence gaps introduced to optimize the sequence alignment. Sequence numbering corresponds to the full-length proteins including their signal sequences. The conserved cysteine residues (highlighted in cyan) form five disulphide bridges, drawn in black lines and labelled as I-V. Notably, Smo has a different cysteine pair arrangement in disulphide bridge IV (Nachtergaele et al., 2013; Rana et al., 2013). Cysteine residues of Fz4 are numbered with blue filled boxes below the sequence alignment. The red boxes denote the residues of Fz4 that contact Norrin, whereas residues of mFz8 are boxed in blue to indicate binding to xWnt8 index finger and in yellow for interaction with xWnt8 palmitoleic acid. Coloured lines above secondary structure elements indicate three specificity-conferring Fz4-CRD loops that interact with Norrin: blue for loop I; green for loop II; yellow for loop III (the assignments correspond to **Figure 4.16A**). The N-glycosylation sites are highlighted in green and those of Fz4 are marked by blue hexagons above the sequence. The purple dots mark residues linked to human retinal diseases (missense mutations; http://www.uniprot.org/uniprot/Q9ULV1) (Nikopoulos et al., 2010b). Red asterisks denote the residues of Fz4 involving in SOS binding. Sequences are from the following UniProt entries: hFz1, Q9UP38; hFz2, Q14332; hFz3, Q9NPG1; hfz4, Q9ULV1; hfz5, Q13467; hFz6, O60353; hFz7, O75084; hfz8, Q9H461; hfz9, O00144; hfz10, Q9ULW2; sfrp1 Q8N474; sfrp2, Q96HF1; sfrp3 Q92765; sfrp4, Q6FHJ7; sfrp5, Q5T4F7; hSmo, Q99835; rMuSk, Q62838; hROR1, Q01973; hROR2, Q01974. (h = human; r = rabbit; sfrp = secreted frizzled related protein; Smo = Smoothened; MuSk = muscle-specific kinase; ROR = tyrosine-protein kinase transmembrane receptor)

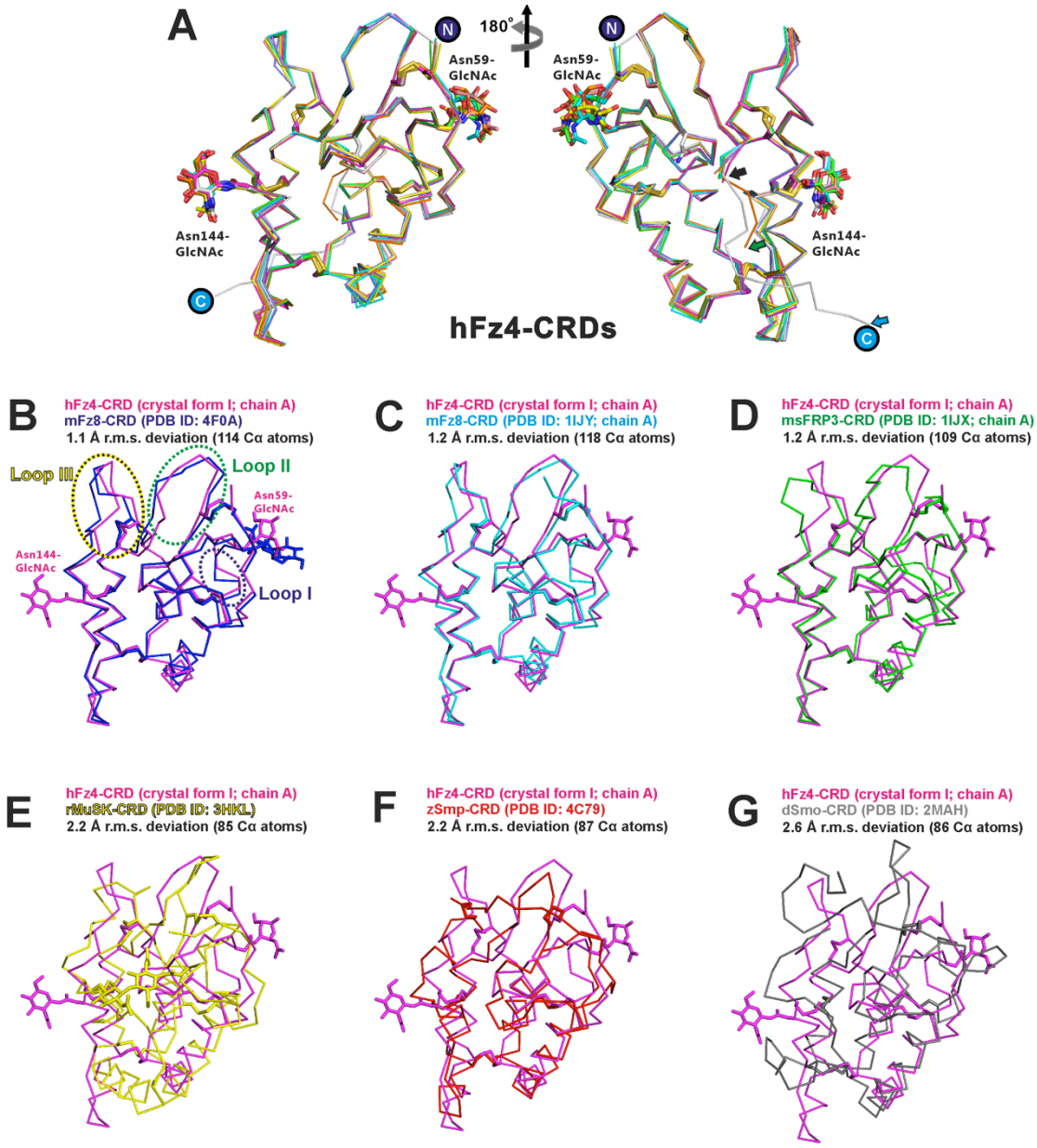


Figure 4.7. Superimposition of Fz4-CRD with CRDs of Fz-like proteins.

Figure 4.7 (continued).
(A) Superimposition of all molecules of unliganded Fz4-CRDs in the asymmetric units from crystal form I and II reveals no major conformational changes. The main difference between all Fz4-CRDs is the length of the C-termini based on whether the quality of the electron density is sufficient for model building (black, green, and cyan arrows indicate residue 162, 165, and 172, respectively). The N-linked glycans are shown as stick models. The encircled N and C indicate the N- and C- termini. See also **Table 4.5** for detailed information on superimposition. **(C)-(H)** Structural comparison of Fz4-CRD with CRDs of Fz-like proteins. Ribbon diagram of superimposition of Fz4-CRD crystal form I (magenta) with **(A)** mFz8-CRD from the complex structure of xWnt8/mFz8-CRD (cyan; PDB ID: 4F0A), **(B)** unliganded mFz8-CRD (cyan; PDB ID: 1IJY), **(C)** msFRP3-CRD (green; PDB ID: 1IJX), **(D)** rMuSk-CRD (yellow; PDB ID: 3HKL), **(E)** zSmo-CRD (red; PDB ID: 4C79), and **(F)** dSmo-CRD (red; PDB ID: 2MAH). N-linked glycans are shown as stick models. Three loop regions of Fz4-CRD used for Norrin binding are highlighted in a blue circle (loop I), green circle (loop II), and yellow circle (loop III). See also **Table 4.6** for detailed information on superimposition. (x = xenopus; m = mouse; r = rabbit; z = zebrafish; d = drosophila)

Table 4.5. Structural comparison of Fz4-CRD proteins.

Pairwise superposition of Fz4-CRD molecules in the asymmetric units from apo and complex structures are revealed as root mean square (r.m.s) deviation (Å)[a] values and the number of aligned Cα atoms (in brackets).

	Fz4-CRD (I)				**Fz4-CRD (II)**				**Norrin/Fz4-CRD$_{methylated}$**	**Norrin/ Fz4-CRD/SOS**
	Chain A	Chain B	Chain C	Chain D	Chain A	Chain B	Chain C	Chain D	hFz4-CRD	hFz4-CRD
Fz4-CRD (I)										
Chain A	–									
Chain B	0.20 (119)	–								
Chain C	0.64 (118)	0.65 (118)	–							
Chain D	0.64 (119)	0.69 (122)	0.30 (118)	–						
Fz4-CRD (II)										
Chain A	0.40 (119)	0.40 (119)	0.51 (118)	0.50 (119)	–					
Chain B	0.61 (119)	0.60 (119)	0.46 (118)	0.39 (119)	0.44 (119)	–				
Chain C	0.59 (118)	0.61 (118)	0.65 (117)	0.62 (118)	0.54 (118)	0.57 (118)	–			
Chain D	0.37 (119)	0.43 (119)	0.54 (118)	0.56 (119)	0.49 (119)	0.55 (119)	0.64 (118)	–		
Norrin/Fz4-CRD$_{methylated}$										
Fz4-CRD	0.62 (114)	0.66 (114)	0.72 (114)	0.74 (114)	0.60 (114)	0.76 (114)	0.65 (113)	0.70 (114)	–	
Norrin/Fz4-CRD/SOS										
Fz4-CRD	0.80 (113)	0.90 (115)	0.92 (113)	0.94 (113)	0.85 (113)	0.98 (113)	0.83 (112)	0.87 (114)	0.63 (115)	–

[a] The r.m.s deviation values were calculated for equivalent Cα atoms using CCP4 program of SUPERPOSE using the SSM algorithm (Krissinel and Henrick, 2004).

Table 4.6. Structural comparison of the CRD domain of Fz4 and Fz related proteins.
Pairwise superposition of apo and complex structures of Fz4-CRD and CRDs of Fz related proteins are shown as root mean square (r.m.s) deviation (Å)[a] values and the number of aligned Cα atoms in brackets. (m = mouse; x = xenopus; r = rabbit; z = sebrafish; d = drosophila; sfrp = secreted frizzled related protein; Smo = Smoothened; MuSk = muscle-specific kinase)

	Fz4-CRD (I)	**Fz4-CRD (II)**	**Norrin/hFz4-CRD$_{methylated}$**	**Norrin/ Fz4-CRD/SOS**	**mFz8-CRD**	**xWnt8/ mFz8-CRD**	**msFRP3-CRD**	**rMuSk-CRD**	**zSmo-CRD**	**dSmo-CRD**
	Chain A	Chain A	Fz4-CRD	Fz4-CRD	Chain A	mFz8-CRD	Chain A	Chain A	Chain A	Chain A
Fz4-CRD (I) Chain A	–									
Fz4-CRD (II) Chain A	0.40 (119)	–								
Norrin/Fz4-CRD$_{methylated}$										
hFz4-CRD	0.62 (114)	0.60 (114)	–							
Norrin/Fz4-CRD/SOS										
hFz4-CRD	0.80 (113)	0.85 (113)	0.63 (115)	–						
mFz8-CRD (PDB: 1IJY) Chain A	1.24 (118)	1.14 (117)	1.11 (110)	1.32 (111)	–					
xWnt8/mFz8-CRD (PDB: 4F0A)										
mFz8-CRD	1.10 (114)	1.05 (114)	1.16 (110)	1.27 (110)	0.62 (117)	–				
msFRP3-CRD (PDB: 1IJX) Chain A	1.21 (109)	1.06 (106)	1.27 (104)	1.38 (112)	1.40 (110)	1.21 (105)	–			
rMuSk-CRD (PDB: 3HKL) Chain A	2.23 (85)	2.23 (88)	2.26 (87)	2.67 (99)	2.60 (92)	2.52 (88)	2.51 (88)	–		
zSmo-CRD (PDB: 4C79) Chain A	2.17 (87)	2.14 (87)	2.21 (97)	2.14 (86)	2.61 (95)	2.46 (91)	2.40 (87)	2.63 (89)	–	
dSmo-CRD (PDB: 2MAH) Chain A	2.57 (86)	2.82 (86)	2.70 (87)	2.88 (85)	2.84 (86)	2.70 (81)	3.44 (81)	2.73 (83)	2.19 (99)	–

[a]The r.m.s deviation values were calculated for equivalent Cα atoms using CCP4 program SUPERPOSE using the SSM algorithm (Krissinel and Henrick, 2004).

4.6 The monomeric state of Fz-CRDs in solution

Fzs are members of the GPCR family (Nichols et al., 2013), known for formation of receptor dimers although it is unclear whether dimerization is mediated by the CRD, transmembrane helices or intracellular domain. In the case of Fz4, β-galactosidase complementation in combination with bioluminescence resonance energy transfer and split-yellow fluorescence protein assays suggest that Fz4 exists as dimer on the cell membrane in the absence of Norrin or Wnts (Kaykas et al., 2004; Ke et al., 2013). However, the ligand-independent receptor dimerization of Fz4 is not sufficient to active signalling (Ke et al., 2013; Xu et al., 2004). This kind of inactive pre-dimerization has also been reported for growth hormone, erythropoietin, and prolactin receptors (Gadd and Clevenger, 2006; Gent et al., 2002; Kubatzky et al., 2001).

Interestingly, I found that the Fz4-CRD structures have a conserved dimeric assembly with r.m.s. deviation of 0.7 Å over 238 equivalent Cα atoms from two crystal forms (**Figure 4.8A**). The dimer interface has an average 1330 $Å^2$ buried surface area, in agreement with the characteristics of known protein-protein interfaces (Lawrence and Colman, 1993). However, the Fz4-CRD dimer (front-to-front) is distinct from the previously reported Fz8-CRD dimer (back-to-back; **Figure 4.8B**), which has previously been suggested to mediate receptor dimerization (Dann et al., 2001). To verify the dimer assembly of Fz-CRDs observed in the crystal structure also occurs in solution, I used size-exclusion chromatography coupled to multiple angle light scattering (SEC-MALS). SEC-MALS results (**Figure 4.9A-D** and **Table 4.7**) show Fz4-, Fz5- and Fz8-CRDs exist

as monomers in solution up to a concentration of 50 μM, in agreement with previously reported SEC studies of Fz8-CRD and SEC-MALS analyses of other Fz-like receptors of MuSK-CRD and Smo-CRD (Nachtergaele et al., 2013; Stiegler et al., 2009). SAXS measurements further support the conclusion that Fz4-CRD is a monomer in solution up to a concentration of 290 μM (**Table 4.2** and **Figure 4.9E-F**). Taken together, my SEC-MALS and SAXS results reveal Fz-CRDs exist as monomers and suggest that this region may not be involved in receptor dimerization, indeed multiple GPCRs dimerize through their heptathelical transmembrane domains (Rios et al., 2001).

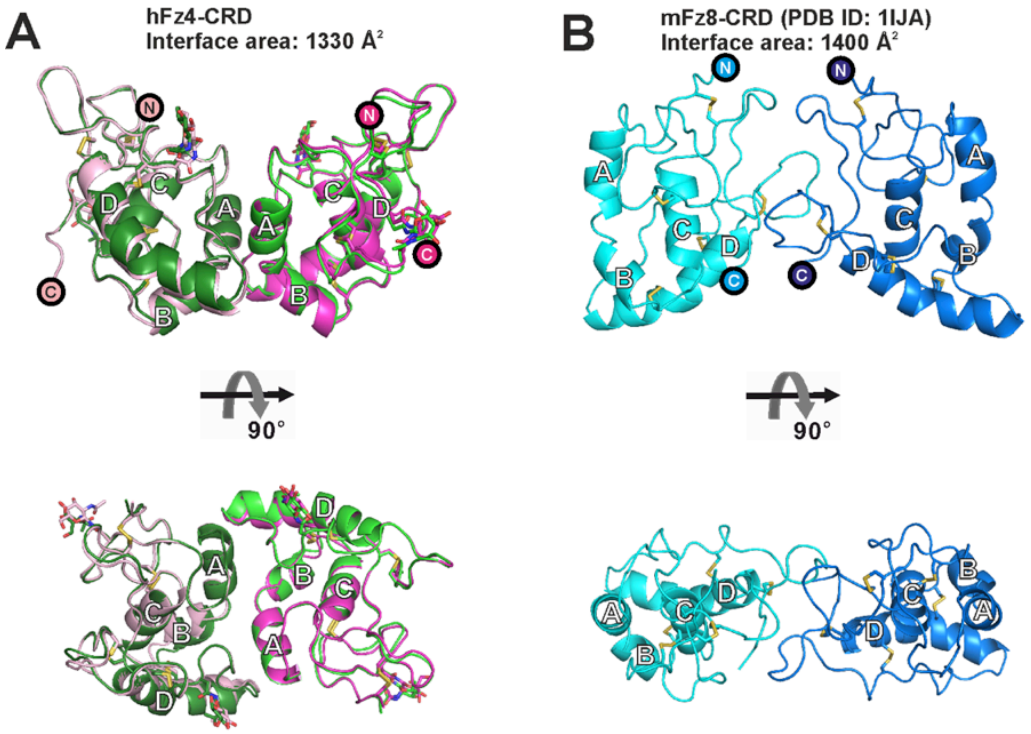


Figure 4.8. Distinct dimeric assembly of Fz4-CRD and mouse Fz8-CRD observed from crystal structures.
(A) The superimposition of Fz4-CRDs from two crystal forms, coloured as pink and magenta for crystal form I and green and forest for crystal form II. **(B)** The structure of dimeric mouse Fz8-CRD (PDB: 1IJA) coloured as cyan and blue. The encircled N and C denote the N- and C-termini.

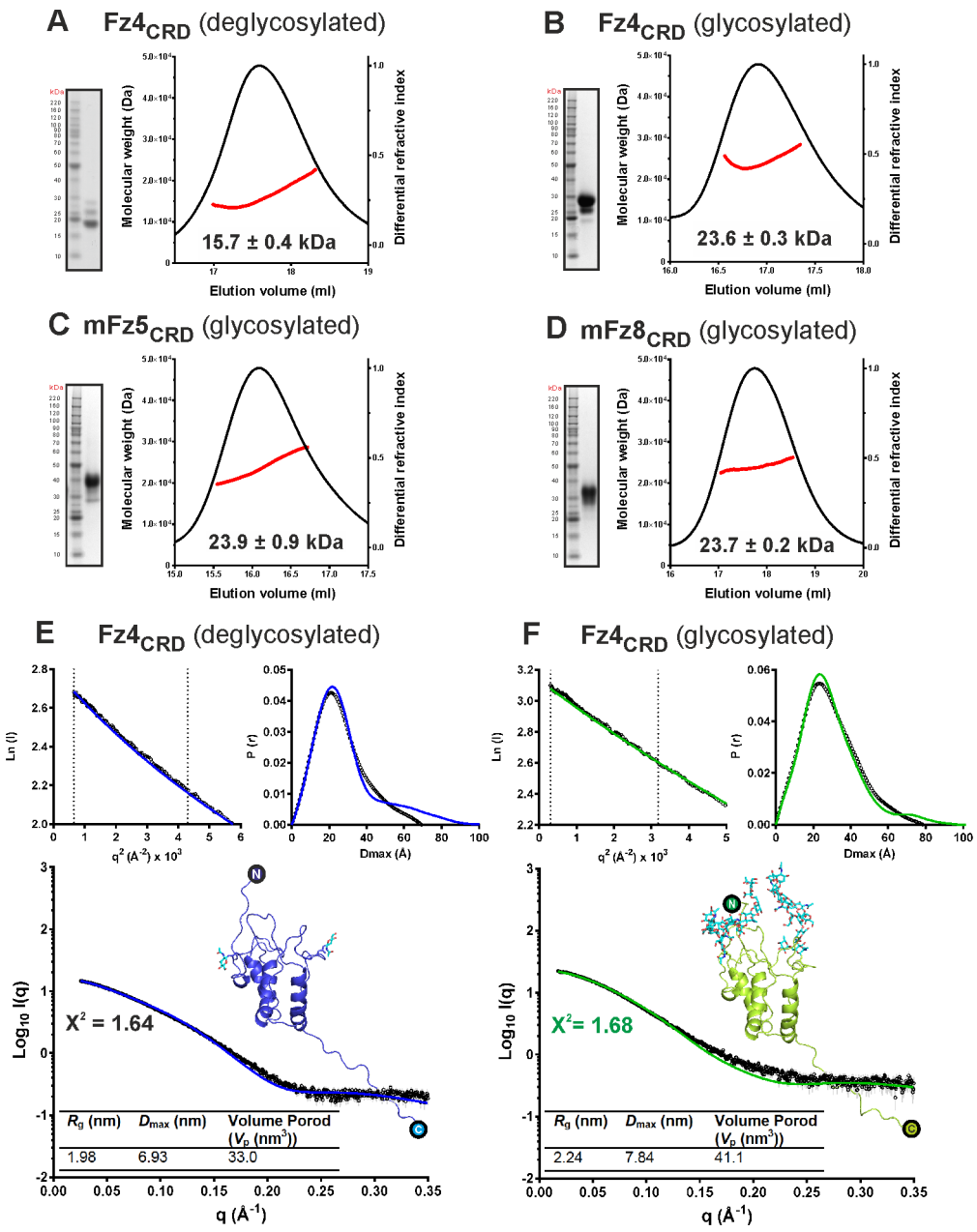


Figure 4.9. SEC-MALS and SAXS analyses of Fz-CRD proteins, related to Table 4.2 and Table 4.7.

Fz-CRD proteins form monomeric states in solution, although Fz4-CRD and Fz8-CRD are observed in dimeric assemblies in crystal structures (**Figure 4.8**) **(A)-(D)** SEC-MALS experiments of Fz-CRDs. **(A)** Deglycosylated Fz4-CRD produced from HEK293T cells in presence of kifunensine with limited glycosylation and treated with Endo-F_1. **(B-D)** Glycosylated Fz-CRDs produced from HEK293T cells with full glycosylation. **(B)** Glycosylated Fz4-CRD. **(C)** Glycosylated mouse Fz5-CRD. **(D)** Glycosylated mouse Fz8-CRD. The red line represents the molecular weight (right ordinate axis) and black lines show the differential refractive index (left ordinate axis) as well as SDS-PAGE (Inset). The numbers denote the corresponding molecular weights of each peak in kDa. **(E)** and **(F)** SAXS analyses

of deglycosylated and glycosylated Fz4-CRD solution structures. The experimental scattering data (black circles) and calculated scattering patterns (coloured lines) are shown to a maximal momentum transfer of q = 0.35 Å^{-1}, and the Fz4-CRD solution structure model is shown in cartoon representation. The upper left inset shows the experimental (black circles) and calculated (coloured lines) Guinier region. The dashed lines delimit the range of fitting for R_g analysis ($R_g \cdot S \leq 1.3$). The upper right inset shows the experimental (black circles) and calculated (coloured lines) pair distance distribution $P(r)$ curve. The measured molecular weights of 15.9 kDa and 19.9 kDa that were obtained from forward scattering of sample ($I(0)$) by comparison with reference bovine serum albumin and by dividing the Volume Porod by 1.66, respectively, are close to the molecular weight of monomeric deglycosylated Fz4-CRD (17.1 kDa). The estimates of molecular weights of glycosylated Fz4-CRD were 23.7 kDa and 24.7 kDa, respectively, close to the molecular weight of glycosylated monomer (21.4 kDa)

Table 4.7. **Molecular properties of the proteins determined by size-exclusion chromatography coupled to multiple angle light scattering (SEC-MALS).**

The measured molecular weights ($MW_{Measured}$) are in general agreement with theoretical molecular weights ($MW_{Theoretical}$) predicated based on the primary sequence plus 2.35 kDa per N-linked glycosylation site for protein produced in HEK293T cells, or 203 Da per site for deglycosylated proteins. SEC-MALS results suggest Fz-CRDs are monomers in solution and Norrin/Fz4-CRD forms a 2:2 complex.

Protein	Number of N-glyc sites	Glyc state	$MW_{Theoretical}$ (kDa) (+ N-glyc)	$MW_{Measured}$ (KDa)	Protein assembly
Fz4-CRD	2	deglyc[a]	16.7 (17.1)	15.7 ± 0.4	monomer
Fz4-CRD	2	glyc[b]	16.7 (21.4)	23.6 ± 0.3	monomer
mFz5-CRD	2	glyc[b]	17.5 (22.2)	23.9 ± 0.9	monomer
mFz8-CRD	2	glyc[b]	17.4 (22.1)	23.7 ± 0.2	monomer
Norrin/Fz4-CRD	4 (2:2 complex)	deglyc[a]	60.5 (61.3) (2:2 complex)	60.1 ± 0.4	2:2 complex
	2 (2:1 complex)		43.8 (44.2) (2:1 complex)		
Norrin/Fz4-CRD	4 (2:2 complex)	glyc[b]	60.5 (69.9) (2:2 complex)	61.3 ± 0.5	2:2 complex
	2 (2:1 complex)		43.8 (48.5) (2:1 complex)		

[a]The proteins were produced from HEK293T cells in the presence of the N-glycosylation processing inhibitor, kifunensine, resulting in limited glycosylation, and were treated with endoglycosidase-F_1 (see **Chapter 2 Materials and Methods** for detailed procedure).

[b]The proteins were produced from HEK293T cells with full glycosylation.

4.7 The crystal structure of human Norrin in complex with Fz4-CRD

Due to the limited structural knowledge available to link disease-associated mutations to functional understanding of Norrin and Fz4 pairs, the novel protein expression strategies described in **Chapter 3** were developed to produce sufficient complex protein for structural studies. Despite extensive efforts, Norrin/Fz4-CRD complex failed to generate diffracting crystals, until I either dimethylated surface-exposed lysine resides (Walter et al., 2006) or co-crystallized with the heparin mimic sucrose octasulfate (SOS) in response to previous studies showing the interaction of Norrin with glycosaminoglycans of HSPGs (Ohlmann et al., 2010; Perez-Vilar and Hill, 1997; Smallwood et al., 2007; Xu et al., 2004). Crystal structures of methylated complex (Norrin/Fz4-$CRD_{methylated}$; **Figure 4.2D-F**) and native complex bound with SOS (Norrin/Fz4-CRD/SOS) were determined at 2.3Å and 3.0Å resolution, respectively (**Table 4.1**). These two complex structures reveal different stoichiometries: Norrin/Fz4-$CRD_{methylated}$ is a 2:1 complex (**Figure 4.10A-B**), whereas Norrin/Fz4-CRD/SOS complex in a 2:2 stoichiometry shows a symmetric butterfly-shaped architecture (**Figure 4.11**). Superposition reveals a conserved complex binding interface, however there is a small difference in the orientation of the Fz4-CRD molecules possibly due to the tighter crystal packing in Norrin/Fz4-$CRD_{methylated}$ (**Figure 4.10C**). Each of the Fz4-CRDs interacts one-to-one with a separate Norrin chain, providing a Fz4 binding site with about 1680 $Å^2$ buried surface area (Complexation Significance Score is 1; The score (0-1) is defined as a maximal fraction of the total free energy of binding that belongs to the interface in stable

assemblies) and the two Fz4-CRDs diverge from the Norrin dimer without contacting each other (**Figure 4.11**). The arrangement of the C-termini of the complexed Fz4-CRDs is suitable for signalling in membrane-proximal regions.

To investigate the preference for complex formation in a 2:1 or 2:2 stoichiometry, I performed SEC-MALS and SAXS measurements. SEC-MALS results reveal Norrin interacts with Fz4-CRD in a 2:2 stoichiometry (**Figure 4.12A**), in agreement with a prior immunoprecipitation assay (Ke et al., 2013). SAXS measurements further support the crystal architecture of the 2:2 model (**Figure 4.12B**). The complex architecture of Norrin/Fz4-CRD is unique, distinct from other ligand and receptor or ligand and antagonist pairs of cystine knot growth factors, including transforming growth factor-β (TGF-β), bone morphogenetic protein (BMP), platelet-derived growth factor (PDGF), vascular endothelial growth factors (VEGF) and their corresponding receptors (**Figure 4.13**).

Neither Norrin nor Fz4-CRD undergoes large conformational changes upon complex formation, in particular the Fz4 binding sites are highly conserved (**Figure 4.14A-B**; **Table 4.4** and **4.5**). Complex formation reduces the structural flexibility (crystallographic B factor values) at the protein and SOS binding interface (**Figure 4.14C-D**). Interestingly, superposition of Norrin/Fz4-CRD complex with MBP-Norrin reveals that the Fz4-CRD partially clashes with MBP (**Figure 4.15**), this suggests that MBP may interfere with the Norrin interaction with Fz4-CRD consistant with MBP-Norrin only having 50% of the signalling activity of untagged Norrin in cell based assays (Ke et al., 2013).

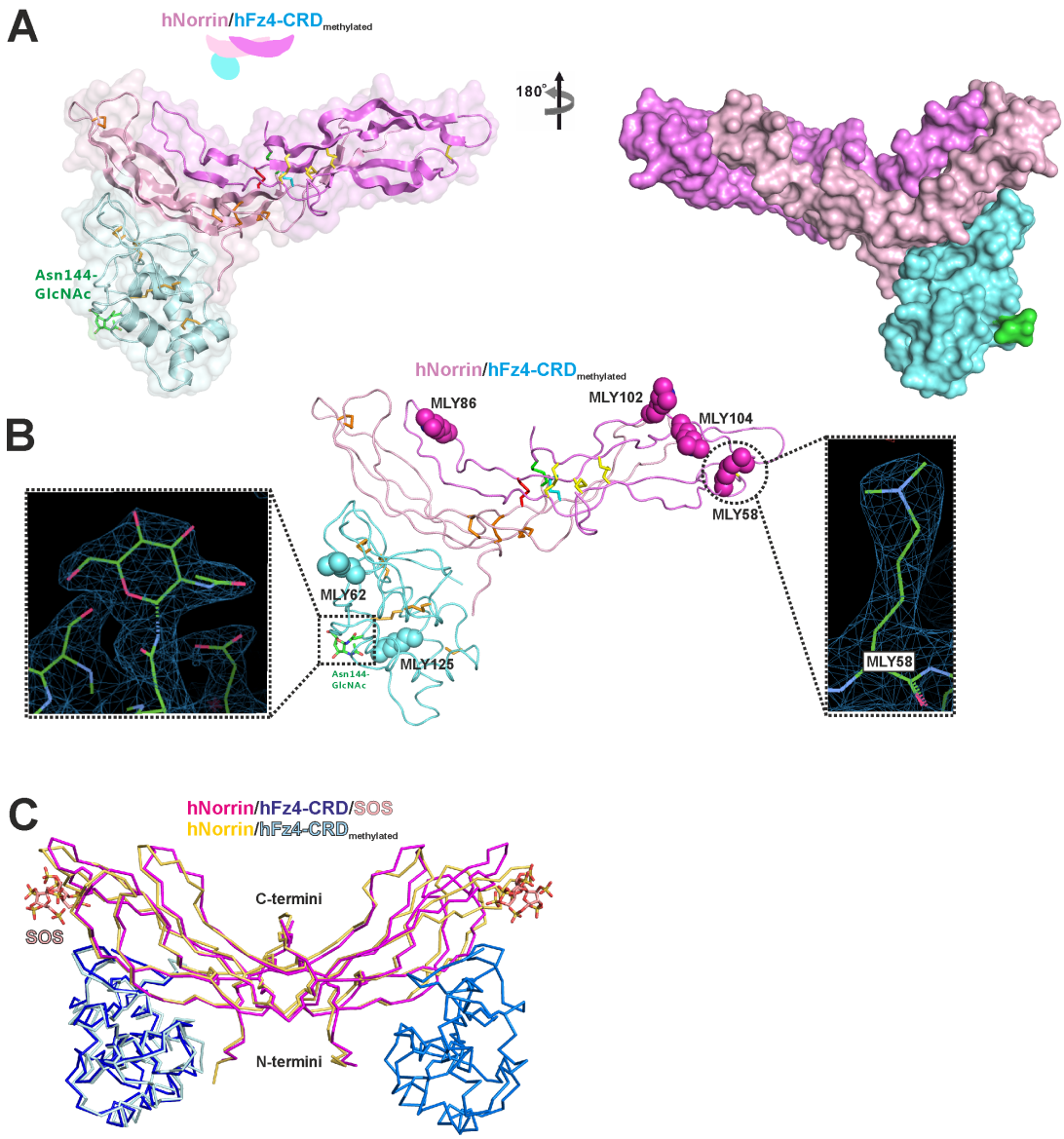


Figure 4.10. Crystal structure of methylated Norrin/Fz4-CRD complex and structural comparison.

(A) The crystal structure of Norrin/Fz4-CRD$_{methylated}$ forms a 2:1 complex (Norrin dimer, shown as pink and magenta and Fz4-CRD, show as cyan), which loses one molecule of Fz4-CRD during crystal lattice formation. The surface lysine residues are dimethylated to facilitate crystal lattice formation (Walter et al., 2006). The disulphide bonds are shown as sticks. The N-linked glycans are coloured in green. The encircled N and C denote the N- and C-termini. **(B)** Dimethylated lysine (MLY) residues on the protein surface are shown as sphere models. Close-up view of $2|F_O|-|F_C|$ electron density maps for MLY and N-glycans are contoured at 1.0 σ as blue mesh. **(C)** Norrin (yellow)/Fz4-CRD (cyan)$_{methylated}$ was superposed onto the Norrin (magenta)/Fz4-CRD (blue)/SOS (wheat) complex using Norrin as a reference.

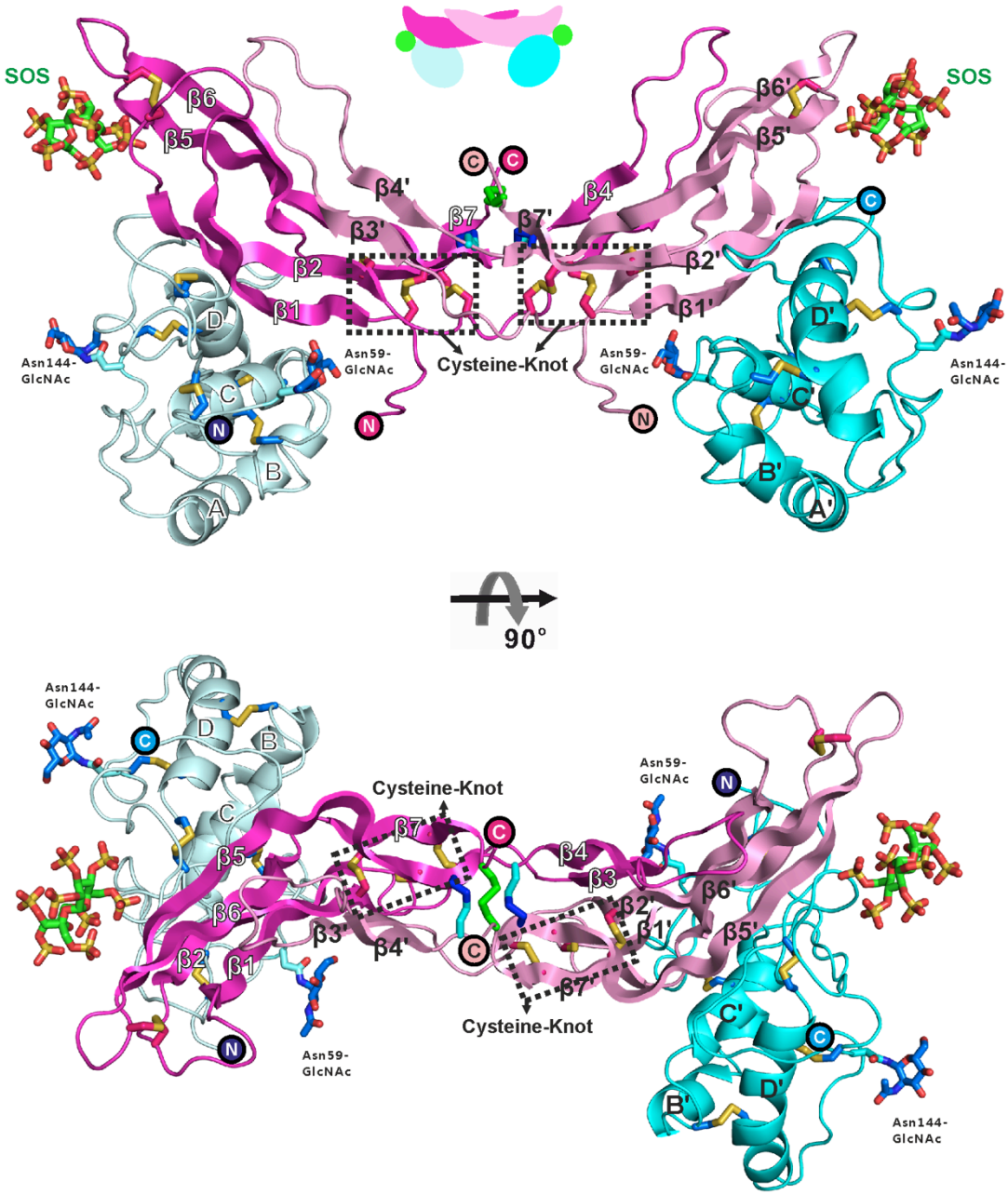


Figure 4.11. Crystal structure of Norrin/Fz4-CRD/SOS.
Ribbon representation of Norrin (magenta and pink) in complex with Fz4-CRD (cyan and pale cyan) and SOS (green; synthetic heparin analogue) as a 2:2 symmetric complex, illustrating secondary structure nomenclature. The intramolecular disulphide bonds are shown as sticks in blue for Fz4-CRD and magenta for Norrin. Three intermolecular disulphide bridges of Norrin coloured as in **Figure 4.1**. The molecules of N-linked glycans and SOS are shown as blue and green sticks, respectively.

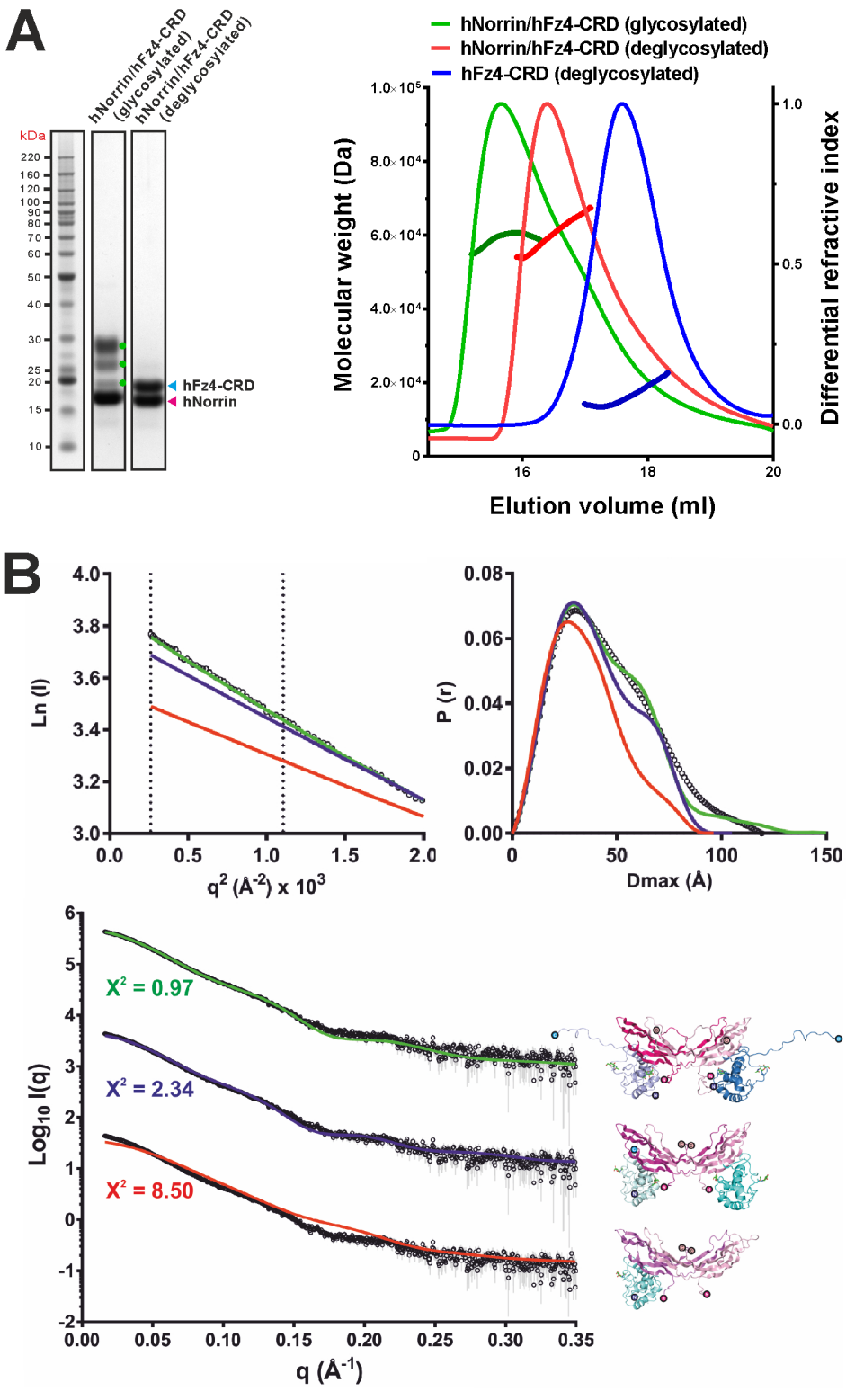


Figure 4.12. Solution behaviour of Norrin/Fz4-CRD complex.
(A) The SEC peak fraction shown in SDS-PAGE reveals Norrin in complex with Fz4-CRD (triplet bands for glycosylated Fz4-CRD, marked as green circles, represent glycosylation heterogeneity). SEC-MALS analyses reveal 2:2 complex of Norrin/Fz4-CRD (green and red lines for glycosylated and deglycosylated states, respectively) and monomer of Fz4-CRD (blue line) in solution. The profile

of molecular weight (right ordinate axis) and differential refractive index (left ordinate axis) are shown as thick and thin lines, respectively. **(B)** SAXS analysis of Norrin/Fz4-CRD solution structure and stoichiometry. Experimental scattering data (black circles) and calculated scattering patterns (coloured lines) are shown to a maximal momentum transfer of q = 0.35 $Å^{-1}$. Individual data: fit pairs are displaced along an arbitrary y axis to allow for better visualization. Bottom curve: Norrin/Fz4-CRD 1:2 complex crystal structure (red line). Middle curve: Norrin/Fz4-CRD 2:2 complex crystal structure (blue line). Top curve: modelled Norrin/Fz4-CRD 2:2 complex crystal structure (green line). Structural models are shown in cartoon representation. The top right inset shows the experimental (black circles) and calculated (coloured lines) Guinier region. The dashed lines delimit the range of fitting for R_g analysis ($R_g \cdot S \leq 1.3$). The bottom right inset shows the experimental (black circles) and calculated (coloured lines) pair distance distribution $P(r)$ curves.

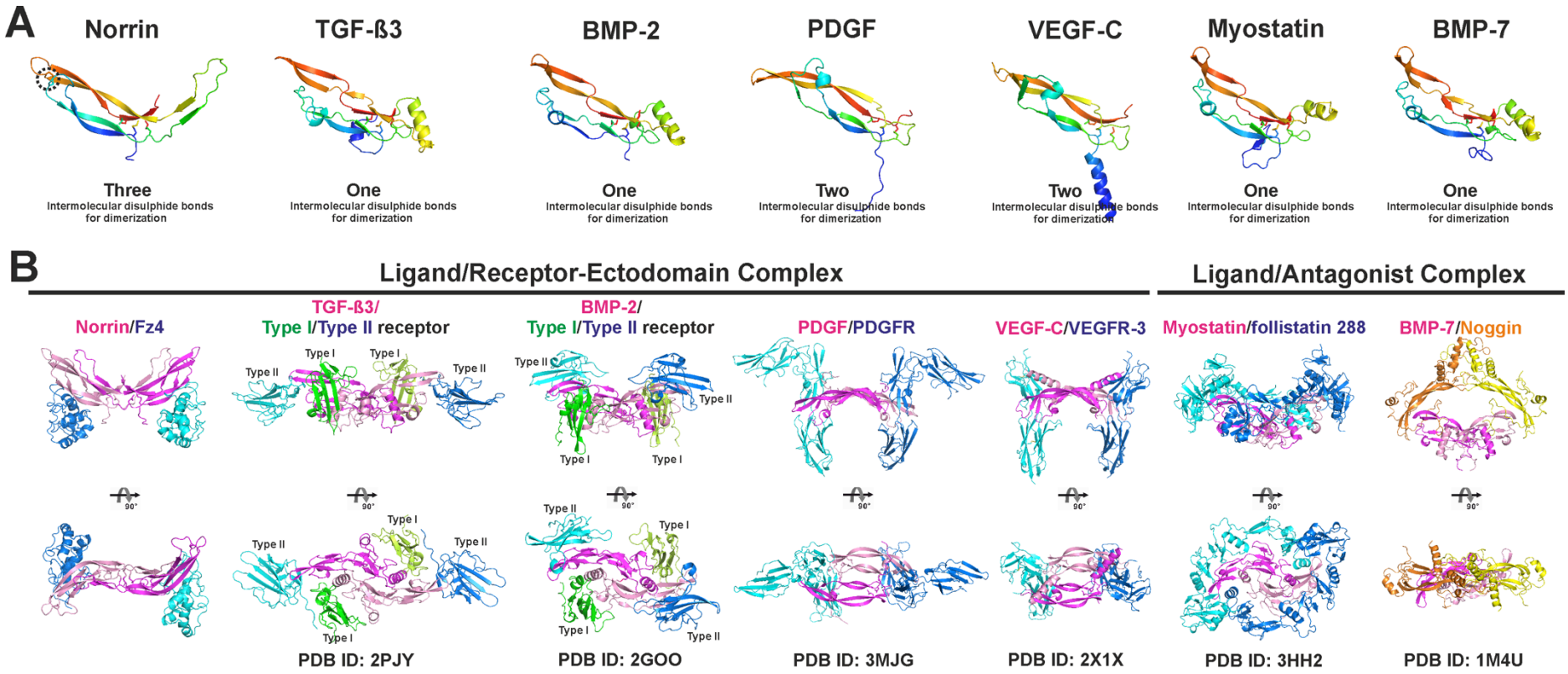


Figure 4.13. Structural comparison of cystine knot growth factors **monomers and their ternary complexes.**

Figure 4.13 (continued).
The structure of Norrin is distinct from other cystine knot growth factors and Norrin has a unique three intermolecular disulphide bonds arrangement, rather than the one or two intermolecular disulphide bonds found in other TGF-β superfamily proteins. The Norrin specific intramolecular disulphide bond is highlighted with a black dotted circle. The complex interface of Norrin/Fz4-CRD is unique. Norrin uses β1, β2, β5, and β6 for interaction with Fz4-CRD, which is an all helix structure unlike the mainly β-strand structures of cystine knot growth factor binding partners. **(A)** Cartoon representation of a single chain of cystine knot growth factors, coloured as rainbow from blue N-terminus to red C-terminus. Each structure was superimposed with the Norrin monomer and presented in the same view. **(B)** Comparison of ternary complex formation is shown as a ribbon diagram of ligand/receptor-ectodomain and ligand/antagonist complex, including Norrin (dimer, magenta and pink) and Fz4-CRDs (cyan and blue), transforming growth factor-β3 (TGF-β3; dimer, magenta and pink) in complex with Type I (green and lemon) and Type II (blue and cyan) receptors, bone morphogenetic protein (BMP-2; dimer, magenta and pink) bound with Type I (green and lemon) and Type II (blue and cyan) receptors, platelet-derived growth factor (PDGF; dimer, magenta and pink) in complex with its receptors (PDGFR; blue and cyan), vascular endothelial growth factor-C (VEGF-C; dimer, magenta and pink) in complex with its receptors (VEGFR-3; blue and cyan), myostatin (dimer, magenta and pink) and its antogonists (follistatin 288; blue and cyan), and BMP-7 (dimer, magenta and pink) bound with its antagonists (Noggin; orange and yellow). The PDB identifiers are shown below the structural representation.

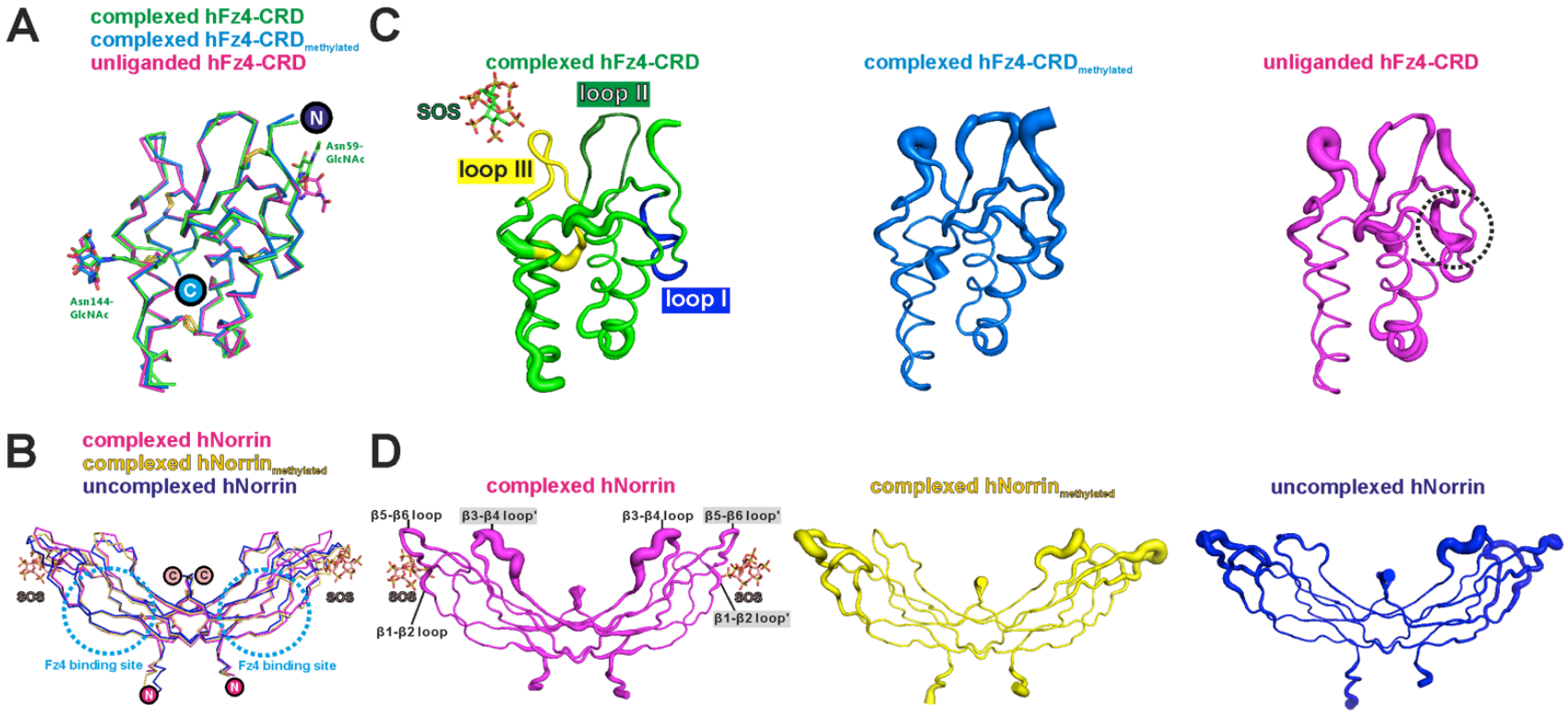


Figure 4.14. There are no large conformational changes; however, there are changes in structural flexibility upon complex formation and SOS binding.

Figure 4.14 (continued).
(A) There are no large conformational changes of Fz4-CRDs upon complex formation. Superimposition of Fz4-CRD (green) from Norrin/Fz4-CRD/SOS complex with Fz4-CRD (cyan) from Norrin/Fz4-CRD$_{methylated}$ and unliganded Fz4-CRD (magenta) crystal form II (chain D) is presented as a ribbon diagram. N-linked glycans are shown as stick models. The encircled N and C denote the N- and C-termini. **(B)** There are no large conformational changes of the Fz4 binding site on the Norrin structures. Structural comparisons of Norrin (magenta) from Norrin/Fz4-CRD/SOS complex, Norrin (yellow) from Norrin/Fz4-CRD$_{methylated}$ and uncomplexed Norrin (blue) crystal form I (chain A and B) are shown as a ribbon diagram. The cyan dotted circles denote the Fz4 binding site on Norrin. The encircled N and C denote the N- and C-termini. **(C)** Representative Fz4-CRDs with colour-coding corresponding to **(A)** displayed according to the B factor of the Cα atoms as defined by the diameter of the Cα tube (small tube means structural rigidity; large tube indicates structural flexibility). Fz4-CRD loops for Norrin binding are highlighted as blue (loop I), green (loop II), and yellow (loop III). The flexibilities of loop I and III are reduced upon complex formation and SOS binding, respectively. **(D)** Representative Norrin with colour-coding corresponding to **(B)** displayed according to the B factor of the Cα atoms. The SOS binding site (mainly on β5-β6 loop) becomes rigid upon SOS binding (ligand induced fit). See also **Table 4.4 and 4.5** for detailed information of superimpositions.

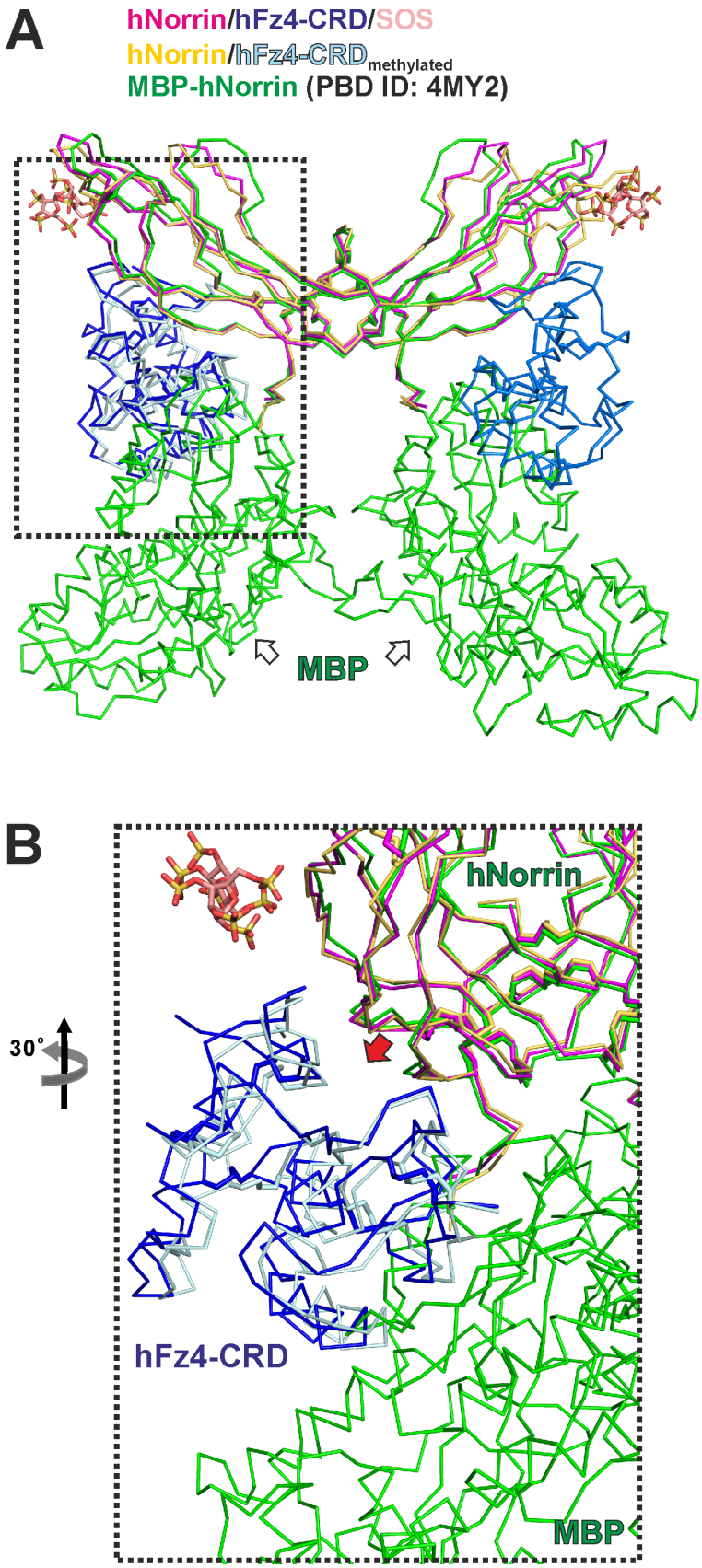


Figure 4.15. Structural comparison of Norrin/Fz4-CRD complex with MBP-Norrin.

Figure 4.15 (continued).
Structural analyses indicate that MBP of MBP-Norrin would interfere with Fz4-CRD binding to Norrin. This observation may explain why MBP-Norrin only retains half of the signal activity of untagged Norrin (Ke et al., 2013). **(A)** Superimposition of MBP-Norrin (green; PDB ID: 4MY2) onto Norrin structures of Norrin (magenta)/ Fz4-CRD (blue)/SOS (wheat) and Norrin (yellow)/ Fz4-CRD $(cyan)_{methylated}$. **(B)** Close-up view of steric clashes (indicated by a red arrow) between Fz4-CRD and MBP.

4.8 Norrin has distinct binding sites for Fz4, Lrp5/6, and HSPGs

The Fz4 binding site (**Figure 4.16A**) has contributions from Norrin hairpin A and B (including β1, β2, β5, and β6) and contacts with three loops (I, II, and III; **Figure 4.3**) and one residue (Phe96 for hydrophobic interaction) on helix C of Fz4-CRD (**Figure 4.6**). The integrity of the architecture of hairpin A and B is stabilized via Norrin unique disulphide bridge II (**Figure 4.16A**). Disruption of this disulphide bridge affects Fz4-CRD binding ability and signalling activity (Smallwood et al., 2007).

Specifically, Fz4-CRD loop I binds to Norrin by hydrogen bond interactions (**Figure 4.16B**). Fz4-CRD loop II provides extensive hydrophobic contacts to Norrin plus one salt-bridge interaction of Fz4-CRD Lys109 with Norrin Asp46 (**Figure 4.16C**). Fz4-CRD loop III interacts with Norrin via extensive hydrogen bond networks and additional hydrophobic contacts (**Figure 4.16D**). The conclusion that this is the functionally relevant Fz4 binding site is further supported by the observation that interface-contact residues highly overlap with disease-associated mutations (**Figure 4.3** and **4.6**; **Table 4.8**). Interactions with SOS (**Figure 4.2G**) involve the positively charged side chains of Lys58, Arg107, Arg109, and Arg115 on Norrin plus His154 and Asn155 on Fz4-CRD loop III (**Figure 4.16E**), these residues define a likely HSPG binding site. This binding site is in agreement with prior studies of Norrin interactions with extracellular matrix and heparin (Ohlmann et al., 2010; Perez-Vilar and Hill, 1997), as well as the binding affinity of Norrin with Fz4-CRD which is enhanced in the presence of

heparin (Smallwood et al., 2007). Very recently Capurro *et al*., reported that Fz-CRDs including Fz4 bind directly to the glycosaminoglycans of Glypican-3 (Capurro et al., 2014), one of the HSPGs in the human genome, and that the interactions are involved in signalling complex formation. In combination, these observations corroborate my structural finding that Fz4-CRD directly interacts with SOS.

Wnt interaction with co-receptor Lrp5/6-ECD is an essential factor for activation of canonical Wnt signalling (Bourhis et al., 2010; Grumolato et al., 2010), and signalling is also highly dependent on the Norrin and Lrp5/6-ECD interaction (Ke et al., 2013; Xu et al., 2004). To identify potential Norrin residues involved in this interaction, I performed a comprehensive analysis based on the criteria: solvent exposure (not at Norrin dimer interface), implicated by disease-associated mutations, and neither Fz4-CRD nor HSPGs binding sites (**Table 4.8**). Five residues (Lys54, Arg90, Arg97, Gly112, and Arg121) relevant to diseases were highlighted by this analysis and surprisingly they form a continuous positively charged patch, with a concave-shape, on the nearly opposite side of the Norrin surface from the Fz4 binding site (**Figure 4.16F**). Interestingly, previous structural studies revealed an acidic charged region on the Lrp6-ECD surface, which appears well suited to interact with this positively charged patch (Ahn et al., 2011; Bourhis et al., 2011; Chen et al., 2011; Cheng et al., 2011). The identification of this patch as the Lrp5/6 binding surface is further supported by previous systematic mutational studies, which indicate that the mutation of Norrin residues K54E, R90E, R97E, or R121E impairs the signalling activity but

does not affect Fz4-CRD binding. I cannot exclude the possibility that other factors bind at this surface and that this is the cause of the reduction of signalling activity. One possibility to consider is Tspan-12; however, it has been reported that Norrin does not directly interact with Tspan-12, although Norrin mediated signalling does require Tspain-12 to enhance activity (Junge et al., 2009). I therefore propose this concave-shaped patch (**Figure 4.16F**) as the Lrp5/6 binding site.

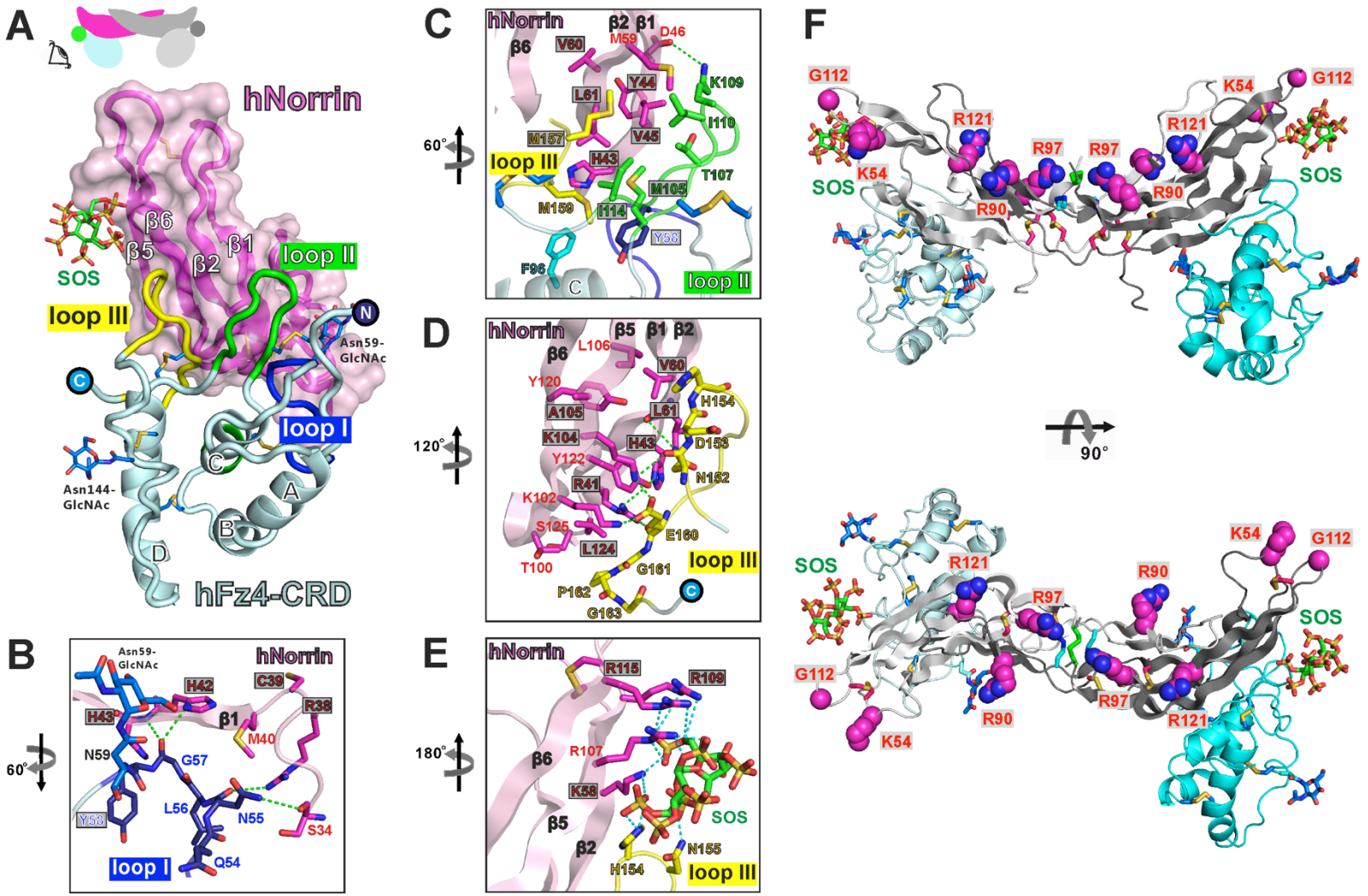


Figure 4.16. Detailed interactions of binding sites.

Figure 4.16 (continued).
(A) Interactions of the Norrin/Fz4-CRD/SOS complex in side view coloured as in **Figure 4.11**. The loops of Fz4-CRD involving in Norrin binding are coloured in blue (loop I), green (loop II), and yellow (loop III). Structural features are described in **Figure 4.11**. **(B-E)** Detailed view of the binding interface in the Norrin/Fz4-CRD/SOS complex. Colour-coding and rotation corresponds to **(A**). Selected residues involved in binding are shown as sticks and coloured in red (Norrin), blue (loop I), green (loop II), yellow (loop III), and cyan (Phe96 on helix C of Fz4-CRD) and those associated with disease mutations are highlighted in grey filled black boxes. Dotted lines denote hydrogen bonds. To give a better view of the diagram, some residues with minor contributions to the interface are omitted; see **Table 4.8** for the detailed information on binding sites. **(B)** Interactions between Fz4-CRD loop I (blue) and Norrin (magenta). **(C)** Norrin (magenta) interaction with Fz4-CRD loop II (green) and part of loop III (yellow) showing the contribution of hydrophobic interactions. **(D)** Interactions of Fz4-CRD loop III (yellow) with Norrin (magenta). **(E)** SOS (green sticks) binding to Norrin (magenta) and Fz4-CRD loop III (yellow). **(F)** Cartoon representation of Norrin (grey) in complex with Fz4-CRD (cyan). Disulphide bonds, SOS, and N-linked glycans are shown as sticks with colour-coding as in **Figure 4.11.** Residues in the potential Lrp5/6 binding site are shown as sphere models (atom colouring: magenta, carbon; blue, nitrogen; red, oxygen). The grey filled boxes highlight residues associated with disease mutations (**Figure 4.3** and **Table 4.8**).

Table 4.8. Classification of Norrin functional domains and disease-associated mutations, related to Figure 4.3.

The Norrin sequence (residues 25-133; mature form) is used for analyses and categorization (including dimer interface, Fz4 binding site, HSPGs binding site and Lrp5/6 binding site) on basis of the structural and functional results presented here in combination with previous studies (Ke et al., 2013; Smallwood et al., 2007). Norrin disease-association mutations (including missense, frame-shift, nonsense) are identified from several retinal disorders including Norrie Disease, Familial Exudative Vitreoretinopathy, Retinopathy Of Prematurity, Coats' disease, Persistent Fetal Vasculature, Primary Retinal Dysplasia, Venous Insufficiency, and Primary Hyperplastic Persistent Vitreous. The information on Norrin disease-association mutations is taken from one key reference (Nikopoulos et al., 2010b) and the following two websites.

http://www.uniprot.org/uniprot/Q00604

http://www.medmolgen.uzh.ch/research/eyediseases/norriedisease/Norrinmutations.html

Footnotes for some resides involved in two distinct binding sites.

[a] Residue Tyr44 uses its side-chain for dimer interface contact, whereas its backbone is involved in the Fz4 binding site.

[b] Residues Arg97 and Arg121 use their backbones for dimer interface contacts, whereas their side-chains are involved in the putative Lrp5/6 binding site.

[c] Residues Tyr120 and Tyr122 use their backbones for dimer interface contacts, whereas their side-chains are involved in the Fz4 binding site.

Residues	Dimer interface	Fz4 binding site	HSPGs binding site	Lrp5/6 binding site	Disease-association mutations		
LYS 25							
THR 26							
ASP 27							
SER 28							
SER 29					S29X		
PHE 30							
ILE 31							
MET 32							
ASP 33		Fz4 binding					
SER 34		Fz4 binding					
ASP 35					D35fs		
PRO 36		Fz4 binding					
ARG 37							
ARG 38		Fz4 binding			R38C		
CYS 39					C39R		
MET 40		Fz4 binding					
ARG 41		Fz4 binding			R41K	R41S	R41T
HIS 42		Fz4 binding			H42E	H42R	
HIS 43		Fz4 binding			H43Q	H43R	H43fs
TYR 44	Dimer inf[a]	Fz4 binding[a]			Y44C	Y44X	

VAL 45		Fz4 binding			V45E	V45M	V45fs
ASP 46		Fz4 binding					
SER 47		Fz4 binding					
ILE 48	Dimer inf						
SER 49	Dimer inf						
HIS 50	Dimer inf						
PRO 51	Dimer inf						
LEU 52							
TYR 53							
LYS 54				Lrp5/6 binding	K54N		
CYS 55					C55R	C55F	
SER 56							
SER 57					S57X		
LYS 58		Fz4 binding	HSPGs binding		K58N		
MET 59		Fz4 binding					
VAL 60		Fz4 binding			V60E		
LEU 61		Fz4 binding			L61F	L61I	L61P
LEU 62	Dimer inf						
ALA 63	Dimer inf				A63D	A63S	
ARG 64	Dimer inf						
CYS 65	Dimer inf				C65W	C65Y	
GLU 66	Dimer inf						
GLY 67	Dimer inf				G67E	G67R	
HIS 68	Dimer inf						
CYS 69	Dimer inf				C69S	C69fs	
SER 70	Dimer inf						
GLN 71	Dimer inf						
ALA 72	Dimer inf						
SER 73	Dimer inf				S73X		
ARG 74	Dimer inf				R74C		
SER 75	Dimer inf				S75C	S75P	
GLU 76	Dimer inf						
PRO 77	Dimer inf						
LEU 78	Dimer inf						
VAL 79	Dimer inf						
SER 80	Dimer inf						
PHE 81	Dimer inf						
SER 82							
THR 83	Dimer inf						
VAL 84	Dimer inf						
LEU 85	Dimer inf						
LYS 86							
GLN 87							
PRO 88	Dimer inf						

PHE 89	Dimer inf				F89L	F89fs		
ARG 90				Lrp5/6 binding	R90C	R90P		
SER 91	Dimer inf							
SER 92					S92P			
CYS 93	Dimer inf				C93R			
HIS 94	Dimer inf				H94fs			
CYS 95	Dimer inf				C95F	C95R	C95Y	C95X
CYS 96	Dimer inf				C96W	C96Y	C96fs	
ARG 97	Dimer inf[b]			Lrp5/6 binding[b]	R97P			
PRO 98	Dimer inf				P98L			
GLN 99								
THR 100		Fz4 binding						
SER 101	Dimer inf				S101F			
LYS 102		Fz4 binding						
LEU 103	Dimer inf				L103V			
LYS 104		Fz4 binding			K104N	K104Q		
ALA 105		Fz4 binding			A105T			
LEU 106		Fz4 binding						
ARG 107			HSPGs binding					
LEU 108	Dimer inf				L108P			
ARG 109			HSPGs binding		R109X			
CYS 110					C110G	C110R	C110S	C110X
SER 111								
GLY 112				Lrp5/6 binding	G112E			
GLY 113								
MET 114								
ARG 115			HSPGs binding		R115L			
LEU 116	Dimer inf							
THR 117	Dimer inf							
ALA 118	Dimer inf				A118D			
THR 119	Dimer inf							
TYR 120	Dimer inf[c]	Fz4 binding[c]			Y120C	Y120X		
ARG 121	Dimer inf[b]			Lrp5/6 binding[b]	R121G	R121L	R121W	R121Q
TYR 122	Dimer inf[c]	Fz4 binding[c]						
ILE 123	Dimer inf				I123N			
LEU 124		Fz4 binding			L124F			
SER 125		Fz4 binding 5						
CYS 126					C126S	C126X		
HIS 127								
CYS 128					C128R	C128X		
GLU 129								
GLU 130								

CYS 131	**Dimer inf**				
ASN 132	**Dimer inf**				**N132fs**
SER 133					

4.8.1 Verification of Fz4 binding site

Overall, the Fz4 binding site (**Figure 4.17A**) comprising hydrophobic interactions interspersed with hydrophilic patches (complementarily charged; **Figure 4.17B**) is in excellent agreement with previously reported disease-associated mutations of Norrin and Fz4-CRD (**Figure 4.17C**), as well as consistent with a high level of surface residue conservation (**Figure 4.17D**). To dissect the Fz4 binding site, I selected Norrin interface residues for mutagenesis (**Figure 4.17A**) and performed a binding assay by using surface plasmon resonance (SPR) experiments. Untagged and monomeric Fz4-CRD binding to a SPR chip coupled with Norrin was measured. The SPR measurements show a micromolar equilibrium dissociation constant between Norrin and Fz4-CRD: binding is surface density independent (**Figure 4.17E** and **4.18**). Mutations of either H43N/V45T or L61N/A63S, which result in the introduction of an N-linked glycosylation site in the Fz4 binding site on Norrin, completely abolish the interaction (**Figure 4.19B-C**). Norrin disease-associated mutants V45E and L61P/A63D lose the binding affinity with Fz4-CRD (**Figure 4.17E** and **4.19D-E**). Two Norrin mutants, R41E/H43E and R38E/R41S/H43E/K102E/K104E, designed to disrupt hydrophilic interactions of the Fz4 binding site, show profoundly impaired the interactions with Fz4-CRD (**Figure 4.19F-G**). I further corroborated the Fz4 binding site by introducing an N-linked glycosylation site on the β1-β2 loop or β5-β6 loop of Norrin, which are outside the binding interface (**Figure 4.17A**). As expected, these Norrin mutants, L52N/K54S and M114N/L116S, show the same binding affinity with *K*d values of 1.3 μM and 1.1 μM, respectively, as wild-type (**Figure 4.19H-I**).

The cell-based Wnt/β-catenin responsive luciferase assays (**Figure 4.17F**) further support the significance of the Fz4 binding site. Norrin mutants losing binding to Fz4-CRD also fail to induce the luciferase reporter activity (**Figure 4.17F**), in excellent agreement with the SPR results (**Figure 4.17E** and **4.19**) and prior genetic data (Ke et al., 2013; Smallwood et al., 2007; Xu et al., 2004). But, the Norrin L52N/K54S mutant also reveals a modest reduction of reporter activity (**Figure 4.17F**). This is in agreement with my previous analysis of binding sites because Lys54 is a disease mutation site and proposed to interact with Lrp5/6-ECD (**Figure 4.16F**) for transduction of signalling. The Norrin M114N/L116S mutant exhibits half of the signalling activity of wild-type (**Figure 4.17F**), presumably because the mutation sites are located adjacent to Arg115, a key residue involved in SOS binding and thereby may affect the interactions with HSPGs. Taken together, mutagenesis in combination with SPR and cell-based assays validates the observed Fz4 binding site from the crystal structures and provides insights into how missense mutations on Norrin disrupt the interaction with Fz4 and lead to impair the signalling.

Previous cell surface histochemical assays have indicated that Norrin binds to Fz4-CRD and does not detectably interact with the other 9 Fz-CRDs (Smallwood et al., 2007; Xu et al., 2004). However, quantitative determinations of the binding affinity of Norrin with different Fz-CRDs are lacking. I used SPR experiments to measure the affinities of Norrin with mouse Fz5- and Fz8-CRD as well as with human Fz7-CRD, Fz-CRDs were in monomeric states without artificial

dimerization effects resulting from Fc fusion. SPR measurements (**Figure 4.17G** and **4.20**) show that Norrin has greatest affinity with Fz4-CRD (*K*d: 1 μM), intermediate affinities to Fz5- and Fz8-CRD with about 40-fold and 60-fold decrease in binding affinities (*K*d: 42 μM and *K*d: 64 μM, respectively), and no binding to Fz7-CRD. In combination, these results confirm that Norrin binding to Fz4-CRD is a selective and high affinity-binding pairing relative to interactions with other Fz-CRDs. However, it remains to be clarified whether the low affinity interactions of Norrin with other Fzs play any functional role *in vivo*.

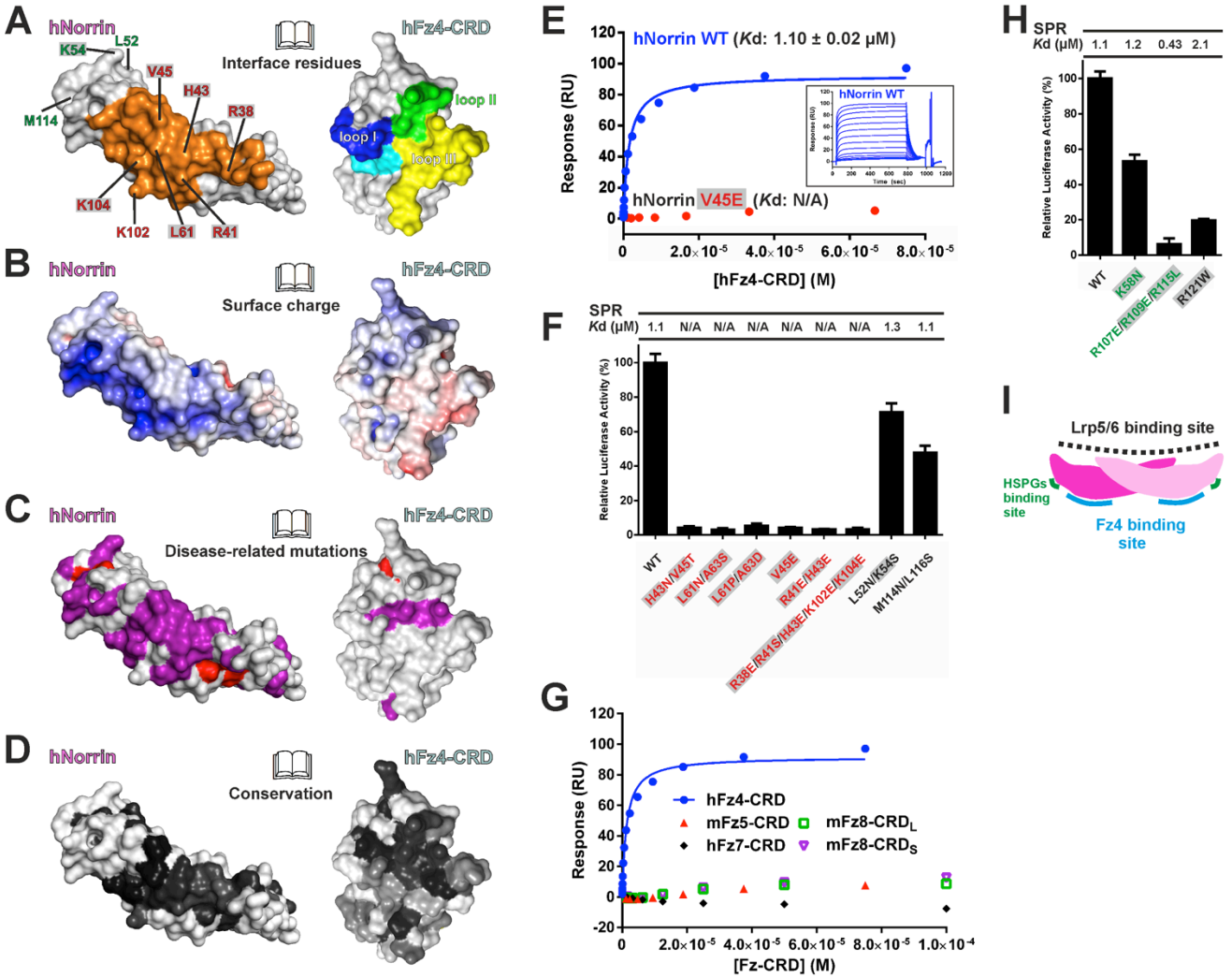


Figure 4.17. Biophysical and functional characterisation of binding sites.

Figure 4.17 (continued).
The Norrin/Fz4-CRD complex is shown in surface representation in an open book view. The N-linked glycans of Fz4-CRD are omitted. **(A)** Interface residues are coloured orange on Norrin and blue (loop I), green (loop II), yellow (loop III), and cyan (Phe96) on Fz4-CRD, see also **Figure 4.6**. Mutation sites of Norrin used in biophysical and cellular assays are labelled (red, residues involved in Fz4-CRD binding; grey filled box, residues associated with diseases; green, residues located outside the Fz4 binding site). **(B)** Norrin and Fz4-CRD coloured by electrostatic potential from red (acidic; 7 k_bT/e_c) to blue (basic; 7 k_bT/e_c). **(C)** Disease-associated mutations are mapped onto the surface of Norrin and Fz4-CRD and concentrated at the face of the Fz4 binding site. Missense mutations are shown in purple and missense mutations of cysteine residues are highlighted in red, see also **Figure 4.3** and **4.6**. **(D)** Colour-coded surfaces according to sequence conservation from white (not conserved) to black (conserved) based on alignments of sequences from vertebrates. **(E)** Binding properties of the Norrin and Fz4-CRD interaction. SPR equilibrium experiments show that Fz4-CRD binds to Norrin wild-type (WT) with a binding constant (*K*d) of 1.1 μM, but not to Norrin V45E mutant (data shown as not applicable (N/A)), identified from diseases. The inset for the SPR sensorgrams is of equilibrium-based binding assays with reference subtraction. See also **Figure 4.19** for all SPR experiments. **(F)** Luciferase reporter assays indicate that mutations on the Fz4 binding site affect signalling activities in agreement with SPR analyses (see also **Figure 4.17E** and **4.19**) The *K*d values from SPR measurements are shown above the plot of the luciferase assay. HEK293STF cells were co-transfected with receptors (Fz4, Lrp6, and Tspan12), Renilla luciferase vector, and either Norrin WT or the indicated Norrin mutants. The luciferase activities were analysed as described in **Chapter 2 Materials and Methods** and normalized to a maximum activity value (100%) of Norrin WT. Error bars indicate standard deviations (n = 3). Residues involving in the Fz4 binding site and residues without contact with Fz4-CRD are coloured red and black, respectively. Grey filled boxed highlighted residues are associated with diseases (**Table 4.8**). **(G)** Norrin discriminates between different Fz-CRDs. SPR results reveal that Norrin specifically binds to Fz4-CRD. **(H)** Luciferase reporter assays for Norrin HSPGs binding site mutants (K58N and R107E/R109E/R115L) and potential Lrp5/6 binding site mutant (R121W). The *K*d values from SPR measurements (**Figure 4.21** and **4.23**) are shown above the plot of the luciferase assays. Grey filled boxes highlight the residues associated with diseases (**Table 4.8**). The luciferase activities were normalized to the maximum activity value (100%) of Norrin WT. Error bars indicate standard deviations (n = 3). **(I)** Cartoon model of Norrin showing three distinct surface patches for Fz4, HSPGs, and Lrp5/6 binding sites.

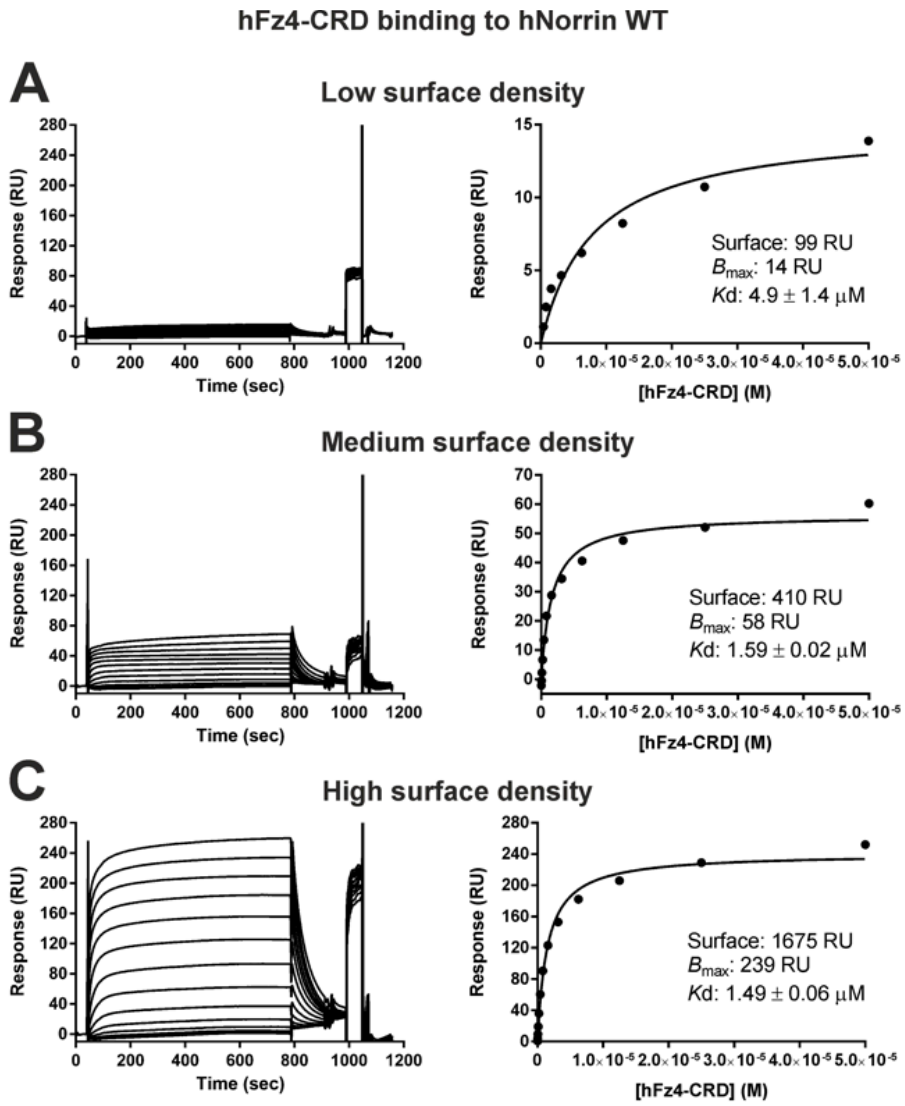


Figure 4.18. SPR equilibrium binding experiments for the Norrin and Fz4-CRD interaction.

SPR measurements reveal that surface density does not affect the binding affinity between Fz4-CRD and Norrin, although low surface density gives weaker affinity comparing to medium and high surface density. Three different densities of biotinylated Norrin proteins (low, medium, and high) were immobilized to the surface of a biosensor CM5 chip and a series of concentrations of Fz4-CRD were injected as analyte for the SPR assays. The sensorgrams (right panels) and fitted plots of equilibrium binding response (left panels; 1:1 Langmuir binding model) against a series of concentrations of Fz4-CRD are shown. For all injections, the experimental traces reached equilibrium and returned to baseline after regeneration (see also **Chapter 2 Materials and Methods** for the detailed SPR procedure). The binding parameters are shown as Surface (the amounts of biotinylated Norrin coated onto sensor chip), B_{max} (the maximum response), *K*d (binding constant), and RU (response unit). All experiments were performed in duplicate.

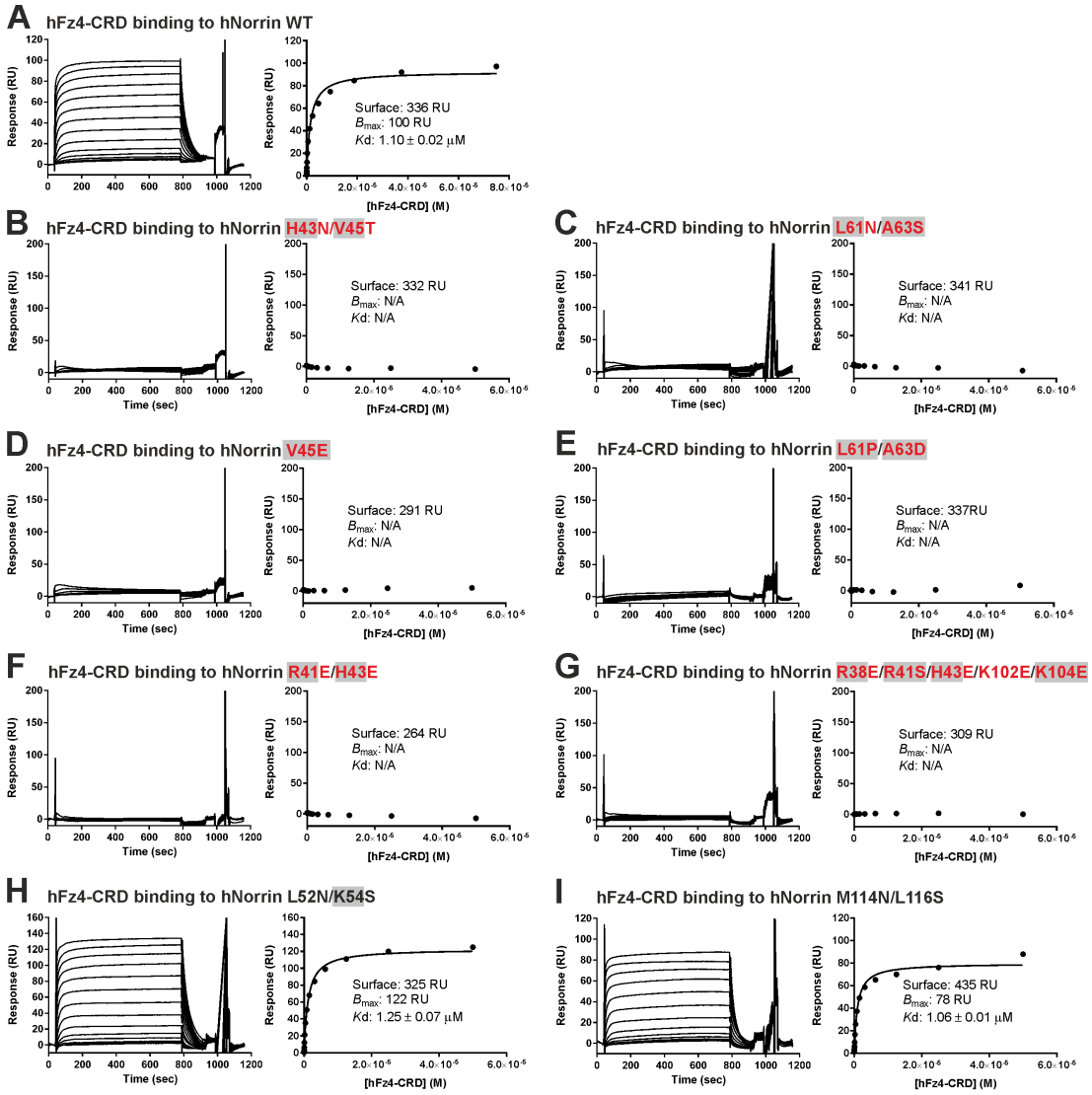


Figure 4.19. SPR measurements support the crystal structures and explain disease-associated mutations on the Fz4 binding site.

Figure 4.19 (continued).
SPR equilibrium binding experiments using human Fz4-CRD as analyte and biotinylated human Norrin wild-type (WT) and mutants as immobilized ligands on CM5 sensor chips. SPR sensorgrams (right panels) and equilibrium binding plots (left panels) against a series of concentrations of Fz4-CRD are presented. For all injections of analytes, the primary experimental traces reached equilibrium and returned to baseline after regeneration. The binding parameters are given as **Figure 4.18**. N/A indicates not applicable for calculation of *K*d. All experiments were performed in duplicate. Residues belonging to disease-associated mutation sites are highlighted as filled grey boxes. See also **Figure 4.17A** for the locations of mutation sites. **(A)** The interaction of Norrin WT with Fz4-CRD has a *K*d of 1.1 μM, weaker than previously published results, the discrepancy may be due to the present binding assays being done with monomeric Fz4-CRD using SPR experiments. Xu *et al*., used an ELISA assay to give an affinity of 3-4 nM for mouse Norrin fused with C-terminal alkaline phosphatase binding to mouse Fz4-CRD with a C-terminal Fc fusion, which dimerized through the disulphide bonds in the Fc tag (Xu et al., 2004). Ke *et al*., reported *K*d values of 11 nM and 5 nM for the interaction between Norrin carrying a N-terminal MBP fusion and Fc-tagged dimeric Fz4-CRD using an AlphaScreen luminescence assay and biolayer interferometry, respectively (Ke et al., 2013). **(B)** and **(C)** Introduction of an N-linked glycosylation site on the Fz binding site of Norrin results in the complete loss of Fz4-CRD binding. **(D)** and **(E)** Norrin mutants identified from diseases show no binding to Fz4-CRD. **(F)** and **(G)** Mutations designed to disrupt the hydrogen bond and salt bridge interactions of the Fz4 binding site completely abolish the binding to Fz4-CRD. **(H)** and **(I)** Introduction of an N-linked glycosylation site on the Norrin surface locating outside the Fz4 binding site does not affect the binding affinity of Norrin to Fz4-CRD.

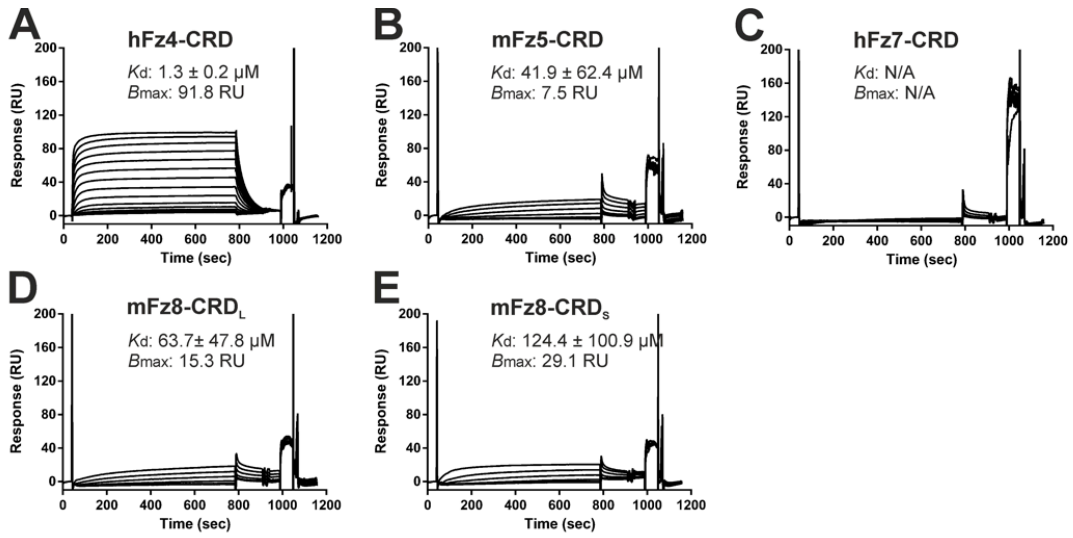


Figure 4.20. SPR equilibrium binding data (Norrin binding to Fz-CRDs) in sensorgram representation, related to Figure 4.17G.

Biotinylated human Norrin proteins were immobilized onto a CM5 sensor chip to give 410 response units (RU) and different Fz-CRD proteins were used as analytes. For all injections, the experimental traces reached equilibrium and returned to baseline after regeneration. The injected human Fz4-CRD proteins have a concentration ranging from 2.3 nM to 75 µM. Protein concentrations ranging from 0.3 µM to 150 µM (mouse Fz5-CRD) or 0.2 µM to 100 µM (human Fz7-CRD, mouse Fz8-CRD_S, and mouse Fz8-CRD_L) were used for SPR experiments. The sensorgrams of mFz5-CRD, mFz8-CRD_L (residues 30-170; longer version containing 1st and 2nd N-linked glycosylation sites), and mFz8-CRD_S (residues 30-15; shorter version lacking 2nd N-linked glycosylation site), show low responses and give weak *K*d values of 42 µM, 64 µM, and 124 µM, respectively, using the 1:1 Langmuir binding model for calculation of equilibrium binding response. Because of the limitations of detection, these *K*d values are too low to measure accurately, resulting in variable standard deviations. The binding affinity of Fz7-CRD to Norrin is not sufficient to calculate a *K*d. All experiments were performed in duplicate. See also **Figure 4.17G** for the fitted plots of the equilibrium binding response experiments.

4.8.2 Verification of the HSPGs binding site

To assess the proposed HSPGs binding site (**Figure 4.16E**), I prepared Norrin mutants: K58N and R107E/R109E/R115L, where K58N and R115L are disease-associated mutations (**Figure 4.3** and **Table 4.8**). Triple mutations of R107E/R109E/R115L nearly abolish signalling activity in the luciferase reporter assays (**Figure 4.17H**) and lose heparin binding ability (**Figure 4.21A**), but do not affect Fz4-CRD binding (**Figure 4.21B**). The Norrin K58N mutant exhibits half of the reporter activity (**Figure 4.17H**), but retains the interaction with Fz4-CRD (**Figure 4.21B**). My results are in agreement with previous functional studies indicating that mutations of K58E, R107E, R109E, and R115E affect signalling activity but do not interfere with Fz4-CRD binding (Smallwood et al., 2007). Therefore, I suggest this area is a HSPGs binding site rather than as originally proposed the Lrp5/6 binding site (Ke et al., 2013). Furthermore, I found that SOS could inhibit luciferase reporter activity when Norrin was pre-incubated with SOS before stimulation (**Figure 4.22**). Taken together, my functional assays support the HSPGs binding site observed in the crystal structure (**Figure 4.11**) and allows me to suggest that HSPGs and Fz4 binding sites are independent, and activation of Norrin mediated signalling requires HSPGs. This observation is highly relevant to the concept of HSPGs as co-receptors, which interact with Wnts to form a morphogen gradient on cell surfaces and to facilitate Wnt engagement with Fz receptors, leading to the transduction of signalling (Binari et al., 1997; Lin and Perrimon, 1999).

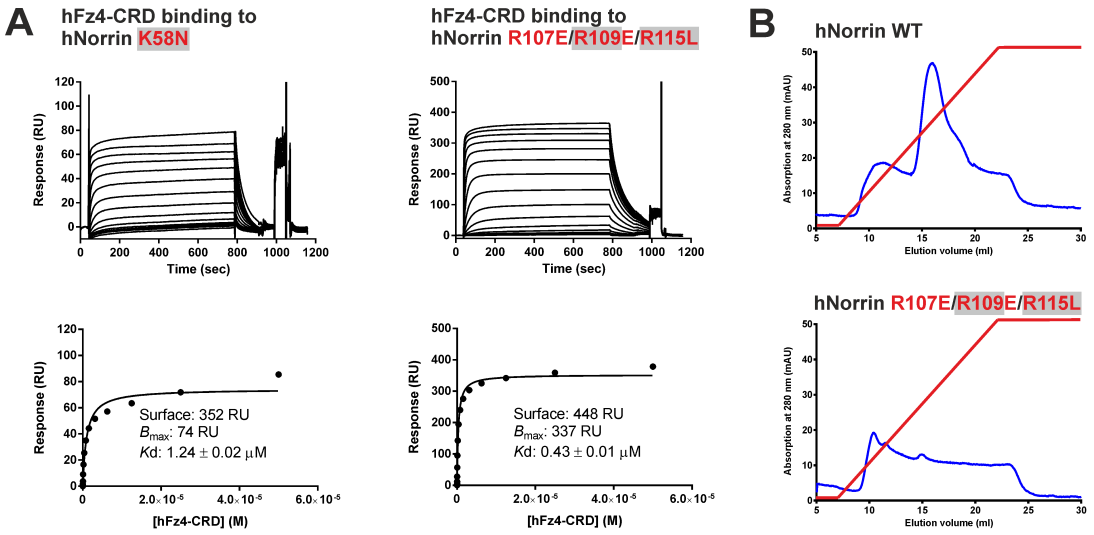


Figure 4.21. Heparin binding and SPR assays of HSPGs binding site mutations (Norrin K58N and R107E/R109E/R115L).
Norrin mutants of K58N and R107E/R109E/R115L are designed to disrupt the HSPGs binding site. Mutations do not affect the binding of Norrin to Fz4-CRD **(A)**, but result in loss of ability to interact with heparin affinity column **(B)** and activate signalling. Residues belonging to disease-associated mutation sites are highlighted as filled grey boxes. **(A)** In SPR equilibrium binding experiments, biotinylated human Norrin K58N or R107E/R109E/R115L proteins were coated onto a CM5 sensor chip and a series of concentration of Fz4-CRD proteins as analyte were injected into the chip. Graphs show sensorgrams (top panels) and fitted plot (bottom panels). Best-fit binding curves are calculated by using a 1:1 Langmuir binding model. The binding parameters are given below the traces of fitted plots. All experiments were performed in duplicate. **(B)** Heparin affinity chromatography of Norrin WT and mutant R107E/R109E/R115L. Norrin WT bound to the column and was eluted with 1.3 M NaCl, whereas Norrin mutant R107E/R109E/R115L lost the binding ability.

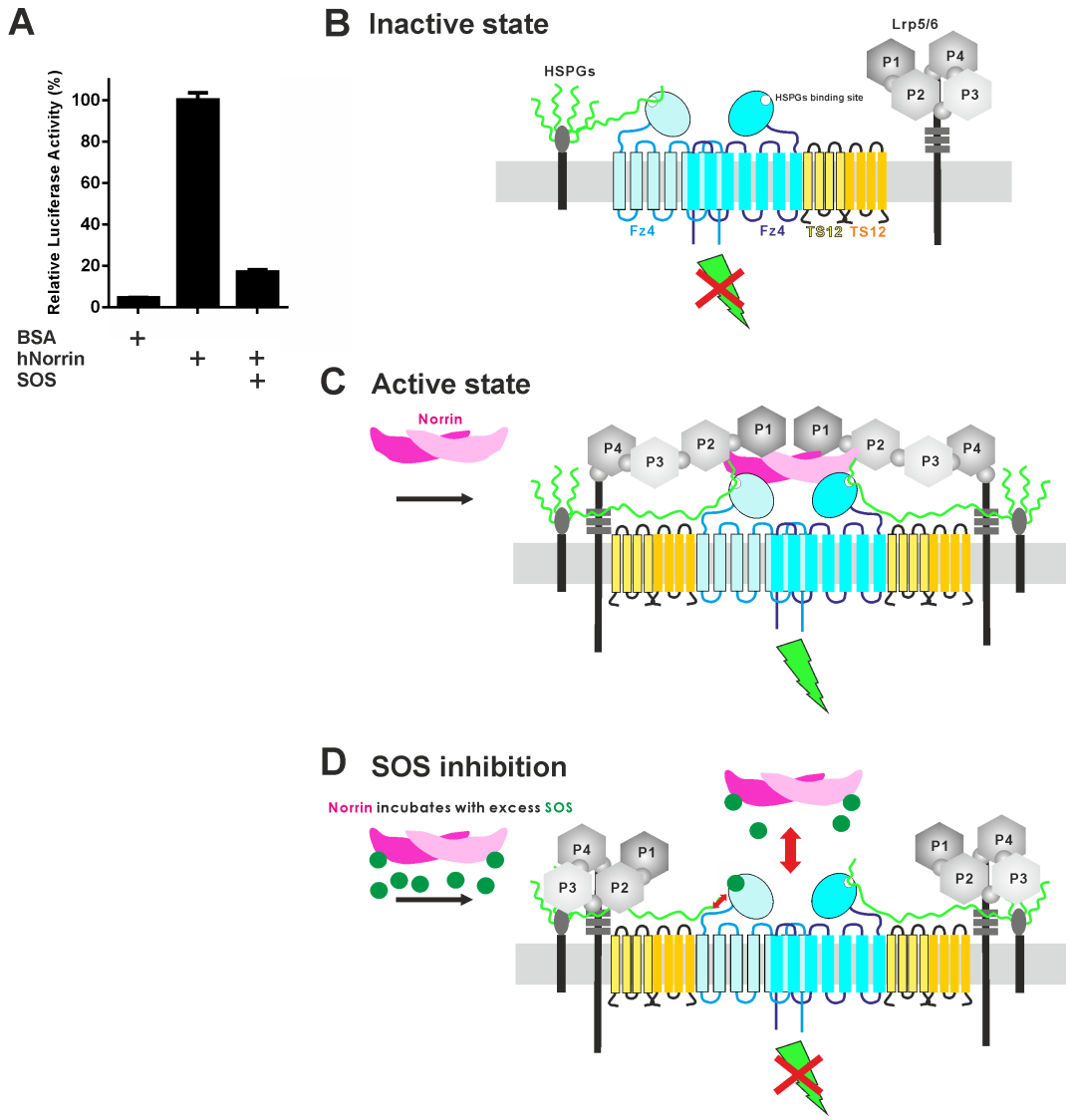


Figure 4.22. SOS inhibits the Norrin mediated Wnt/β-catenin signalling.
(A) HEK 293STF cells were co-transfected with human receptors (Fz4, Lrp6, and Tspan-12) and control *Renilla* luciferase plasmid. Protein samples (BSA, Norrin, and Norrin preincubated with SOS, separately) are stimulated post 6hr transfection. Luciferase reporter activities were then measured after 2 days as describe in **Chapter 2**. The luciferase reporter activities were normalized to a maximum activity value of 100%, using Norrin WT as reference. Error bars indicate standard deviations (n=3). The cartoon models **(B)** Inactive state and **(C)** Active state. Our structural and functional analyses suggest that HSPGs serve as co-receptors to promote the interaction between Norrin and Fz4-CRD and are involved in receptor clustering for signal transduction. **(D)** Inhibition of HSPGs function in Norrin mediated signalling is expected to reduce the signalling activity. The molecules of SOS were used to investigate the hypothesis.

4.8.3 Analyses of Lrp5/6 binding site on Norrin

To test the proposed Lrp5/6 binding site (**Figure 4.16F**), I generated the Norrin disease-associated mutant R121W because Arg121 is a mutational hotspot (four missense mutations, R121G, R121L, R121W, and R121Q) (**Figure 4.3** and **Table 4.8**). As expected, mutation of R121W significantly impairs the signalling activity in luciferase assays (**Figure 4.17H**), but does not affect the interaction with Fz4-CRD in SPR binding experiments (**Figure 4.23A**). In addition, I know that activation of Norrin mediated signalling requires Norrin binding to Fz4-CRD, Lrp5/6-ECD, and HSPGs. Thus, I suggest Arg121 plays a critical role in Lrp5/6-ECD binding.

Wnt antagonist, Sclerostin (SOST) is in a monomeric state in solution, and uses its N*X*I motif within a flexible loop to interact with Lrp5/6-ECD to block Wnt signalling (Bourhis et al., 2011; Holdsworth et al., 2012). However, the motif does not exist in Norrin (**Figure 4.3**), but the corresponding position is substituted in Norrin by Arg90 (**Figure 4.23B**). Interestingly, Norrin residues Lys54, Arg97, Gly112, and Arg121 within the proposed Lrp5/6 binding site are also structurally conserved in SOST (**Figure 4.23B**). These observations imply that SOST may have other epitopes for Lrp5/6 binding in addition to the N*X*I motif, in agreement with recently reported SOST mutagenesis and molecular modeling studies suggesting that SOST uses the N*X*I motif for binding to Lrp5/6-P1E1 and other epitopes for interacting with Lrp5/6-P2E2 (Boschert et al., 2013). It may be worthwhile to revisit the surface patches of SOST implicated in interaction with Lrp5/6-ECD. Our proposed Lrp5/6 binding site also provides an

explanation for a lack of prior observations of binding: Norrin as a C-terminal fusion with alkaline phosphatase could not detect directly interactions with Lrp5/6 in previous histochemical assays, because the C-terminal AP would interfere with the interaction of Norrin with Lrp5/6-ECD.

In total, I suggest that Norrin has three distinct and independent binding sites for Fz4, LRP5/6, and HSPGs (**Figure 4.17I**) and the arrangement of binding sites would likely enable Norrin to form ternary complex, but a definitive conclusion will require a complex structure and detailed binding assays. However, I cannot formally exclude the possibility that the proposed Lrp5/6 binding site is involved in some other unknown mechanism for regulation of Norrin mediated signalling and the mutations result in the reduction of signalling activity through this unknown mechanism.

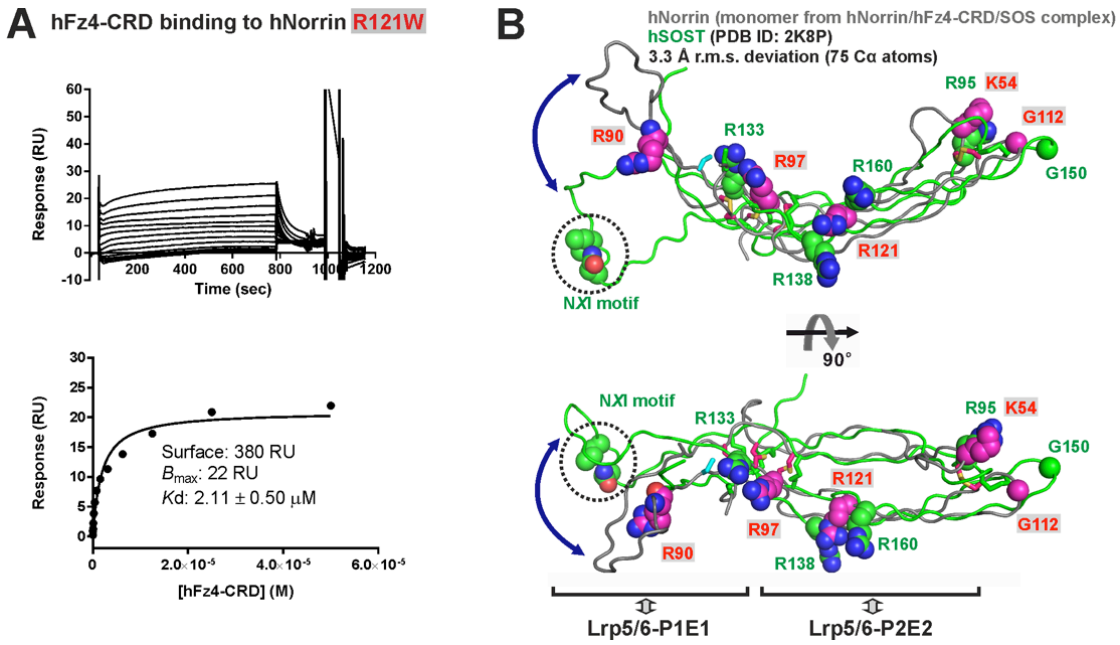


Figure 4.23. SPR binding assay of Norrin mutant R121W and structural comparison of Norrin with SOST.
(A) SPR experiments demonstrate that Norrin R121W mutant retains Fz4-CRD binding ability. Biotinylated human Norrin R121W proteins were coated onto a CM5 sensor chip and a series of concentrations of Fz4-CRD proteins as analyte were injected into the chip for SPR equilibrium binding experiments. Graphs show sensorgrams (top panels) and fitted plot of equilibrium binding response (bottom panels; the binding parameters below the traces) using a 1:1 Langmuir binding model. All experiments were performed in duplicate. **(B)** Superimposition of complexed Norrin (grey) with human SOST (green). Norrin residues on the proposed Lrp5/6 binding site are shown as sphere models (atom colouring: magenta, carbon; blue, nitrogen). The N*X*I (where X can be Ala, Ser, or Trp) motif and residues of SOST with a corresponding position to the Norrin Lrp5/6 binding site are presented as sphere models (atom colouring: green, carbon; blue, nitrogen; red, oxygen).

4.9 Structural comparison of Norrin/Fz4-CRD with Wnt8/Fz8-CRD

Norrin appears to function like Wnt in many aspects including Fz, Lrp5/6 and HSPGs binding, and activation of canonical Wnt/β-catenin signalling, although sharing no discernible sequence and structure homology with Wnts (Janda et al., 2012; Ke et al., 2013; Smallwood et al., 2007). *Xenopus* Wnt8 reveals a two domain structure comprising an N-terminal α-helical domain (NTD) and C-terminal cysteine-rich region (CTD) and resembles a hand-like structure, using extended thumb and index finger to grasp the mouse Fz8-CRD at two distinct sites (Janda et al., 2012). In site 1 (lipid-in-groove), the palmitoleoyl group (PAM) covalently linked to the tip of the thumb on Wnt8 NTD inserts into a hydrophobic groove of Fz8-CRD (**Figure 4.24A**). In site 2 (knob-in-hole), the index finger protruding from the Wnt8 CTD contacts hydrophobic depression in the Fz8-CRD (**Figure 4.24A**). In the Fz binding assays, Norrin revealed a binding specificity to Fz4-CRD but not Fz5-, Fz7- and Fz8-CRD (**Figure 4.17G**) in agreement with previous studies (Smallwood et al., 2007; Xu et al., 2004), whereas Wnts have promiscuous interactions with Fz-CRDs, for example Wnt8 binding to Fz5- and Fz8-CRD plus weak affinity to Fz4-CRD (Janda et al., 2012; Smallwood et al., 2007). Interestingly, genetic studies suggest that the Norrin binding interface on the Fz4-CRD appears to be shared with Wnt8 (Smallwood et al., 2007).

Thus, the Norrin and Fz4 pair seems likely to serve as an interesting comparison system with the Wnt and Fz pair for understanding Wnt functional pleiotropy. I

superimposed Norrin/Fz4-CRD with Wnt8/Fz8-CRD and found that the Fz4 binding site (**Figure 4.17A**) on hFz4-CRD (~800 Å^2 buried area) overlaps with site 2 on Fz8-CRD (~400 Å^2 buried area; **Figure 4.24A** and **4.6**), in agreement with previous systematic mutational mapping studies (Smallwood et al., 2007). The position of the Wnt8 index finger on site 2 for Fz8-CRD binding overlaps with Norrin β1 and β2 and surprisingly these β strands reveal some degree of structural conservation with Wnt8 (**Figure 4.24B**). In addition, Wnt8 residues on site 2 are invariant in all Wnts and the apolar residues in the corresponding positions on Norrin are associated with disease mutations, suggesting importance for Fz binding and activation of signalling. Specifically, Norrin Val45 (key residue for binding and signalling, **Figure 4.17E-3F**; mutation hot spots, **Table 4.8**) is structurally equivalent to Wnt8 Val323, which appears to determine the interaction with Fz8-CRD and affect signalling activity (Kumar et al., 2014). Interestingly, the role of Wnt8 residue Trp319 is substituted in Norrin by Ala63 C_β and Arg41 side chain (**Figure 4.24B**). In summary, residues on both site 2 of Wnt and on Norrin are apolar and highly conserved for binding to a depressed 'pocket' region of Fz-CRD via hydrophobic interactions as well as required to activate signalling.

Structural comparison of Fz4-CRD with Fz8-CRD shows no major conformational changes (r.m.s. deviation of 1.3 Å over 110 equivalent Cα atoms; **Figure 4.24A**). In particular, Fz8-CRD shares a high degree of conservation of the site 1 interface (lipid-in-groove) with Fz4-CRD, except the side chains of hydrophobic residues on the bottom of the groove show small conformational changes upon PAM

insertion (**Figure 4.24C**). Residues of Wnt and Fz (**Figure 4.6**) are highly conserved for site 1 (Janda et al., 2012). Wnt palmitoylation on site 1 is essential to maintain its full biological activity (Takada et al., 2006) and may limit Wnt spatial movement on the cell membrane (Alexandre et al., 2014), which appears to require lipid binding proteins for long-range movement (Mulligan et al., 2012). It has been suggested that site 1 would likely be a conserved common (not specific) binding module for Wnt and Fz pairs, necessary to mediate the lipid-in-groove interaction.

Nevertheless, Norrin binding to Fz4-CRD, corresponding to site 2 on Fz8-CRD, is sufficient for activation of signalling and the interface is also enough to allow Norrin to discriminate between Fz-CRDs for binding (**Figure 4.17G**). However, Norrin has a 2-fold larger interface with the Fz-CRD than Wnt8. The observation that site 2 binding alone is sufficient, is in agreement with results reported using a water-soluble mini-Wnt7a, which can activate signalling (von Maltzahn et al., 2013), and mini-Wnt8 (only containing CTD) interactions with Fz5- and Fz8-CRD in micromolar affinities, but weak binding to Fz4-CRD (Janda et al., 2012). Taken together, structural analyses presented here in combination with previous functional data allow me to suggest that the site 2 interface is enough to interact with Fz-CRD and activate signalling as well as to determine the Fz binding specificity, whereas the site 1 interface may be used to achieve full activity of Wnt signalling, enhance binding affinity, cross-react with multiple Fz-CRDs, and/or limit Wnt movement.

To understand the Norrin discrimination of Fz4-CRD from Fz-CRDs at the molecular level (**Figure 4.17G**), I analyzed the Fz4 binding site superimposed onto Fz8-CRD. In Fz4-CRD loop I (**Figure 4.24D**), Fz4-CRD Asn55 forming a salt bridge with Norrin Ser34 (**Figure 4.16B**) is replaced by Fz8-CRD Gly45. In Fz4-CRD loop II (**Figure 4.24E**), Fz4-CRD Lys109 forming a hydrogen bond with Norrin Asp46 (**Figure 4.16C**) is substituted by mFz8-CRD Asp99. In Fz4-CRD loop III (**Figure 4.24F**), Fz4-CRD Asn152 side chain amide forming a hydrogen bond with Norrin Leu61 backbone carbonyl oxygen (**Figure 4.24F**) is replaced by Fz8-CRD Gly142. In addition, Fz4-CRD Glu160 forming salt bridges with Norrin Lys102 and Lys104 is substituted by Fz8-CRD Asp150 (**Figure 4.24F**). In agreement with previous mutational experiments using block substitution of Fz8-CRD into Fz4-CRD, these residue substitutions affect Fz4-CRD binding to Norrin (Smallwood et al., 2007). Importantly, the kinds of contact residue substitutions may contribute to ligand binding preferences.

My structural analysis also found that Fz4-CRD Gly161 and Pro162 on C-terminal loop III are substituted by Fz8-CRD Tyr151 and Asn152 (both residues with sidechains only built as C_β atoms in the Wnt8/Fz8-CRD coordinates). Asn152 is the second N-linked glycosylation site of Fz8-CRD, which is conserved (**Figure 4.6**), except in Fz3-, Fz4-, and Fz6-CRD. This second N-linked glycosylation site appear to possibly determine Norrin binding preferences with Fz-CRDs. Thus, I generated two versions of Fz8-CRD: mFz8-CRD_L contains two N-linked glycosylation sites, and Fz8-CRD_S only contains the 1st N-linked glycosylation site. No difference between Fz8-CRD_L and Fz8-CRD_S for Norrin binding is detected

(**Figure 4.17G**). Therefore, the N-linked glycans do not contribute to complex interaction.

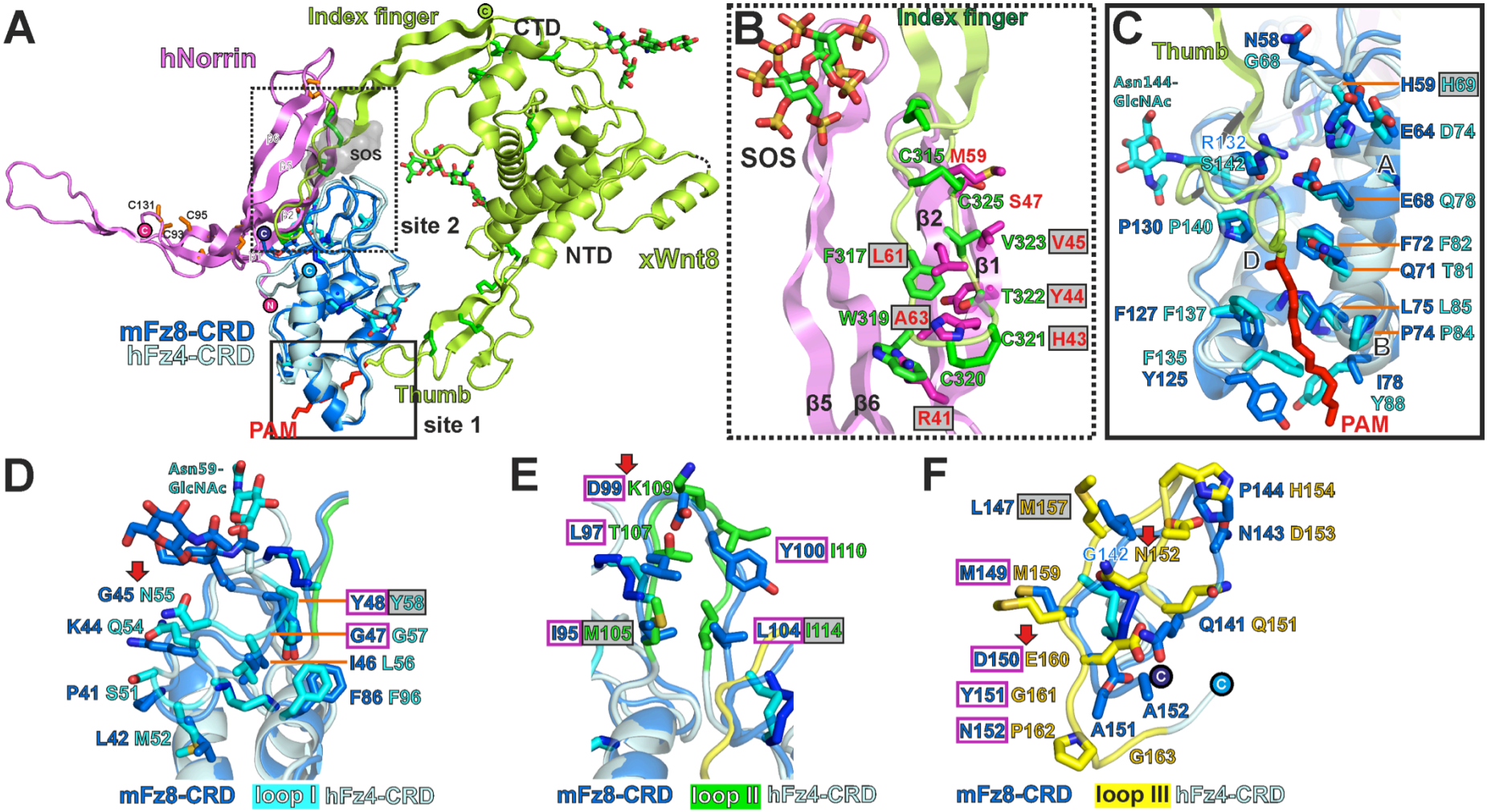


Figure 4.24. Structural comparison of Norrin/Fz4-CRD with Wnt8/Fz8-CRD.

Figure 4.24 (continued).
(A) Superposition of 1:1 complex of Norrin (magenta)/Fz4-CRD (cyan) with Wnt8 (green)/Fz8-CRD (blue) (PDB ID: 4F0A) on the basis of the Fz-CRDs. The disulphide bonds and palmitoleoyl (PAM) covalently attached to the thumb region of Wnt8 are shown as sticks. N-linked glycans are shown as cyan (Fz4-CRD), blue (Fz8-CRD), and green (Wnt8) sticks. The SOS molecule is shown as grey surface in semi-transparent view. N- and C-termini are indicated as encircled N and C. **(B**) The index finger region of Wnt8 on site 2 for Fz8-CRD binding structurally overlays Norrin (β1 and β2) for Fz4-CRD binding. Residues of Wnt8 and Norrin for interactions with Fz8- and Fz4-CRD are shown as green and magenta sticks, respectively. Residues of Norrin associated with disease mutations are highlighted in grey filled black boxes. **(C)** Detailed comparison of site 1 for PAM binding. Fz4-CRD (cyan) and Fz8-CRD (blue) have conserved conformation and contact residues for interaction with PAM, except for orientation changes of Tyr88 and Phe135 of Fz4-CRD. Residue of Fz4-CRD His69 is related to diseases (**Figure 4.6**). **(D)-(F)** Detailed structural comparison of Fz4-CRD (cyan) and Fz8-CRD (blue) for interaction with Norrin and Wnt8, respectively. The selected residues of Fz4-CRD and Fz8-CRD on loop 1 (cyan), loop II (green), and loop III (yellow) are shown as sticks. Residues of Fz8-CRD for Wnt8 binding (site 2) are boxed in purple see also **Figure 4.6**. Fz4-CRD residues associated with diseases are highlighted with grey filled black boxes. Red arrows indicate the residue substitutions between Fz4- and Fz8-CRD that may affect Norrin binding. Two residues (Tyr151 and Asn152) of Fz8-CRD at the C-terminus are built as Ala residues in the coordinates of Wnt8 /Fz8-CRD (PDB ID: 4F0A).

4.10 Model of Norrin-induced receptor clustering and signallosome formation

Taking in combination my above studies and previous findings for Norrin and Wnt signalling, I propose a model for Norrin-induced receptor clustering and signallosome formation (**Figure 4.25**). Co-receptor HSPGs may use a *cis*- or *trans*-model to recruit secreted Norrin for either simultaneously or separately making interactions with Lrp5/6-ECD and the CRD of inactive predimerized Fz4, engaged with homodimeric Tspan12 (Ke et al., 2013). Tspan12 has been suggested to play the role of enhancement of receptor clustering (Junge et al., 2009). In the cytoplasm, Dishevelled binds to the C-terminal tail of Fz4 (containing KTxxxW motif) and self-assembles to oligomers via its DIX domain (Schwarz-Romond et al., 2007), leading to Axin recruitment to the cytoplasmic domain of Lrp5/6 for phosphorylation via glycogen synthase kinase 3 (GSK3) and casein kinase 1 (CK1) and signallsome formation (Bilic et al., 2007). Thus, Norrin binding possibly clusters receptors for signallsome formation through extracellular to intracellular region, leading to signalling.

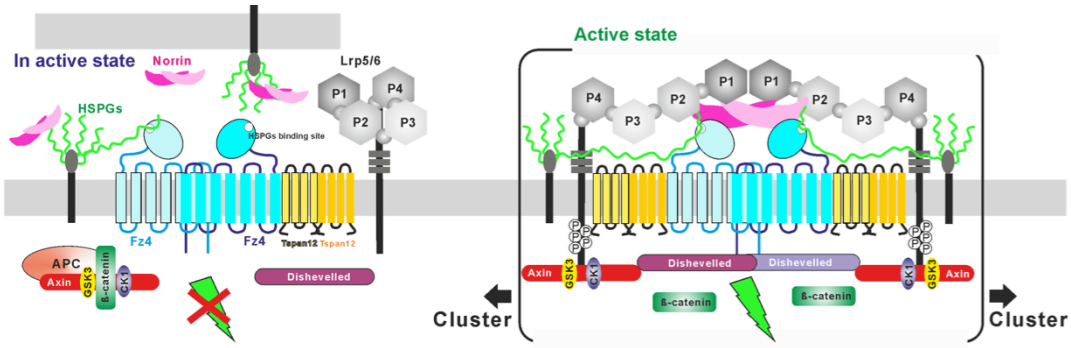


Figure 4.25. Cartoon model of Norrin-induced receptor clustering and signallosome formation.
Ternary complex formation of Fz4, Lrp5/6, and HSPGs as well as Tspan12 after Norrin binding in the extracellular region is important for receptor clustering and signalling (green lightning bolt). Dishevelled and Axin complex are proposed to assemble as signallosome via the DIX-domain in the intracellular region. APC, adenomatous polyposis coli; GSK3, glycogen synthase kinase 3; CK1, casein kinase 1; HSPGs, heparan sulfate proteoglycans.

4.11 Future perspectives

As described in **Chapter 4,** I use multiple approaches to understand Norrin mediated signalling from atomic structures to cell-based studies. The investigations presented in the thesis not only support and correct the previous studies in Fz4 binding, but also provide new insights into HSPGs and Lrp5/6 binding. Structural comparison of Norrin/Fz4-CRD with Wnt8/Fz8-CRD extends our current knowledge of how Fz receptors discriminate the ligand for binding and how two distinct ligands activate signalling via binding to Fz receptors. My discoveries raise several interesting questions, which it will be worthwhile to investigate more in the future.

Regarding HSPGs binding, HSPGs facilitated ligand-receptor binding has also been discovered in fibroblast growth factor (FGF) interactions with FGF receptor (Pellegrini et al., 2000; Schlessinger et al., 2000) and Hedgehog with interference Hedgehog receptor (McLellan et al., 2006). The structure of Norrin/Fz4-CRD complex bound with SOS reveals that SOS appears to be a mediator acting to bring Norrin and Fz4-CRD together to form a complete HSPGs binding site. The finding encourages us to revisit the role of HSPGs, which may not only function to recruit ligands for interaction with receptors or to facilitate the formation of receptor clusters for the signalling amplification, but also to enhance ligand and receptor binding in the extracellular region. I therefore suggest that a universal screen of ligand and receptor pairs in the presence of HSPGs may provide us with some very surprising discoveries, which were unsuspected previously.

Specifically, it will also be interesting to investigate whether mutations of the HSPGs binding site on Fz4 affect signalling activity and determine the binding constants of Norrin interaction with the different glycosaminoglycan chains of proteoglycans (such as heparan and chondroitin sulfates) as well as to study the effects of different lengths of glycosaminoglycan fragments on the behaviour of Norrin in solution. In addition, if Norrin has a significant preference for heparan or chondroitin sulfates, further cellular studies will be worthwhile to investigate the possible differences in biological outcome for cells treated with either heparitinase or chondroitinase.

For the contribution of Lrp5/6 binding to Norrin mediated signalling, the proposed Lrp5/6 binding site on Norrin requires validation and further mapping. Therefore extensive mutational studies in combination with biophysical SPR binding and cellular reporter assays are required. As shown in **Figure 3.16**, the ternary complex of Norrin/Fz4-CRD/Lrp5/6-P1E1P2E2 was successfully purified; however, I still lack diffracting crystals. The preliminary crystallization and X-ray diffraction data are not enough to define whether ternary complex crystals were obtained or not. I suggest that further modification of expression constructs, and optimization of buffer conditions to improve the thermal stability of ternary complex for crystallization, may be needed to produce crystals diffracting to a reasonable resolution. In addition, it may be worth applying a chemical cross-linking technique in the preparation of the ternary complex for crystallization. Because the current knowledge of how Lrp5/6-ECD interacts with Wnt and Norrin is limited in biophysical and cellular analyses, it

will be worthwhile to determine the stoichiometry of the ternary complex of Norrin/Fz4-CRD/Lrp5/6-ECD by SEC-MALS in combination with SAXS. Finally, generation of structural information for the ternary complex by X-ray crystallography in combination of SAXS and cryo-electron microscopy will be a critical step toward a better understanding of the Lrp5/6 binding module.

As shown in **Figure 4.24 D-F**, the structural comparison of Fz4- and Fz8-CRD suggests that a few key residues contribute to the discrimination of Norrin binding. These remain to be verified by further mutagenesis and SPR binding assays. It will also be very interesting to generate Norrin mutants that have different preferences for binding to other Fz-CRDs (Further discussion in **Chapter 5**).

Furthermore, the proposed Norrin-induced receptor clustering and signallosome formation (**Figure 4.25**) remains to be investigated. One worthwhile step forward will be to attempt to verify the general features of the model by super-resolution light microscopy.

Chapter 5

Further discussion

5.1 Therapeutic potential of Norrin for retinal disorders

Previously reported mice genetic studies reveal that expression of ectopic Norrin can rescue pathologic retinal vascularization (Ohlmann et al., 2005; Ohlmann et al., 2010). Hence, Norrin has been suggested to be a target for therapy of genetic retinal disorders and vitreoretinal diseases. However, the technical difficulty of production of recombinant Norrin has hampered progress to assess its proposed therapeutic potential. As described in **Chapter 3**, I have developed efficient mammalian expression strategies to produce biologically active recombinant Norrin in milligram quantities. The protein sample was used for crystallization and the crystal structure of Norrin reveals an unusual elongated flat dimer structure linked by three intermolecular disulphide bonds, described in **Chapter 4.4.**

In the future, it will be very worthwhile to use an animal model to investigate whether injection of recombinant Norrin into the eye of Norrin-deficient mice can rescue the impaired intraretinal vascular architecture. The results would be a milestone for evaluation of whether it is worthwhile to take recombinant Norrin into clinical trials. It will also be very interesting to assess whether recombinant Norrin can be used to prevent ophthalmic disorders, including age-related macular degeneration and diabetic retinopathy. In combination, my D.Phil studies open up new avenues to explore the possible uses of recombinant Norrin as a therapeutic agent for ophthalmic vascular disorders.

5.2 Future structural studies on Norrin and related signalling

As discussed in **Chapter 4.11**, the structure determination of the ternary complex of Norrin/Fz4-CRD/Lrp6-ECD will be a milestone for our better understanding of how signalling is activated via the binding of Norrin to Lrp6-ECD and Fz4-CRD, because activation of signalling requires the presence of Fz4 receptor and Lrp5/6 co-receptor simultaneously. In contrast to several crystal structures of Lrp6-ECD in complex with the Wnt antagonist Dickkof or peptide (Ahn et al., 2011; Bourhis et al., 2011; Cheng et al., 2011), no structure of Lrp5/6-ECD binding to agonist (Wnt and Norrin) is available. Structural information will reveal how antagonist competes with agonist for Lrp5/6 binding. In addition, Ettenberg *et al*., recently reported that a monoclonal antibody antagonizing Lrp6-ECD shows inhibition of tumor growth (Ettenberg et al., 2010). In combination, the ternary structure would not only provide us with important insights into the basic mechanism of signal transduction, but also provide information to guide the development of drugs targeting aberrant Wnt signalling. The more ambitious aim will be to co-crystallize Norrin with full-length Fz4 receptor and Lrp5/6 co-receptor.

Recently two structural reports reveal that endogenous lipids bind to Smo-CRD to modulate Smo activity. This binding mode is analogous to the binding pocket of Fz-CRD used to bind to the palmitoleoyl group of Wnt ligands (Nachtergaele et al., 2013; Rana et al., 2013). The lipid modification of Wnts is necessary for their full biological activity (Takada et al., 2006). This therefore raises the possibility

that drugs (small molecules) can be designed to target the lipid-binding site on Fz proteins for inhibition of Wnt-Fz interactions for therapeutic purposes.

Interestingly, unlike the specificity of Norrin paired with Fz4-CRD, Fz4-CRD has be found to interact with multiple Wnts (Wnt2b, Wnt3a, Wnt5a, and Wnt8a) and the non-Wnt proteins Tsukushi, a secreted leucine-rich repeat-containing protein, and complement C1q (Hsieh et al., 1999; Mikels and Nusse, 2006; Naito et al., 2012; Ohta et al., 2011; Ring et al., 2011; Smallwood et al., 2007). In contrast to the Norrin/Fz4 pair that regulates retinal vascularization (Xu et al., 2004), the Tsukushi/Fz4 pair is involved in the differentiation of peripheral eye structures (Ohta et al., 2011) and the C1q/Fz4 pair modulates mammalian aging (Naito et al., 2012). These observations raise two questions. How does Fz4-CRD interact with the three distinct ligands of Norrin, Tsukushi, and C1q? The more advanced question is how Fz4 transduces the three different biological functions while interacting with these respective ligands. It therefore will be very interesting to determine the complex structures of Tsukushi/Fz4-CRD and C1q/ Fz4-CRD. This structural information in combination with functional assays will provide important insights for the development of engineered protein molecules for modulation of specific biological functions.

Very recently, Deng *et al*., reported that Norrin directly binds to the extracellular domain of leucine-rich repeat-containing G-protein-coupled receptor 4 (Lgr4) and can activate Wnt signalling via Lgr4 in cell-based luciferase reporter assays (Deng et al., 2013). Interestingly, Lgr4 is also the cell receptor for interaction with secreted glycoprotein R-spondins to enhance Wnt signaling (Carmon et al.,

2011; Glinka et al., 2011; Ruffner et al., 2012). However, the molecular mechanism is poorly defined so far. It therefore will be worthwhile to investigate the complex structure of Norrin/Lgr4.

5.3 Application of engineered Norrin mutants

As shown in **Figure 4.17**, Norrin exploits its 109 amino acids (mature form) for multiple functions including dimerization and interactions with Fz4-CRD, Lrp5/6, and HSPGs via distinct patches (**Table 4.8**). Three classes of Norrin mutants were created for functional studies and all mutants fail to activate signalling: class A mutants (such as L61N/A63S and V45E) lose Fz4-CRD binding affinity but appear to retain the interactions with Lrp5/6 and HSPGs, class B mutants (such as R107E/R109E/R115L) lose HSPGs binding ability, but retain binding to Fz4-CRD and Lrp5/6, and class C mutants (such as R121W) retain interactions with Fz4-CRD and HSPGs, but appear to lose Lrp5/6 binding. These engineered Norrin mutants may provide a valuable platform for basic research to understand Norrin and Wnt signalling, for development of cancer therapy, and for drug delivery into the brain as discussed in the next section.

5.3.1 Implication in understanding the signalling mechanism

Profound questions in Wnt signaling centre on the specificity and promiscuity of Wnt and Fz pairs, and which pairs are responsible for the effect in certain biological functions and disease processes. Current knowledge of Wnt signalling suggests that most Wnts target multiple Fzs, but not all. Therefore, it would be interesting to distinguish the signalling and biological outputs from individual mono-specific intereactions of Wnt and Fz. The class B mutants I have produced so far could be used to block Wnts binding to Fz4-CRD. Directed evolution or structure-based mutagenesis could be attempted to generate divergent Norrin mutants including proteins that show either specific binding to other Fz-CRDs or

promiscuous interactions with multiple Fz-CRDs. These Norrin mutants would also potentially be able to probe the specific role of Wnt and Fz pairs and to replace Wnts to investigate the individual biological function of Fzs.

5.3.2 Application in anti-cancer drug development

As expected, aberrant regulation of Wnt signaling is associated with human cancers (Clevers and Nusse, 2012). The therapeutic inhibition of Wnt signaling in extracellular space for cancer treatment is an attractive aim for drug discovery. The monoclonal antibody (mAb) OMP-18R5 inhibits Wnt signalling by binding to Fz1-, Fz2-, Fz5-, Fz7-, and Fz8-CRDs resulting in reduced growth and tumorigenicity of tumors (Gurney et al., 2012) and has just completed Phase I clinical trials (Kahn, 2014). A second protein drug, OMP-54F28, a Fz8-CRD fusion with Fc, shows retardation of the growth of tumors (DeAlmeida et al., 2007) and has started Phase I clinical trial (Kahn, 2014). Another mAb antagonizing Lrp6-EC also shows inhibition of tumor growth (Ettenberg et al., 2010). Very recently, Planutis *et al*., reported that Norrin production by colorectal cancers regulate angiogenesis in the tumor microenvironment (Planutis et al., 2014). Thus, my engineered mutants are potential blocking agents for inhibition of cancers caused by abnormal Wnt or Norrin signalling. In addition, my structural information identifying the determinants of ligand specificity on the Fz-CRD loops can provide insights for the development of a new generation of mAbs against Fz-CRDs with single-reactivity rather than cross-reactivity.

5.3.3 Application to drug delivery in the brain

The blood-brain barrier (BBB) is a natural system that protects the brain from neurotoxin and bacterial infections, and maintains brain homeostasis by providing a highly selective permeability mechanism (Engelhardt and Liebner, 2014). However, the BBB causes difficulty for the delivery of therapeutic and diagnostic agents to the brain for the treatment of brain disorders unless the drugs have high lipid solubility and a molecule weight less than 4-500 Da (Aryal et al., 2014). Development of a transient and non-invasive method to increase the permeability of the BBB for drug delivery is a challenging but eagerly awaited aim (Aryal et al., 2014). Interestingly, Norrin mediated signalling plays an essential role in the maintenance of BBB integrity. Previously reported genetic studies revealed that mosaic deletion of Fz4 in mature cerebellar vascular endothelial cells results in the increase of BBB permeability without altering the general architecture of the BBB. Conversely, ectopic expression of Norrin in Norrin-deficient mice restores the integrity of BBB in the cerebellum (Wang et al., 2012; Zhou et al., 2014). Engineered class B and C Norrin mutants lose the ability to transduce signaling, but retain their binding affinities for Fz4-CRD. This suggests a novel strategy to block Norrin mediated signalling. Our engineered mutants could potentially be used to temporarily increase BBB permeability for delivery of therapeutic drugs to the brain for brain related diseases, including Alzheimer's and Huntington’s disease, and brain cancer, without permanent change of BBB architecture.

Appendices

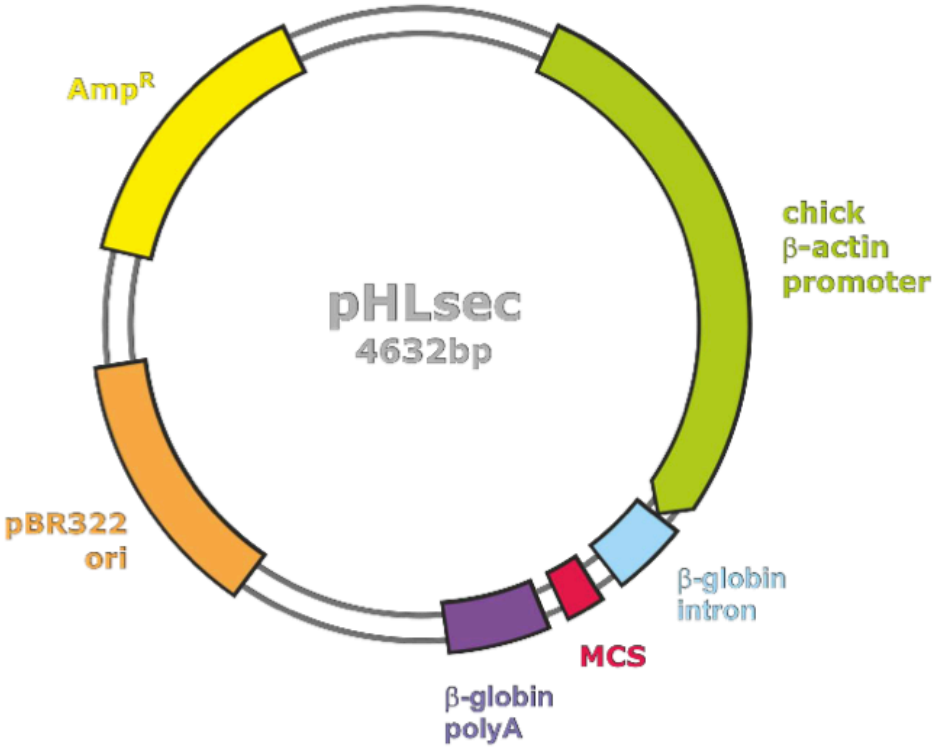
Appendix 1. Polylinkers of pLEXm based vector variants

(A) The vector of pHLsec

General features of pHLsec: The N-terminal Kozak sequence is highlighted in green and chick receptor protein tyrosine phosphatase sigma (RPTPσ) signal peptide (SP) in light purple, the C-terminal hexahistadine tag (KHHHHHH) is shown in blue and stop codons in black, while specific restriction enzyme sites are underlined.

```
EcoRIHindIII Kozak M  G  I  L  P  S  P  G  M  P  A  L  L  S  L  V  S  L  L  S  V  L  L  M
GAATTCAAGCTTGCCACCATGGGGATCCTTCCCAGCCCTGGGATGCCTGCGCTGCTCTCCCTCGTGAGCCTTCTCTCCGTGCTGCTGATG
 G  C  V  A  E  T  G           G  T  K  H  H  H  H  H  H  *  *      XhoI
GGTTGCGTAGCTGAAACCGGT …Insert… GGTACCAAGCACCACCATCACCATCACTAATGATCACTCGAG
               AgeI             KpnI
```

The vector map of pHLsec is shown as follows. Figure provided by Dr. A. R. Aricescu and based on reference (Aricescu et al., 2006).



(B) The vector of pHLsec-1D4 (a gift from Drs. N. Mitakidis and A. R. Aricescu, University of Oxford, UK)

The unique feature: The C-terminal hexahistadine tag (KHHHHHH) is replaced with the Rho-1D4 epitope coloured in red (TETSQVAPA), recognized by Rhodopsin 1D4 antibody.

```
EcoRI HindIIIKozak M  G  I  L  P  S  P  G  M  P  A  L  L  S  L  V  S  L  L  S  V  L  L  M
GAATTCAAGCTTGCCACCATGGGGATCCTTCCCAGCCCTGGGATGCCTGCGCTGCTCTCCCTCGTGAGCCTTCTCTCCGTGCTGCTGATG
 G  C  V  A  E  T  G           G  T  E  T  S  Q  V  A  P  A  *  *     XhoI
GGTTGCGTAGCTGAAACCGGT …Insert… GGTACCGAGACCAGCCAGGTGGCCCCTGCATAATGATCACTCGAG
               AgeI            KpnI
```

(C) The vector of pHLIgK-1D4

The unique feature: The SP of RPTPσ in pHLsec-1D4 was substituted for the SP of Murine Igκ-chain (Coloma et al., 1992).

```
EcoRI  Kozak M  E  T  D  T  L  L  L  W  V  L  L  L  W  V  P  G  S  T  G  D  T  G
GAATTCGCCACCATGGAGACAGACACACTCCTGCTATGGGTACTGCTGCTCTGGGTTCCAGGTTCCACTGGTGACACCGGT…Insert…
 G  T  E  T  S  Q  V  A  P  A  *  *     XhoI                                AgeI
GGTACCGAGACCAGCCAGGTGGCCCCTGCATAATGATCACTCGAG
KpnI
```

(D) The vector of pHLSta-1D4

The unique feature: The SP of RPTPσ in pHLsec-1D4 was substituted for the SP of human stanniocalcin-1 (Liu et al., 2009)

```
EcoRI  Kozak M  L  Q  N  S  A  V  L  L  V  L  V  I  S  A  S  A  T  H  E  A  E  Q  T  G
GAATTCGCCACCATGCTCCAAAACTCAGCAGTGCTTCTGGTGCTGGTGATCAGTGCTTCTGCAACCCATGAGGCGGAGCAGACCGGT…Insert
 G  T  E  T  S  Q  V  A  P  A  *  *     XhoI                                      AgeI
GGTACCGAGACCAGCCAGGTGGCCCCTGCATAATGATCACTCGAG
KpnI
```

(E) The vector of pHLAzu-1D4

The unique feature: The SP of RPTPσ in pHLsec-1D4 was substituted for the SP of human azurocidin (Olczak and Olczak, 2006)

EcoRI Kozak M T R L T V L A L L A G L L A S S R A G S S P L L D

GAATTCGCCACCATGACCCGGCTGACAGTCCTGGCCCTGCTGGCTGGTCTGCTGGCGTCCTCGAGGGCCGGCTCCAGCCCCCTTTTGGAC

T G G T E T S Q V A P A * * XhoI

ACCGGT…Insert…GGTACCGAGACCAGCCAGGTGGCCCCTGCA**TAATGA**TCACTCGAG

AgeI KpnI

(F) The vector of pHLArt-1D4

The unique feature: The SP of RPTPσ in pHLsec-1D4 was substituted for the SP of artifact (Barash et al., 2002)

EcoRI Kozak M W W R L W W L L L L L L L L W P M V W A T G

GAATTCGCCACCATGTGGTGGCGCCTGTGGTGGCTGCTGCTGCTGCTGCTGCTGTGGCCCATGGTGTGGGCCACCGGT…Insert…

G T E T S Q V A P A * * XhoI AgeI

GGTACCGAGACCAGCCAGGTGGCCCCTGCATAATGATCACTCGAG

KpnI

(G) The vector of pHLSer-1D4

The unique feature: The SP of RPTPσ in pHLsec-1D4 was substituted for the SP of rat serum albumin (Shi et al., 2011; Zou and Sun, 2004)

EcoRI Kozak M K W V T F L L L L F I S G S A F S T G

GAATTCGCCACCATGAAATGGGTCACCTTCCTGCTGCTGCTGTTCATCAGCGGCAGCGCCTTCAGCACCGGT…Insert…

G T E T S Q V A P A * * XhoI AgeI

GGTACCGAGACCAGCCAGGTGGCCCCTGCA**TAATGA**TCACTCGAG

KpnI

(H) The vector of pHL-FC-1D4

The unique feature: The vector is modified from pHL-FCHis vector (Aricescu et al., 2006) and it contains a **3C protease cleavage** site followed by three **GGS linker** sequences, the **human IgGγ1 hinge and Fc** regions and finally a Rho-1D4 tag.

```
EcoRI HindIIIKozak M  G  I  L  P  S  P  G  M  P  A  L  L  S  L  V  S  L  L  S  V  L  L  M
GAATTCAAGCTTGCCACCATGGGGATCCTTCCCAGCCCTGGGATGCCTGCGCTGCTCTCCCTCGTGAGCCTTCTCTCCGTGCTGCTGATG
 G  C  V  A  E  T  G
GGTTGCGTAGCTGAAACCGGT.........................Insert.................................
               AgeI
 KpnI
 G  T  L  E  V  L  F  Q  G  P  G  G  S  G  G  S  G  G  S  K  S  C  D  K  T  H  T  C  P  P
GGTACCCTGGAAGTGCTGTTTCAGGGCCCCGGGGGCTCTGGCGGAAGCGGCGGATCTAAATCTTGTGACAAAACTCACACATGCCCACCG
 C  P  A  P  E  L  L  G  G  P  S  V  F  L  F  P  P  K  P  K  D  T  L  M  I  S  R  T  P  E
TGCCCAGCACCTGAACTCCTGGGGGGACCGTCAGTCTTCCTCTTCCCCCCAAAACCCAAGGACACCCTCATGATCTCCCGGACCCCTGAG
 V  T  C  V  V  V  D  V  S  H  E  D  P  E  V  K  F  N  W  Y  V  D  G  V  E  V  H  N  A  K
GTCACATGCGTGGTGGTGGACGTGAGCCACGAAGACCCTGAGGTCAAGTTCAACTGGTACGTGGACGGCGTGGAGGTGCATAATGCCAAG
 T  K  P  R  E  E  Q  Y  N  S  T  Y  R  V  V  S  V  L  T  V  L  H  Q  D  W  L  N  G  K  E
ACAAAGCCGCGGGAGGAGCAGTACAACAGCACGTACCGTGTGGTCAGCGTCCTCACCGTCCTGCACCAGGACTGGCTGAATGGCAAGGAG
 Y  K  C  K  V  S  N  K  A  L  P  A  P  I  E  K  T  I  S  K  A  K  G  Q  P  R  E  P  Q  V
TACAAGTGCAAGGTCTCCAACAAAGCCCTCCCAGCCCCCATCGAGAAAACCATCTCCAAAGCCAAAGGGCAGCCCCGAGAACCACAGGTG
 Y  T  L  P  P  S  R  D  E  L  T  K  N  Q  V  S  L  T  C  L  V  K  G  F  Y  P  S  D  I  A
TACACCCTGCCCCCATCCCGGGATGAGCTGACCAAGAACCAGGTCAGCCTGACCTGCCTGGTCAAAGGCTTCTATCCCAGCGACATCGCC
 V  E  W  E  S  N  G  Q  P  E  N  N  Y  K  A  T  P  P  V  L  D  S  D  G  S  F  F  L  Y  S
GTGGAGTGGGAGAGCAATGGGCAGCCGGAGAACAACTACAAGGCCACGCCTCCCGTGCTGGACTCCGACGGCTCCTTCTTCCTCTACAGC
 K  L  T  V  D  K  S  R  W  Q  Q  G  N  V  F  S  C  S  V  M  H  E  A  L  H  N  H  Y  T  Q
AAGCTCACCGTGGACAAGAGCAGGTGGCAGCAGGGGAACGTCTTCTCATGCTCCGTGATGCATGAGGCTCTGCACAACCACTACACGCAG
 K  S  L  S  L  S  P  G  K  S  T  E  T  S  Q  V  A  P  A  *  *  XhoI
AAGAGCCTCTCCCTGTCTCCGGGTAAATCCACAGAGACAAGCCAGGTGGCCCCTGCCTAATGACTCGAG
```

(I) The vector of pHL-AP-1D4

The unique feature: The vector is modified from pHLsec vector (Aricescu et al., 2006) and it contains a **3C protease cleavage** site followed by three **GGS linker** sequences, the **human alkaline phosphatase** and finally a Rho-1D4 tag.

```
EcoRI HindIIIKozak M  G  I  L  P  S  P  G  M  P  A  L  L  S  L  V  S  L  L  S  V  L  L  M
GAATTCAAGCTTGCCACCATGGGGATCCTTCCCAGCCCTGGGATGCCTGCGCTGCTCTCCCTCGTGAGCCTTCTCTCCGTGCTGCTGATG
 G  C  V  A  E  T  G
GGTTGCGTAGCTGAAACCGGT.........................Insert.....................................
               AgeI
 KpnI
 G  T  L  E  V  L  F  Q  G  P  G  G  S  G  G  S  G  G  S  I  I  P  V  E  E  E  N  P  D  F
GGTACCCTGGAAGTGCTGTTTCAGGGCCCCGGGGGCTCTGGCGGAAGCGGCGGATCTATCATCCCAGTTGAGGAGGAGAACCCAGACTTC
 W  N  R  E  A  A  E  A  L  G  A  A  K  K  L  Q  P  A  Q  T  A  A  K  N  L  I  I  F  L  G
TGGAACCGCGAGGCAGCCGAGGCCCTGGGTGCCGCCAAGAAGCTGCAGCCTGCACAGACAGCCGCCAAGAACCTCATCATCTTCCTGGGC
 D  G  M  G  V  S  T  V  T  A  A  R  I  L  K  G  Q  K  K  D  K  L  G  P  E  I  P  L  A  M
GATGGGATGGGGGTGTCTACGGTGACAGCTGCCAGGATCCTAAAAGGGCAGAAGAAGGACAAACTGGGGCCTGAGATACCCCTGGCCATG
 D  R  F  P  Y  V  A  L  S  K  T  Y  N  V  D  K  H  V  P  D  S  G  A  T  A  T  A  Y  L  C
GACCGCTTCCCATATGTGGCTCTGTCCAAGACATACAATGTAGACAAACATGTGCCAGACAGTGGAGCCACAGCCACGGCCTACCTGTGC
 G  V  K  G  N  F  Q  T  I  G  L  S  A  A  A  R  F  N  Q  C  N  T  T  R  G  N  E  V  I  S
GGGGTCAAGGGCAACTTCCAGACCATTGGCTTGAGTGCAGCCGCCCGCTTTAACCAGTGCAACACGACACGCGGCAACGAGGTCATCTCC
 V  M  N  R  A  K  K  A  G  K  S  V  G  V  V  T  T  T  R  V  Q  H  A  S  P  A  G  T  Y  A
GTGATGAATCGGGCCAAGAAAGCAGGGAAGTCAGTGGGAGTGGTAACCACCACACGAGTGCAGCACGCCTCGCCAGCCGGCACCTACGCC
 H  T  V  N  R  N  W  Y  S  D  A  D  V  P  A  S  A  R  Q  E  G  C  Q  D  I  A  T  Q  L  I
CACACGGTGAACCGCAACTGGTACTCGGACGCCGACGTGCCTGCCTCCGCCCGCCAGGAGGGGTGCCAGGACATCGCTACGCAGCTCATC
 S  N  M  D  I  D  V  I  L  G  G  G  R  K  Y  M  F  R  M  G  T  P  D  P  E  Y  P  D  D  Y
TCCAACATGGACATTGACGTGATCCTAGGTGGAGGCCGAAAGTACATGTTTCGCATGGGAACCCCAGACCCTGAGTACCCAGATGACTAC
 S  Q  G  G  T  R  L  D  G  K  N  L  V  Q  E  W  L  A  K  R  Q  G  A  R  Y  V  W  N  R  T
AGCCAAGGTGGGACCAGGCTGGACGGGAAGAATCTGGTGCAGGAATGGCTGGCGAAGCGCCAGGGTGCCCGGTATGTGTGGAACCGCACT
 E  L  M  Q  A  S  L  D  P  S  V  T  H  L  M  G  L  F  E  P  G  D  M  K  Y  E  I  H  R  D
GAGCTCATGCAGGCTTCCCTGGACCCGTCTGTGACCCATCTCATGGGTCTCTTTGAGCCTGGAGACATGAAATACGAGATCCACCGAGAC
 S  T  L  D  P  S  L  M  E  M  T  E  A  A  L  R  L  L  S  R  N  P  R  G  F  F  L  F  V  E
TCCACACTGGACCCCTCCCTGATGGAGATGACAGAGGCTGCCCTGCGCCTGCTGAGCAGGAACCCCCGCGGCTTCTTCCTCTTCGTGGAG
 G  G  R  I  D  H  G  H  H  E  S  R  A  Y  R  A  L  T  E  T  I  M  F  D  D  A  I  E  R  A
GGTGGTCGCATCGACCATGGTCATCATGAAAGCAGGGCTTACCGGGCACTGACTGAGACGATCATGTTCGACGACGCCATTGAGAGGGCG
 G  Q  L  T  S  E  E  D  T  L  S  L  V  T  A  D  H  S  H  V  F  S  F  G  G  Y  P  L  R  G
GGCCAGCTCACCAGCGAGGAGGACACGCTGAGCCTCGTCACTGCCGACCACTCCCACGTCTTCTCCTTCGGAGGCTACCCCCTGCGAGGG
 S  S  I  F  G  L  A  P  G  K  A  R  D  R  K  A  Y  T  V  L  L  Y  G  N  G  P  G  Y  V  L
```

AGCTCCATCTTCGGGCTGGCCCCTGGCAAGGCCCGGGACAGGAAGGCCTACACGGTCCTCCTATACGGAAACGGTCCAGGCTATGTGCTC

K D G A R P D V T E S E S G S P E Y R Q Q S A V P L D E E T

AAGGACGGCGCCCGGCCGGATGTTACCGAGAGCGAGAGCGGGAGCCCCGAGTATCGGCAGCAGTCAGCAGTGCCCCTGGACGAAGAGACC

H A G E D V A V F A R G P Q A H L V H G V Q E Q T F I A H V

CACGCAGGCGAGGACGTGGCGGTGTTCGCGCGCGGCCCGCAGGCGCACCTGGTTCACGGCGTGCAGGAGCAGACCTTCATAGCGCACGTC

M A F A A C L E P Y T A C D L A P P A G T T D A A H P G K S

ATGGCCTTCGCCGCCTGCCTGGAGCCCTACACCGCCTGCGACCTGGCGCCCCCCGCCGGCACCACCGACGCCGCGCACCCGGGGAAGTCC

T E T S Q V A P A * * XhoI

ACAGAGACAAGCCAGGTGGCCCCTGCCTAATGACTCGAG

(J) The vector of pHL-mVenus-1D4

The unique feature: The vector is modified from pHL-mVenus (a gift from Drs. A. Clayton and A. R. Aricescu, University of Oxford, UK) and it contains a **3C protease cleavage** site followed by **linker** sequences, the **monoVenus** and finally a Rho-1D4 tag.

```
EcoRI HindIIIKozak M  G  I  L  P  S  P  G  M  P  A  L  L  S  L  V  S  L  L  S  V  L  L  M
GAATTCAAGCTTGCCACCATGGGGATCCTTCCCAGCCCTGGGATGCCTGCGCTGCTCTCCCTCGTGAGCCTTCTCTCCGTGCTGCTGATG
 G  C  V  A  E  T  G
GGTTGCGTAGCTGAAACCGGT.......................Insert.................................
               AgeI
 KpnI
 G  T  L  E  V  L  F  Q  G  P  G  S  G  G  S  G  G  S  M  V  S  K  G  E  E  L  F  T  G  V
GGTACCCTGGAAGTGCTGTTTCAGGGCCCCGGCTCTGGCGGAAGCGGCGGATCTATGGTGAGCAAGGGCGAGGAGCTGTTCACCGGGGTG
 V  P  I  L  V  E  L  D  G  D  V  N  G  H  K  F  S  V  S  G  E  G  E  G  D  A  T  Y  G  K
GTGCCCATCCTGGTCGAGCTGGACGGCGACGTAAACGGCCACAAGTTCAGCGTGTCCGGCGAGGGCGAGGGCGATGCCACCTACGGCAAG
 L  T  L  K  L  I  C  T  T  G  K  L  P  V  P  W  P  T  L  V  T  T  L  G  Y  G  L  Q  C  F
CTGACCCTGAAGCTGATCTGCACCACCGGCAAGCTGCCCGTGCCCTGGCCCACCCTCGTGACCACCCTGGGCTACGGCCTGCAGTGCTTC
 A  R  Y  P  D  H  M  K  Q  H  D  F  F  K  S  A  M  P  E  G  Y  V  Q  E  R  T  I  F  F  K
GCCCGCTACCCCGACCACATGAAGCAGCACGACTTCTTCAAGTCCGCCATGCCCGAAGGCTACGTCCAGGAGCGCACCATCTTCTTCAAG
 D  D  G  N  Y  K  T  R  A  E  V  K  F  E  G  D  T  L  V  N  R  I  E  L  K  G  I  D  F  K
GACGACGGCAACTACAAGACCCGCGCCGAGGTGAAGTTCGAGGGCGACACCCTGGTGAACCGCATCGAGCTGAAGGGCATCGACTTCAAG
 E  D  G  N  I  L  G  H  K  L  E  Y  N  Y  N  S  H  N  V  Y  I  T  A  D  K  Q  K  N  G  I
GAGGACGGCAACATCCTGGGGCACAAGCTGGAGTACAACTACAACAGCCACAACGTCTATATCACCGCCGACAAGCAGAAGAACGGCATC
 K  A  N  F  K  I  R  H  N  I  E  D  G  G  V  Q  L  A  D  H  Y  Q  Q  N  T  P  I  G  D  G
AAGGCCAACTTCAAGATCCGCCACAACATCGAGGACGGCGGCGTGCAGCTCGCCGACCACTACCAGCAGAACACCCCCATCGGCGACGGC
 P  V  L  L  P  D  N  H  Y  L  S  Y  Q  S  K  L  S  K  D  P  N  E  K  R  D  H  M  V  L  L
CCCGTGCTGCTGCCCGACAACCACTACCTGAGCTACCAGTCCAAGCTGAGCAAAGACCCCAACGAGAAGCGCGATCACATGGTCCTGCTG
 E  F  V  T  A  A  G  I  T  L  G  M  D  E  L  Y  K  S  T  E  T  S  Q  V  A  P  A  *  *  XhoI
GAGTTCGTGACCGCCGCCGGGATCACTCTCGGCATGGACGAGCTGTACAAGTCCACAGAGACAAGCCAGGTGGCCCCTGCCTAATGACTCGAG
```

(K) The vector of pHL-mVenus-12H

The vector has the same backbone as **pHL-mVenus-1D4**. But, a Rho-1D4 tag of **pHL-mVenus-1D4** was replaced by the tag of HHHHHHSGSHHHHHH.

(L) The vector of pHLsec-8H-SUMO-1D4

The unique feature: The vector is modified from pHL**sec**-**1D4** and it contains an **octahistidine** tag followed by an engineered **SUMO** tag and **linker** sequences as well as a **3C protease cleavage** site. Inserts can be cloned into the vector by using the XmaI and KpnI sites.

```
EcoRI HindIIIKozak M  G  I  L  P  S  P  G  M  P  A  L  L  S  L  V  S  L  L  S  V  L  L  M
GAATTCAAGCTTGCCACCATGGGGATCCTTCCCAGCCCTGGGATGCCTGCGCTGCTCTCCCTCGTGAGCCTTCTCTCCGTGCTGCTGATG
                AgeI
 G  C  V  A  E  T  G  S  H  H  H  H  H  H  H  H  S  S  G  S  D  S  E  V  N  Q  E  A  K  P
GGTTGCGTAGCTGAAACCGGTAGCCACCACCATCACCATCACCACCACAGCAGCGGCAGCGACAGCGAAGTGAACCAGGAAGCCAAGCCC
 E  V  K  P  E  V  K  P  E  T  H  I  N  L  K  V  S  D  G  S  S  E  I  F  F  K  I  K  K  T
GAAGTGAAACCTGAAGTGAAGCCCGAGACACACATCAACCTGAAGGTGTCCGACGGCAGCAGCGAGATCTTCTTCAAGATCAAGAAAACC
 T  P  L  R  R  L  M  E  A  F  A  K  R  Q  G  K  E  M  D  S  L  T  F  L  Y  D  G  I  E  I
ACCCCCCTGCGGCGGCTGATGGAAGCCTTTGCCAAGCGGCAGGGCAAAGAGATGGACAGCCTGACCTTCCTGTACGACGGCATCGAGATC
 Q  A  D  Q  T  P  E  D  L  D  M  E  D  N  D  I  I  E  A  H  R  E  Q  I  S  G  T  G  S  G
CAGGCCGACCAGACCCCCGAGGACCTGGACATGGAAGATAACGACATCATCGAGGCCCACAGAGAGCAGATCAGCGGCACAGGCTCTGGC
 L  E  V  L  F  Q  G  P  G          G  T  E  T  S  Q  V  A  P  A  *  *     XhoI
CTGGAAGTGCTGTTCCAGGGCCCCGGG…Insert…GGTACCGAGACCAGCCAGGTGGCCCCTGCATAATGATCACTCGAG
                    XmaI             KpnI
```

(M) The vector of pHLsec-STR-8H-SUMO-1D4

The unique feature: The vector is modified from pHLSec-**8H**-**SUMO**-**1D4** and it contains a **Strep-Tag II** prior to an **octahistidine** tag followed by an engineered **SUMO** tag and **linker** sequences as well as a **3C protease cleavage** site. Inserts can be cloned into the vector by using the XmaI and KpnI sites.

```
EcoRI HindIIIKozak M  G  I  L  P  S  P  G  M  P  A  L  L  S  L  V  S  L  L  S  V  L  L  M
GAATTCAAGCTTGCCACCATGGGGATCCTTCCCAGCCCTGGGATGCCTGCGCTGCTCTCCCTCGTGAGCCTTCTCTCCGTGCTGCTGATG
                AgeI
 G  C  V  A  E  T  G  S  A  W  S  H  P  Q  F  E  K  G  S  S  H  H  H  H  H  H  H  H  S  S
GGTTGCGTAGCTGAAACCGGTTCCGCCTGGTCCCACCCCCAGTTCGAGAAGGGCAGCAGCCACCACCATCACCATCACCACCACAGCAGC
 G  S  D  S  E  V  N  Q  E  A  K  P  E  V  K  P  E  V  K  P  E  T  H  I  N  L  K  V  S  D
GGCAGCGACAGCGAAGTGAACCAGGAAGCCAAGCCCGAAGTGAAACCTGAAGTGAAGCCCGAGACACACATCAACCTGAAGGTGTCCGAC
 G  S  S  E  I  F  F  K  I  K  K  T  T  P  L  R  R  L  M  E  A  F  A  K  R  Q  G  K  E  M
GGCAGCAGCGAGATCTTCTTCAAGATCAAGAAAACCACCCCCCTGCGGCGGCTGATGGAAGCCTTTGCCAAGCGGCAGGGCAAAGAGATG
 D  S  L  T  F  L  Y  D  G  I  E  I  Q  A  D  Q  T  P  E  D  L  D  M  E  D  N  D  I  I  E
GACAGCCTGACCTTCCTGTACGACGGCATCGAGATCCAGGCCGACCAGACCCCCGAGGACCTGGACATGGAAGATAACGACATCATCGAG
 A  H  R  E  Q  I  S  G  T  G  S  G  L  E  V  L  F  Q  G  P  G          G  T  E  T  S  Q
GCCCACAGAGAGCAGATCAGCGGCACAGGCTCTGGCCTGGAAGTGCTGTTCCAGGGCCCCGGG…Insert…GGTACCGAGACCAGCCAG
 V  A  P  A  *  *     XhoI                                XmaI            KpnI
GTGGCCCCTGCATAATGATCACTCGAG
```

Appendix 2. List of Formulae

Formula 1:

$$I_{\mathrm{hkl}} = |F_{\mathrm{hkl}}|^2$$

where $F_{\mathrm{hkl}} = \sum_j f_{\mathrm{j}} \exp\left(2\pi i(hx_{\mathrm{j}} + ky_{\mathrm{j}} + lz_{\mathrm{j}})\right) exp(-B_{\mathrm{j}} sin^2\vartheta/\lambda^2)$

and f_{j} is the atomic scattering factor.

Formula 2:

$$R_{\mathrm{work}} = \frac{\sum_{hkl} \left| |F_{\mathrm{obs}}| - |F_{\mathrm{calc}}| \right|}{\sum_{hkl} |F_{\mathrm{obs}}|}$$

where $|F_{\mathrm{obs}}|$ are the experimentally observed structure factor amplitudes and $|F_{\mathrm{calc}}|$ are the structure factor amplitudes calculated from the model.

Formula 3:

$$R_{\mathrm{free}} = \frac{\sum_{test\ set\ hkl} \left| |F_{\mathrm{obs}}| - |F_{\mathrm{calc}}| \right|}{\sum_{test\ set\ hkl} |F_{\mathrm{obs}}|}$$

calculated as R_{work} but only with 5% of data that have been excluded from the refinement.

Appendix 3. Abbreviations

AC	Affinity chromatography
APC	Adenomatous polyposis coli
AP	Alkaline phosphatase
BBB	Blood-brain barrier
BRB	Blood-retina barrier
β-TRCP1	β-transducin repeat-containing protein 1
B_{max}	The SPR signal value (in RUs) obtained at the receptor saturation level
°C	Celsius
cDNA	Complementary Deoxyribonucleic Acid
CCP4	Collaborative Computing Project 4
CHAPS	A zwitterionic detergent, 3-[(3-Cholamidopropyl)dimethylammonio]-1-propanesulfonate, $C_{32}H_{58}N_2O_7S$
CK1	Casein kinase 1
CNBr-1D4	CNBr-activated beads conjugated 1D4 antibody
CRD	Cysteine-rich domain
CV	Column volume
DMEM	Dulbecco's modified eagle's medium
ECL	Enhanced chemilluminescence
EDTA	Ethylenediaminetetraacetic acid, $C_{10}H_{16}N_2O_8$
Endo-F_1	Endoglycosidase-F_1
FCS	Fetal calf serum
FPLC	Fast protein liquid chromatography
FEVR	Familial exudative vitreoretinopathy
FC	Human IgGγ1 FC region
GAG	glycosaminoglycans
GlcNAc	N-Acetylglucosamine
GPCR	G protein-coupled receptor
GSK3	Glycogen synthase kinase
iHDAC	Histone deacetylase inhibitors

HEK293T	Human embryonic kidney 293 cells expressing SV40 type T antigen
HEK293S	Human embryonic kidney 293 cells GnTI deficient
HEPES	*N*-[2-Hydroxyethyl]piperazine-*N'*-[2-ethanesulphonic acid]
HRP	Horseradish peroxidase
HSPG	heparan sulfate proteoglycan
IMAC	Immobilised metal affinity chromatography
kDa	Kilodalton
K_d	Dissociation constant
LB	Luria-Bertani Media
Lrp5	Low density lipoprotein receptor related protein
MBP	Maltose binding protein
NDP	Norrie disease protein
OPPF	Oxford protein production facility
PBS	Phosphate-buffered saline
PCR	Polymerase chain reaction
pdb	Protein data bank
PEI	Polyethylenimine
PCP	planar cell polarity
SB	Sodium Butyrate
SDS-PAGE	Sodium dodecyl sulphate polyacrylamide gel electrophoresis
SP	Signal peptide
SPR	Surface Plasmon Resonance
sFRP	Secreted Frizzled-related protein
SEC	Size-exclusion chromatography
SUMO	Small ubiquitin-like modifier
SOS	Sucrose Octasulfate
TCF/LEF	T cell factor/lymphoid enhancer factor family
TGF	Transforming growth factor
Tris	Tris(hydroxymethyl)aminomethane, $(HOCH_2)_3CNH_2$

TM	Transmembrane domain
Tspan-12	Tetraspanin-12
Tween 20	A polysorbate surfactant, polyoxyethylene (20) sorbitan monolaurate
VPA	Valproic acid
Rho-1D4	TETSQVAPA The epitope recognized by anti-rhodopsin antibody 1D4
ROP	Retinopathy Of Prematurity
8xHis	Octa-Histidine tag

References

Aberle, H., Bauer, A., Stappert, J., Kispert, A., and Kemler, R. (1997). beta-catenin is a target for the ubiquitin-proteasome pathway. EMBO J *16*, 3797-3804.
Adams, P.D., Afonine, P.V., Bunkoczi, G., Chen, V.B., Davis, I.W., Echols, N., Headd, J.J., Hung, L.W., Kapral, G.J., Grosse-Kunstleve, R.W.*, et al.* (2010). PHENIX: a comprehensive Python-based system for macromolecular structure solution. Acta Crystallogr D Biol Crystallogr *66*, 213-221.
Adams, P.D., Grosse-Kunstleve, R.W., Hung, L.W., Ioerger, T.R., McCoy, A.J., Moriarty, N.W., Read, R.J., Sacchettini, J.C., Sauter, N.K., and Terwilliger, T.C. (2002). PHENIX: building new software for automated crystallographic structure determination. Acta Crystallogr D Biol Crystallogr *58*, 1948-1954.
Ahn, V.E., Chu, M.L., Choi, H.J., Tran, D., Abo, A., and Weis, W.I. (2011). Structural basis of Wnt signaling inhibition by Dickkopf binding to LRP5/6. Dev Cell *21*, 862-873.
Alegria-Schaffer, A., Lodge, A., and Vattem, K. (2009). Performing and optimizing Western blots with an emphasis on chemiluminescent detection. Methods Enzymol *463*, 573-599.
Alexandre, C., Baena-Lopez, A., and Vincent, J.P. (2014). Patterning and growth control by membrane-tethered Wingless. Nature *505*, 180-185.
Anastas, J.N., and Moon, R.T. (2013). WNT signalling pathways as therapeutic targets in cancer. Nature reviews Cancer *13*, 11-26.
Angers, S., and Moon, R.T. (2009). Proximal events in Wnt signal transduction. Nat Rev Mol Cell Biol *10*, 468-477.
Aricescu, A.R., Lu, W., and Jones, E.Y. (2006). A time- and cost-efficient system for high-level protein production in mammalian cells. Acta Crystallogr D Biol Crystallogr *62*, 1243-1250.
Aryal, M., Arvanitis, C.D., Alexander, P.M., and McDannold, N. (2014). Ultrasound-mediated blood-brain barrier disruption for targeted drug delivery in the central nervous system. Advanced drug delivery reviews *72*, 94-109.
Ashkenazy, H., Erez, E., Martz, E., Pupko, T., and Ben-Tal, N. (2010). ConSurf 2010: calculating evolutionary conservation in sequence and structure of proteins and nucleic acids. Nucleic Acids Res *38*, W529-533.
Backliwal, G., Hildinger, M., Kuettel, I., Delegrange, F., Hacker, D.L., and Wurm, F.M. (2008). Valproic acid: a viable alternative to sodium butyrate for enhancing protein expression in mammalian cell cultures. Biotechnol Bioeng *101*, 182-189.
Baeg, G.H., Lin, X., Khare, N., Baumgartner, S., and Perrimon, N. (2001). Heparan sulfate proteoglycans are critical for the organization of the extracellular distribution of Wingless. Development *128*, 87-94.
Baker, N.A., Sept, D., Joseph, S., Holst, M.J., and McCammon, J.A. (2001). Electrostatics of nanosystems: application to microtubules and the ribosome. Proc Natl Acad Sci U S A *98*, 10037-10041.
Bao, J., Zheng, J.J., and Wu, D. (2012). The structural basis of DKK-mediated inhibition of Wnt/LRP signaling. Sci Signal *5*, pe22.
Barash, S., Wang, W., and Shi, Y. (2002). Human secretory signal peptide description by hidden Markov model and generation of a strong artificial signal

peptide for secreted protein expression. Biochem Biophys Res Commun *294*, 835-842.
Battye, T.G., Kontogiannis, L., Johnson, O., Powell, H.R., and Leslie, A.G. (2011). iMOSFLM: a new graphical interface for diffraction-image processing with MOSFLM. Acta Crystallogr D Biol Crystallogr *67*, 271-281.
Berger, W., Meindl, A., van de Pol, T.J., Cremers, F.P., Ropers, H.H., Doerner, C., Monaco, A., Bergen, A.A., Lebo, R., Warburg, M.*, et al.* (1992a). Isolation of a candidate gene for Norrie disease by positional cloning. Nat Genet *1*, 199-203.
Berger, W., van de Pol, D., Warburg, M., Gal, A., Bleeker-Wagemakers, L., de Silva, H., Meindl, A., Meitinger, T., Cremers, F., and Ropers, H.H. (1992b). Mutations in the candidate gene for Norrie disease. Hum Mol Genet *1*, 461-465.
Bhanot, P., Brink, M., Samos, C.H., Hsieh, J.C., Wang, Y., Macke, J.P., Andrew, D., Nathans, J., and Nusse, R. (1996). A new member of the frizzled family from Drosophila functions as a Wingless receptor. Nature *382*, 225-230.
Bilic, J., Huang, Y.L., Davidson, G., Zimmermann, T., Cruciat, C.M., Bienz, M., and Niehrs, C. (2007). Wnt induces LRP6 signalosomes and promotes dishevelled-dependent LRP6 phosphorylation. Science *316*, 1619-1622.
Binari, R.C., Staveley, B.E., Johnson, W.A., Godavarti, R., Sasisekharan, R., and Manoukian, A.S. (1997). Genetic evidence that heparin-like glycosaminoglycans are involved in wingless signaling. Development *124*, 2623-2632.
Boschert, V., van Dinther, M., Weidauer, S., van Pee, K., Muth, E.M., Ten Dijke, P., and Mueller, T.D. (2013). Mutational analysis of sclerostin shows importance of the flexible loop and the cystine-knot for Wnt-signaling inhibition. PLoS One *8*, e81710.
Bourhis, E., Tam, C., Franke, Y., Bazan, J.F., Ernst, J., Hwang, J., Costa, M., Cochran, A.G., and Hannoush, R.N. (2010). Reconstitution of a frizzled8.Wnt3a.LRP6 signaling complex reveals multiple Wnt and Dkk1 binding sites on LRP6. J Biol Chem *285*, 9172-9179.
Bourhis, E., Wang, W., Tam, C., Hwang, J., Zhang, Y., Spittler, D., Huang, O.W., Gong, Y., Estevez, A., Zilberleyb, I.*, et al.* (2011). Wnt antagonists bind through a short peptide to the first beta-propeller domain of LRP5/6. Structure *19*, 1433-1442.
Brunger, A.T. (1993). Assessment of phase accuracy by cross validation: the free R value. Methods and applications. Acta Crystallogr D Biol Crystallogr *49*, 24-36.
Bujacz, G., Wrzesniewska, B., and Bujacz, A. (2010). Cryoprotection properties of salts of organic acids: a case study for a tetragonal crystal of HEW lysozyme. Acta Crystallogr D Biol Crystallogr *66*, 789-796.
Capurro, M., Martin, T., Shi, W., and Filmus, J. (2014). Glypican-3 binds to Frizzled and plays a direct role in the stimulation of canonical Wnt signaling. J Cell Sci *127*, 1565-1575.
Carmon, K.S., Gong, X., Lin, Q., Thomas, A., and Liu, Q. (2011). R-spondins function as ligands of the orphan receptors LGR4 and LGR5 to regulate Wnt/beta-catenin signaling. Proc Natl Acad Sci U S A *108*, 11452-11457.
Chang, V.T., Crispin, M., Aricescu, A.R., Harvey, D.J., Nettleship, J.E., Fennelly, J.A., Yu, C., Boles, K.S., Evans, E.J., Stuart, D.I.*, et al.* (2007). Glycoprotein structural genomics: solving the glycosylation problem. Structure *15*, 267-273.
Chen, S., Bubeck, D., MacDonald, B.T., Liang, W.X., Mao, J.H., Malinauskas, T., Llorca, O., Aricescu, A.R., Siebold, C., He, X.*, et al.* (2011). Structural and functional

studies of LRP6 ectodomain reveal a platform for Wnt signaling. Dev Cell *21*, 848-861.
Chen, V.B., Arendall, W.B., 3rd, Headd, J.J., Keedy, D.A., Immormino, R.M., Kapral, G.J., Murray, L.W., Richardson, J.S., and Richardson, D.C. (2010). MolProbity: all-atom structure validation for macromolecular crystallography. Acta Crystallogr D Biol Crystallogr *66*, 12-21.
Chen, Z.Y., Hendriks, R.W., Jobling, M.A., Powell, J.F., Breakefield, X.O., Sims, K.B., and Craig, I.W. (1992). Isolation and characterization of a candidate gene for Norrie disease. Nat Genet *1*, 204-208.
Cheng, Z., Biechele, T., Wei, Z., Morrone, S., Moon, R.T., Wang, L., and Xu, W. (2011). Crystal structures of the extracellular domain of LRP6 and its complex with DKK1. Nat Struct Mol Biol *18*, 1204-1210.
Clevers, H., and Nusse, R. (2012). Wnt/beta-catenin signaling and disease. Cell *149*, 1192-1205.
Coloma, M.J., Hastings, A., Wims, L.A., and Morrison, S.L. (1992). Novel vectors for the expression of antibody molecules using variable regions generated by polymerase chain reaction. J Immunol Methods *152*, 89-104.
Cowtan, K. (2006). The Buccaneer software for automated model building. 1. Tracing protein chains. Acta Crystallogr D Biol Crystallogr *62*, 1002-1011.
Cowtan, K. (2010). Recent developments in classical density modification. Acta Crystallogr D Biol Crystallogr *66*, 470-478.
Cruciat, C.M., and Niehrs, C. (2013). Secreted and transmembrane wnt inhibitors and activators. Cold Spring Harbor perspectives in biology *5*, a015081.
Csak, K., Szabo, V., Szabo, A., and Vannay, A. (2006). Pathogenesis and genetic basis for retinopathy of prematurity. Frontiers in bioscience : a journal and virtual library *11*, 908-920.
Daly, N.L., and Craik, D.J. (2011). Bioactive cystine knot proteins. Current opinion in chemical biology *15*, 362-368.
Dann, C.E., Hsieh, J.C., Rattner, A., Sharma, D., Nathans, J., and Leahy, D.J. (2001). Insights into Wnt binding and signalling from the structures of two Frizzled cysteine-rich domains. Nature *412*, 86-90.
Davidson, G., Wu, W., Shen, J., Bilic, J., Fenger, U., Stannek, P., Glinka, A., and Niehrs, C. (2005). Casein kinase 1 gamma couples Wnt receptor activation to cytoplasmic signal transduction. Nature *438*, 867-872.
DeAlmeida, V.I., Miao, L., Ernst, J.A., Koeppen, H., Polakis, P., and Rubinfeld, B. (2007). The soluble wnt receptor Frizzled8CRD-hFc inhibits the growth of teratocarcinomas in vivo. Cancer research *67*, 5371-5379.
Deng, C., Reddy, P., Cheng, Y., Luo, C.W., Hsiao, C.L., and Hsueh, A.J. (2013). Multi-functional norrin is a ligand for the LGR4 receptor. J Cell Sci *126*, 2060-2068.
Emsley, P., and Cowtan, K. (2004). Coot: model-building tools for molecular graphics. Acta Crystallogr D Biol Crystallogr *60*, 2126-2132.
Engelhardt, B., and Liebner, S. (2014). Novel insights into the development and maintenance of the blood-brain barrier. Cell and tissue research *355*, 687-699.
Ettenberg, S.A., Charlat, O., Daley, M.P., Liu, S., Vincent, K.J., Stuart, D.D., Schuller, A.G., Yuan, J., Ospina, B., Green, J.*, et al.* (2010). Inhibition of tumorigenesis driven by different Wnt proteins requires blockade of distinct ligand-binding regions by LRP6 antibodies. Proc Natl Acad Sci U S A *107*, 15473-15478.

Evans, P.R., and Murshudov, G.N. (2013). How good are my data and what is the resolution? Acta Crystallogr D Biol Crystallogr *69*, 1204-1214.
Flanagan, J.G., and Cheng, H.J. (2000). Alkaline phosphatase fusion proteins for molecular characterization and cloning of receptors and their ligands. Methods Enzymol *327*, 198-210.
Gadd, S.L., and Clevenger, C.V. (2006). Ligand-independent dimerization of the human prolactin receptor isoforms: functional implications. Mol Endocrinol *20*, 2734-2746.
Gent, J., van Kerkhof, P., Roza, M., Bu, G., and Strous, G.J. (2002). Ligand-independent growth hormone receptor dimerization occurs in the endoplasmic reticulum and is required for ubiquitin system-dependent endocytosis. Proc Natl Acad Sci U S A *99*, 9858-9863.
Glinka, A., Dolde, C., Kirsch, N., Huang, Y.L., Kazanskaya, O., Ingelfinger, D., Boutros, M., Cruciat, C.M., and Niehrs, C. (2011). LGR4 and LGR5 are R-spondin receptors mediating Wnt/beta-catenin and Wnt/PCP signalling. EMBO reports *12*, 1055-1061.
Goldschmidt, L., Cooper, D.R., Derewenda, Z.S., and Eisenberg, D. (2007). Toward rational protein crystallization: A Web server for the design of crystallizable protein variants. Protein Sci *16*, 1569-1576.
Gong, Y., Slee, R.B., Fukai, N., Rawadi, G., Roman-Roman, S., Reginato, A.M., Wang, H., Cundy, T., Glorieux, F.H., Lev, D.*, et al.* (2001). LDL receptor-related protein 5 (LRP5) affects bone accrual and eye development. Cell *107*, 513-523.
Grueninger-Leitch, F., D'Arcy, A., D'Arcy, B., and Chene, C. (1996). Deglycosylation of proteins for crystallization using recombinant fusion protein glycosidases. Protein Sci *5*, 2617-2622.
Grumolato, L., Liu, G., Mong, P., Mudbhary, R., Biswas, R., Arroyave, R., Vijayakumar, S., Economides, A.N., and Aaronson, S.A. (2010). Canonical and noncanonical Wnts use a common mechanism to activate completely unrelated coreceptors. Genes Dev *24*, 2517-2530.
Gurney, A., Axelrod, F., Bond, C.J., Cain, J., Chartier, C., Donigan, L., Fischer, M., Chaudhari, A., Ji, M., Kapoun, A.M.*, et al.* (2012). Wnt pathway inhibition via the targeting of Frizzled receptors results in decreased growth and tumorigenicity of human tumors. Proc Natl Acad Sci U S A *109*, 11717-11722.
Guttman, M., Weinkam, P., Sali, A., and Lee, K.K. (2013). All-atom ensemble modeling to analyze small-angle x-ray scattering of glycosylated proteins. Structure *21*, 321-331.
He, X., Semenov, M., Tamai, K., and Zeng, X. (2004). LDL receptor-related proteins 5 and 6 in Wnt/beta-catenin signaling: arrows point the way. Development *131*, 1663-1677.
Hiraoka, M., Takahashi, H., Orimo, H., Ogata, T., and Azuma, N. (2010). Genetic screening of Wnt signaling factors in advanced retinopathy of prematurity. Mol Vis *16*, 2572-2577.
Holdsworth, G., Slocombe, P., Doyle, C., Sweeney, B., Veverka, V., Le Riche, K., Franklin, R.J., Compson, J., Brookings, D., Turner, J.*, et al.* (2012). Characterization of the interaction of sclerostin with the low density lipoprotein receptor-related protein (LRP) family of Wnt co-receptors. J Biol Chem *287*, 26464-26477.
Holm, L., and Rosenstrom, P. (2010). Dali server: conservation mapping in 3D. Nucleic Acids Res *38*, W545-549.

Holyoak, T., Fenn, T.D., Wilson, M.A., Moulin, A.G., Ringe, D., and Petsko, G.A. (2003). Malonate: a versatile cryoprotectant and stabilizing solution for salt-grown macromolecular crystals. Acta Crystallogr D Biol Crystallogr *59*, 2356-2358.
Hsieh, J.C., Rattner, A., Smallwood, P.M., and Nathans, J. (1999). Biochemical characterization of Wnt-frizzled interactions using a soluble, biologically active vertebrate Wnt protein. Proc Natl Acad Sci U S A *96*, 3546-3551.
Ikeda, S., Kishida, S., Yamamoto, H., Murai, H., Koyama, S., and Kikuchi, A. (1998). Axin, a negative regulator of the Wnt signaling pathway, forms a complex with GSK-3beta and beta-catenin and promotes GSK-3beta-dependent phosphorylation of beta-catenin. EMBO J *17*, 1371-1384.
Janda, C.Y., Waghray, D., Levin, A.M., Thomas, C., and Garcia, K.C. (2012). Structural basis of Wnt recognition by Frizzled. Science *337*, 59-64.
Joiner, D.M., Ke, J., Zhong, Z., Xu, H.E., and Williams, B.O. (2013). LRP5 and LRP6 in development and disease. Trends in endocrinology and metabolism: TEM *24*, 31-39.
Junge, H.J., Yang, S., Burton, J.B., Paes, K., Shu, X., French, D.M., Costa, M., Rice, D.S., and Ye, W. (2009). TSPAN12 regulates retinal vascular development by promoting Norrin- but not Wnt-induced FZD4/beta-catenin signaling. Cell *139*, 299-311.
Kabsch, W. (2010). Xds. Acta Crystallogr D Biol Crystallogr *66*, 125-132.
Kahn, M. (2014). Can we safely target the WNT pathway? Nature reviews Drug discovery *13*, 513-532.
Kato, M., Patel, M.S., Levasseur, R., Lobov, I., Chang, B.H., Glass, D.A., 2nd, Hartmann, C., Li, L., Hwang, T.H., Brayton, C.F.*, et al.* (2002). Cbfa1-independent decrease in osteoblast proliferation, osteopenia, and persistent embryonic eye vascularization in mice deficient in Lrp5, a Wnt coreceptor. The Journal of cell biology *157*, 303-314.
Kaykas, A., Yang-Snyder, J., Heroux, M., Shah, K.V., Bouvier, M., and Moon, R.T. (2004). Mutant Frizzled 4 associated with vitreoretinopathy traps wild-type Frizzled in the endoplasmic reticulum by oligomerization. Nat Cell Biol *6*, 52-58.
Ke, J., Harikumar, K.G., Erice, C., Chen, C., Gu, X., Wang, L., Parker, N., Cheng, Z., Xu, W., Williams, B.O.*, et al.* (2013). Structure and function of Norrin in assembly and activation of a Frizzled 4-Lrp5/6 complex. Genes Dev *27*, 2305-2319.
Kenyon, J.R., and Craig, I.W. (1999). Analysis of the 5' regulatory region of the human Norrie's disease gene: evidence that a non-translated CT dinucleotide repeat in exon one has a role in controlling expression. Gene *227*, 181-188.
Kikuchi, A., Yamamoto, H., and Kishida, S. (2007). Multiplicity of the interactions of Wnt proteins and their receptors. Cell Signal *19*, 659-671.
Krissinel, E., and Henrick, K. (2004). Secondary-structure matching (SSM), a new tool for fast protein structure alignment in three dimensions. Acta Crystallogr D Biol Crystallogr *60*, 2256-2268.
Krissinel, E., and Henrick, K. (2007). Inference of macromolecular assemblies from crystalline state. J Mol Biol *372*, 774-797.
Kubatzky, K.F., Ruan, W., Gurezka, R., Cohen, J., Ketteler, R., Watowich, S.S., Neumann, D., Langosch, D., and Klingmuller, U. (2001). Self assembly of the transmembrane domain promotes signal transduction through the erythropoietin receptor. Curr Biol *11*, 110-115.

Kumar, S., Zigman, M., Patel, T.R., Trageser, B., Gross, J.C., Rahm, K., Boutros, M., Gradl, D., Steinbeisser, H., Holstein, T.*, et al.* (2014). Molecular dissection of Wnt3a-Frizzled8 interaction reveals essential and modulatory determinants of Wnt signaling activity. BMC biology *12*, 44.
Larkin, M.A., Blackshields, G., Brown, N.P., Chenna, R., McGettigan, P.A., McWilliam, H., Valentin, F., Wallace, I.M., Wilm, A., Lopez, R.*, et al.* (2007). Clustal W and Clustal X version 2.0. Bioinformatics *23*, 2947-2948.
Lawrence, M.C., and Colman, P.M. (1993). Shape complementarity at protein/protein interfaces. J Mol Biol *234*, 946-950.
Lin, X., and Perrimon, N. (1999). Dally cooperates with Drosophila Frizzled 2 to transduce Wingless signalling. Nature *400*, 281-284.
Liu, C., Li, Y., Semenov, M., Han, C., Baeg, G.H., Tan, Y., Zhang, Z., Lin, X., and He, X. (2002). Control of beta-catenin phosphorylation/degradation by a dual-kinase mechanism. Cell *108*, 837-847.
Liu, Y., Nguyen, A., Wolfert, R.L., and Zhuo, S. (2009). Enhancing the secretion of recombinant proteins by engineering N-glycosylation sites. Biotechnol Prog *25*, 1468-1475.
Logan, C.Y., and Nusse, R. (2004). The Wnt signaling pathway in development and disease. Annu Rev Cell Dev Biol *20*, 781-810.
Luhmann, U.F., Meunier, D., Shi, W., Luttges, A., Pfarrer, C., Fundele, R., and Berger, W. (2005). Fetal loss in homozygous mutant Norrie disease mice: a new role of Norrin in reproduction. Genesis *42*, 253-262.
MacDonald, B.T., and He, X. (2012). Frizzled and LRP5/6 receptors for Wnt/beta-catenin signaling. Cold Spring Harbor perspectives in biology *4*.
MacDonald, B.T., Tamai, K., and He, X. (2009). Wnt/beta-catenin signaling: components, mechanisms, and diseases. Dev Cell *17*, 9-26.
Malinauskas, T., Aricescu, A.R., Lu, W., Siebold, C., and Jones, E.Y. (2011). Modular mechanism of Wnt signaling inhibition by Wnt inhibitory factor 1. Nat Struct Mol Biol *18*, 886-893.
Malinauskas, T., and Jones, E.Y. (2014). Extracellular modulators of Wnt signalling. Current opinion in structural biology *29C*, 77-84.
Mayo, C.J., Diprose, J.M., Walter, T.S., Berry, I.M., Wilson, J., Owens, R.J., Jones, E.Y., Harlos, K., Stuart, D.I., and Esnouf, R.M. (2005). Benefits of automated crystallization plate tracking, imaging, and analysis. Structure *13*, 175-182.
McCoy, A.J. (2007). Solving structures of protein complexes by molecular replacement with Phaser. Acta Crystallogr D Biol Crystallogr *63*, 32-41.
McDonald, N.Q., and Hendrickson, W.A. (1993). A structural superfamily of growth factors containing a cystine knot motif. Cell *73*, 421-424.
McLellan, J.S., Yao, S., Zheng, X., Geisbrecht, B.V., Ghirlando, R., Beachy, P.A., and Leahy, D.J. (2006). Structure of a heparin-dependent complex of Hedgehog and Ihog. Proc Natl Acad Sci U S A *103*, 17208-17213.
Meindl, A., Berger, W., Meitinger, T., van de Pol, D., Achatz, H., Dorner, C., Haasemann, M., Hellebrand, H., Gal, A., Cremers, F.*, et al.* (1992). Norrie disease is caused by mutations in an extracellular protein resembling C-terminal globular domain of mucins. Nat Genet *2*, 139-143.
Meitinger, T., Meindl, A., Bork, P., Rost, B., Sander, C., Haasemann, M., and Murken, J. (1993). Molecular modelling of the Norrie disease protein predicts a cystine knot growth factor tertiary structure. Nat Genet *5*, 376-380.

Mikels, A.J., and Nusse, R. (2006). Purified Wnt5a protein activates or inhibits beta-catenin-TCF signaling depending on receptor context. PLoS Biol *4*, e115.
Miller, P.S., and Aricescu, A.R. (2014). Crystal structure of a human GABAA receptor. Nature *512*, 270-275.
Molday, R.S., and MacKenzie, D. (1983). Monoclonal antibodies to rhodopsin: characterization, cross-reactivity, and application as structural probes. Biochemistry *22*, 653-660.
Monneret, C. (2005). Histone deacetylase inhibitors. Eur J Med Chem *40*, 1-13.
Mulligan, K.A., Fuerer, C., Ching, W., Fish, M., Willert, K., and Nusse, R. (2012). Secreted Wingless-interacting molecule (Swim) promotes long-range signaling by maintaining Wingless solubility. Proc Natl Acad Sci U S A *109*, 370-377.
Munemitsu, S., Albert, I., Souza, B., Rubinfeld, B., and Polakis, P. (1995). Regulation of intracellular beta-catenin levels by the adenomatous polyposis coli (APC) tumor-suppressor protein. Proc Natl Acad Sci U S A *92*, 3046-3050.
Murshudov, G.N., Vagin, A.A., and Dodson, E.J. (1997). Refinement of macromolecular structures by the maximum-likelihood method. Acta Crystallogr D Biol Crystallogr *53*, 240-255.
Nachtergaele, S., Whalen, D.M., Mydock, L.K., Zhao, Z., Malinauskas, T., Krishnan, K., Ingham, P.W., Covey, D.F., Siebold, C., and Rohatgi, R. (2013). Structure and function of the Smoothened extracellular domain in vertebrate Hedgehog signaling. eLife *2*, e01340.
Nagai, T., Ibata, K., Park, E.S., Kubota, M., Mikoshiba, K., and Miyawaki, A. (2002). A variant of yellow fluorescent protein with fast and efficient maturation for cell-biological applications. Nature biotechnology *20*, 87-90.
Naito, A.T., Sumida, T., Nomura, S., Liu, M.L., Higo, T., Nakagawa, A., Okada, K., Sakai, T., Hashimoto, A., Hara, Y.*, et al.* (2012). Complement C1q activates canonical Wnt signaling and promotes aging-related phenotypes. Cell *149*, 1298-1313.
Nichols, A.S., Floyd, D.H., Bruinsma, S.P., Narzinski, K., and Baranski, T.J. (2013). Frizzled receptors signal through G proteins. Cell Signal *25*, 1468-1475.
Nikopoulos, K., Gilissen, C., Hoischen, A., van Nouhuys, C.E., Boonstra, F.N., Blokland, E.A., Arts, P., Wieskamp, N., Strom, T.M., Ayuso, C.*, et al.* (2010a). Next-generation sequencing of a 40 Mb linkage interval reveals TSPAN12 mutations in patients with familial exudative vitreoretinopathy. Am J Hum Genet *86*, 240-247.
Nikopoulos, K., Venselaar, H., Collin, R.W., Riveiro-Alvarez, R., Boonstra, F.N., Hooymans, J.M., Mukhopadhyay, A., Shears, D., van Bers, M., de Wijs, I.J.*, et al.* (2010b). Overview of the mutation spectrum in familial exudative vitreoretinopathy and Norrie disease with identification of 21 novel variants in FZD4, LRP5, and NDP. Hum Mutat *31*, 656-666.
O'Callaghan C, A., Byford, M.F., Wyer, J.R., Willcox, B.E., Jakobsen, B.K., McMichael, A.J., and Bell, J.I. (1999). BirA enzyme: production and application in the study of membrane receptor-ligand interactions by site-specific biotinylation. Anal Biochem *266*, 9-15.
Ohlmann, A., Scholz, M., Goldwich, A., Chauhan, B.K., Hudl, K., Ohlmann, A.V., Zrenner, E., Berger, W., Cvekl, A., Seeliger, M.W.*, et al.* (2005). Ectopic norrin induces growth of ocular capillaries and restores normal retinal angiogenesis in Norrie disease mutant mice. J Neurosci *25*, 1701-1710.

Ohlmann, A., Seitz, R., Braunger, B., Seitz, D., Bosl, M.R., and Tamm, E.R. (2010). Norrin promotes vascular regrowth after oxygen-induced retinal vessel loss and suppresses retinopathy in mice. J Neurosci *30*, 183-193.
Ohlmann, A., and Tamm, E.R. (2012). Norrin: molecular and functional properties of an angiogenic and neuroprotective growth factor. Prog Retin Eye Res *31*, 243-257.
Ohta, K., Ito, A., Kuriyama, S., Lupo, G., Kosaka, M., Ohnuma, S., Nakagawa, S., and Tanaka, H. (2011). Tsukushi functions as a Wnt signaling inhibitor by competing with Wnt2b for binding to transmembrane protein Frizzled4. Proc Natl Acad Sci U S A *108*, 14962-14967.
Olczak, M., and Olczak, T. (2006). Comparison of different signal peptides for protein secretion in nonlytic insect cell system. Anal Biochem *359*, 45-53.
Paes, K.T., Wang, E., Henze, K., Vogel, P., Read, R., Suwanichkul, A., Kirkpatrick, L.L., Potter, D., Newhouse, M.M., and Rice, D.S. (2011). Frizzled 4 is required for retinal angiogenesis and maintenance of the blood-retina barrier. Invest Ophthalmol Vis Sci *52*, 6452-6461.
Pellegrini, L., Burke, D.F., von Delft, F., Mulloy, B., and Blundell, T.L. (2000). Crystal structure of fibroblast growth factor receptor ectodomain bound to ligand and heparin. Nature *407*, 1029-1034.
Penalva, L.O., and Keene, J.D. (2004). Biotinylated tags for recovery and characterization of ribonucleoprotein complexes. Biotechniques *37*, 604, 606, 608-610.
Perez-Vilar, J., and Hill, R.L. (1997). Norrie disease protein (norrin) forms disulfide-linked oligomers associated with the extracellular matrix. J Biol Chem *272*, 33410-33415.
Pernot, P., Round, A., Barrett, R., De Maria Antolinos, A., Gobbo, A., Gordon, E., Huet, J., Kieffer, J., Lentini, M., Mattenet, M.*, et al.* (2013). Upgraded ESRF BM29 beamline for SAXS on macromolecules in solution. Journal of synchrotron radiation *20*, 660-664.
Peroutka, R.J., Elshourbagy, N., Piech, T., and Butt, T.R. (2008). Enhanced protein expression in mammalian cells using engineered SUMO fusions: secreted phospholipase A2. Protein Sci *17*, 1586-1595.
Petoukhov, M.V., Franke, D., Shkumatov, A.V., Tria, G., Kikhney, A.G., Gajda, M., Gorba, C., Mertens, H.D.T., Konarev, P.V., and Svergun, D.I. (2012). New developments in the ATSAS program package for small-angle scattering data analysis. Journal of Applied Crystallography *45*, 342-350.
Planutis, K., Planutiene, M., and Holcombe, R.F. (2014). A novel signaling pathway regulates colon cancer angiogenesis through Norrin. Scientific reports *4*, 5630.
Poulter, J.A., Ali, M., Gilmour, D.F., Rice, A., Kondo, H., Hayashi, K., Mackey, D.A., Kearns, L.S., Ruddle, J.B., Craig, J.E.*, et al.* (2010). Mutations in TSPAN12 cause autosomal-dominant familial exudative vitreoretinopathy. Am J Hum Genet *86*, 248-253.
Rambo, R.P., and Tainer, J.A. (2011). Characterizing flexible and intrinsically unstructured biological macromolecules by SAS using the Porod-Debye law. Biopolymers *95*, 559-571.
Rana, R., Carroll, C.E., Lee, H.J., Bao, J., Marada, S., Grace, C.R., Guibao, C.D., Ogden, S.K., and Zheng, J.J. (2013). Structural insights into the role of the Smoothened cysteine-rich domain in Hedgehog signalling. Nature communications *4*, 2965.

Reeves, P.J., Callewaert, N., Contreras, R., and Khorana, H.G. (2002). Structure and function in rhodopsin: high-level expression of rhodopsin with restricted and homogeneous N-glycosylation by a tetracycline-inducible N-acetylglucosaminyltransferase I-negative HEK293S stable mammalian cell line. Proc Natl Acad Sci U S A *99*, 13419-13424.
Rehm, H.L., Zhang, D.S., Brown, M.C., Burgess, B., Halpin, C., Berger, W., Morton, C.C., Corey, D.P., and Chen, Z.Y. (2002). Vascular defects and sensorineural deafness in a mouse model of Norrie disease. J Neurosci *22*, 4286-4292.
Richter, M., Gottanka, J., May, C.A., Welge-Lussen, U., Berger, W., and Lutjen-Drecoll, E. (1998). Retinal vasculature changes in Norrie disease mice. Invest Ophthalmol Vis Sci *39*, 2450-2457.
Riese, J., Yu, X., Munnerlyn, A., Eresh, S., Hsu, S.C., Grosschedl, R., and Bienz, M. (1997). LEF-1, a nuclear factor coordinating signaling inputs from wingless and decapentaplegic. Cell *88*, 777-787.
Ring, L., Perobner, I., Karow, M., Jochum, M., Neth, P., and Faussner, A. (2011). Reporter gene HEK 293 cells and WNT/Frizzled fusion proteins as tools to study WNT signaling pathways. Biol Chem *392*, 1011-1020.
Rios, C.D., Jordan, B.A., Gomes, I., and Devi, L.A. (2001). G-protein-coupled receptor dimerization: modulation of receptor function. Pharmacology & therapeutics *92*, 71-87.
Riu, E., Chen, Z.Y., Xu, H., He, C.Y., and Kay, M.A. (2007). Histone modifications are associated with the persistence or silencing of vector-mediated transgene expression in vivo. Mol Ther *15*, 1348-1355.
Robitaille, J., MacDonald, M.L., Kaykas, A., Sheldahl, L.C., Zeisler, J., Dube, M.P., Zhang, L.H., Singaraja, R.R., Guernsey, D.L., Zheng, B.*, et al.* (2002). Mutant frizzled-4 disrupts retinal angiogenesis in familial exudative vitreoretinopathy. Nat Genet *32*, 326-330.
Ruffner, H., Sprunger, J., Charlat, O., Leighton-Davies, J., Grosshans, B., Salathe, A., Zietzling, S., Beck, V., Therier, M., Isken, A.*, et al.* (2012). R-Spondin potentiates Wnt/beta-catenin signaling through orphan receptors LGR4 and LGR5. PLoS One *7*, e40976.
Schlessinger, J., Plotnikov, A.N., Ibrahimi, O.A., Eliseenkova, A.V., Yeh, B.K., Yayon, A., Linhardt, R.J., and Mohammadi, M. (2000). Crystal structure of a ternary FGF-FGFR-heparin complex reveals a dual role for heparin in FGFR binding and dimerization. Mol Cell *6*, 743-750.
Schneidman-Duhovny, D., Hammel, M., and Sali, A. (2010). FoXS: a web server for rapid computation and fitting of SAXS profiles. Nucleic Acids Res *38*, W540-544.
Schwarz-Romond, T., Fiedler, M., Shibata, N., Butler, P.J., Kikuchi, A., Higuchi, Y., and Bienz, M. (2007). The DIX domain of Dishevelled confers Wnt signaling by dynamic polymerization. Nat Struct Mol Biol *14*, 484-492.
Schwarzenbacher, R., Godzik, A., Grzechnik, S.K., and Jaroszewski, L. (2004). The importance of alignment accuracy for molecular replacement. Acta Crystallogr D Biol Crystallogr *60*, 1229-1236.
Seifert, J.R., and Mlodzik, M. (2007). Frizzled/PCP signalling: a conserved mechanism regulating cell polarity and directed motility. Nat Rev Genet *8*, 126-138.
Seitz, R., Hackl, S., Seibuchner, T., Tamm, E.R., and Ohlmann, A. (2010). Norrin mediates neuroprotective effects on retinal ganglion cells via activation of the

Wnt/beta-catenin signaling pathway and the induction of neuroprotective growth factors in Muller cells. J Neurosci *30*, 5998-6010.
Shastry, B.S. (2010). Genetic susceptibility to advanced retinopathy of prematurity (ROP). J Biomed Sci *17*, 69.
Shastry, B.S., Hejtmancik, J.F., and Trese, M.T. (1997a). Identification of novel missense mutations in the Norrie disease gene associated with one X-linked and four sporadic cases of familial exudative vitreoretinopathy. Hum Mutat *9*, 396-401.
Shastry, B.S., Pendergast, S.D., Hartzer, M.K., Liu, X., and Trese, M.T. (1997b). Identification of missense mutations in the Norrie disease gene associated with advanced retinopathy of prematurity. Arch Ophthalmol *115*, 651-655.
Shastry, B.S., and Trese, M.T. (2003). Overproduction and partial purification of the Norrie disease gene product, norrin, from a recombinant baculovirus. Biochem Biophys Res Commun *312*, 229-234.
Sheldrick, G.M. (2010). Experimental phasing with SHELXC/D/E: combining chain tracing with density modification. Acta Crystallogr D Biol Crystallogr *66*, 479-485.
Shi, M., Zhu, J., Wang, R., Chen, X., Mi, L., Walz, T., and Springer, T.A. (2011). Latent TGF-beta structure and activation. Nature *474*, 343-349.
Slabinski, L., Jaroszewski, L., Rychlewski, L., Wilson, I.A., Lesley, S.A., and Godzik, A. (2007). XtalPred: a web server for prediction of protein crystallizability. Bioinformatics *23*, 3403-3405.
Smallwood, P.M., Williams, J., Xu, Q., Leahy, D.J., and Nathans, J. (2007). Mutational analysis of Norrin-Frizzled4 recognition. J Biol Chem *282*, 4057-4068.
Stiegler, A.L., Burden, S.J., and Hubbard, S.R. (2009). Crystal structure of the frizzled-like cysteine-rich domain of the receptor tyrosine kinase MuSK. J Mol Biol *393*, 1-9.
Sun, P.D., and Davies, D.R. (1995). The cystine-knot growth-factor superfamily. Annual review of biophysics and biomolecular structure *24*, 269-291.
Svergun, D. (1992). Determination of the regularization parameter in indirect-transform methods using perceptual criteria. Journal of Applied Crystallography *25*, 495-503.
Takada, R., Satomi, Y., Kurata, T., Ueno, N., Norioka, S., Kondoh, H., Takao, T., and Takada, S. (2006). Monounsaturated fatty acid modification of Wnt protein: its role in Wnt secretion. Dev Cell *11*, 791-801.
Tamai, K., Semenov, M., Kato, Y., Spokony, R., Liu, C., Katsuyama, Y., Hess, F., Saint-Jeannet, J.P., and He, X. (2000). LDL-receptor-related proteins in Wnt signal transduction. Nature *407*, 530-535.
Terwilliger, T.C. (2000). Maximum-likelihood density modification. Acta Crystallogr D Biol Crystallogr *56*, 965-972.
Terwilliger, T.C. (2003). SOLVE and RESOLVE: automated structure solution and density modification. Methods Enzymol *374*, 22-37.
Terwilliger, T.C., Adams, P.D., Read, R.J., McCoy, A.J., Moriarty, N.W., Grosse-Kunstleve, R.W., Afonine, P.V., Zwart, P.H., and Hung, L.W. (2009). Decision-making in structure solution using Bayesian estimates of map quality: the PHENIX AutoSol wizard. Acta Crystallogr D Biol Crystallogr *65*, 582-601.
Thompson, J.D., Higgins, D.G., and Gibson, T.J. (1994). CLUSTAL W: improving the sensitivity of progressive multiple sequence alignment through sequence

weighting, position-specific gap penalties and weight matrix choice. Nucleic Acids Res *22*, 4673-4680.
Toomes, C., Bottomley, H.M., Scott, S., Mackey, D.A., Craig, J.E., Appukuttan, B., Stout, J.T., Flaxel, C.J., Zhang, K., Black, G.C.*, et al.* (2004). Spectrum and frequency of FZD4 mutations in familial exudative vitreoretinopathy. Invest Ophthalmol Vis Sci *45*, 2083-2090.
Trombetta, E.S., and Parodi, A.J. (2003). Quality control and protein folding in the secretory pathway. Annu Rev Cell Dev Biol *19*, 649-676.
von Maltzahn, J., Zinoviev, R., Chang, N.C., Bentzinger, C.F., and Rudnicki, M.A. (2013). A truncated Wnt7a retains full biological activity in skeletal muscle. Nature communications *4*, 2869.
Walter, T.S., Diprose, J.M., Mayo, C.J., Siebold, C., Pickford, M.G., Carter, L., Sutton, G.C., Berrow, N.S., Brown, J., Berry, I.M.*, et al.* (2005). A procedure for setting up high-throughput nanolitre crystallization experiments. Crystallization workflow for initial screening, automated storage, imaging and optimization. Acta Crystallogr D Biol Crystallogr *61*, 651-657.
Walter, T.S., Meier, C., Assenberg, R., Au, K.F., Ren, J., Verma, A., Nettleship, J.E., Owens, R.J., Stuart, D.I., and Grimes, J.M. (2006). Lysine methylation as a routine rescue strategy for protein crystallization. Structure *14*, 1617-1622.
Wang, Y., Rattner, A., Zhou, Y., Williams, J., Smallwood, P.M., and Nathans, J. (2012). Norrin/Frizzled4 signaling in retinal vascular development and blood brain barrier plasticity. Cell *151*, 1332-1344.
Weinkam, P., Pons, J., and Sali, A. (2012). Structure-based model of allostery predicts coupling between distant sites. Proc Natl Acad Sci U S A *109*, 4875-4880.
Willert, K., Brown, J.D., Danenberg, E., Duncan, A.W., Weissman, I.L., Reya, T., Yates, J.R., 3rd, and Nusse, R. (2003). Wnt proteins are lipid-modified and can act as stem cell growth factors. Nature *423*, 448-452.
Willert, K., and Nusse, R. (2012). Wnt proteins. Cold Spring Harbor perspectives in biology *4*, a007864.
Winter, G. (2010). xia2: an expert system for macromolecular crystallography data reduction. Journal of Applied Crystallography *43*, 186-190.
Wong, H.C., Bourdelas, A., Krauss, A., Lee, H.J., Shao, Y., Wu, D., Mlodzik, M., Shi, D.L., and Zheng, J. (2003). Direct binding of the PDZ domain of Dishevelled to a conserved internal sequence in the C-terminal region of Frizzled. Mol Cell *12*, 1251-1260.
Xia, C.H., Liu, H., Cheung, D., Wang, M., Cheng, C., Du, X., Chang, B., Beutler, B., and Gong, X. (2008). A model for familial exudative vitreoretinopathy caused by LPR5 mutations. Hum Mol Genet *17*, 1605-1612.
Xu, Q., Wang, Y., Dabdoub, A., Smallwood, P.M., Williams, J., Woods, C., Kelley, M.W., Jiang, L., Tasman, W., Zhang, K.*, et al.* (2004). Vascular development in the retina and inner ear: control by Norrin and Frizzled-4, a high-affinity ligand-receptor pair. Cell *116*, 883-895.
Xu, S., Cheng, F., Liang, J., Wu, W., and Zhang, J. (2012). Maternal xNorrin, a canonical Wnt signaling agonist and TGF-beta antagonist, controls early neuroectoderm specification in Xenopus. PLoS Biol *10*, e1001286.
Yan, D., and Lin, X. (2009). Shaping morphogen gradients by proteoglycans. Cold Spring Harbor perspectives in biology *1*, a002493.

Yang, H., Li, S., Xiao, X., Guo, X., and Zhang, Q. (2012). Screening for NDP Mutations in 44 Unrelated Patients with Familial Exudative Vitreoretinopathy or Norrie Disease. Curr Eye Res *37*, 726-729.
Yang, H., Xiao, X., Li, S., Mai, G., and Zhang, Q. (2011). Novel TSPAN12 mutations in patients with familial exudative vitreoretinopathy and their associated phenotypes. Mol Vis *17*, 1128-1135.
Yang, Z.R., Thomson, R., McNeil, P., and Esnouf, R.M. (2005). RONN: the bio-basis function neural network technique applied to the detection of natively disordered regions in proteins. Bioinformatics *21*, 3369-3376.
Ye, X., Wang, Y., Cahill, H., Yu, M., Badea, T.C., Smallwood, P.M., Peachey, N.S., and Nathans, J. (2009). Norrin, frizzled-4, and Lrp5 signaling in endothelial cells controls a genetic program for retinal vascularization. Cell *139*, 285-298.
Ye, X., Wang, Y., and Nathans, J. (2010). The Norrin/Frizzled4 signaling pathway in retinal vascular development and disease. Trends Mol Med *16*, 417-425.
Zeng, L., Fagotto, F., Zhang, T., Hsu, W., Vasicek, T.J., Perry, W.L., 3rd, Lee, J.J., Tilghman, S.M., Gumbiner, B.M., and Costantini, F. (1997). The mouse Fused locus encodes Axin, an inhibitor of the Wnt signaling pathway that regulates embryonic axis formation. Cell *90*, 181-192.
Zhang, K., Harada, Y., Wei, X., Shukla, D., Rajendran, A., Tawansy, K., Bedell, M., Lim, S., Shaw, P.X., He, X.*, et al.* (2011). An essential role of the cysteine-rich domain of FZD4 in Norrin/Wnt signaling and familial exudative vitreoretinopathy. J Biol Chem *286*, 10210-10215.
Zhao, Y., Bishop, B., Clay, J.E., Lu, W., Jones, M., Daenke, S., Siebold, C., Stuart, D.I., Jones, E.Y., and Aricescu, A.R. (2011). Automation of large scale transient protein expression in mammalian cells. J Struct Biol *175*, 209-215.
Zhou, Y., Wang, Y., Tischfield, M., Williams, J., Smallwood, P.M., Rattner, A., Taketo, M.M., and Nathans, J. (2014). Canonical WNT signaling components in vascular development and barrier formation. The Journal of clinical investigation.
Zhou, Y.F., and Springer, T.A. (2014). Highly reinforced structure of a C-terminal dimerization domain in von Willebrand factor. Blood *123*, 1785-1793.
Zou, Z., and Sun, P.D. (2004). Overexpression of human transforming growth factor-beta1 using a recombinant CHO cell expression system. Protein Expr Purif *37*, 265-272.